

Response to reviewers

**Owen Callahan (Referee 1)**

**“Muñoz-López and co-authors document evolving fluid sources and conditions during multiple stages of deformation through a combination of field, petrographic, and geochemical analysis of an exhumed thrust in the Pyrenees. The manuscript is generally well written, with only minor grammatical or stylistic edits, and the quality of the work is robust. I do think that the manuscript could be improved with relatively minor edits, specifically with regards to motivation, descriptions of geologic units, and inclusion of a better synthesis figure”.**

We thank the referee for his constructive comments, which greatly helped to improve the quality of the manuscript.

**General Comments:**

**“The motivation for the study should be stated clearly and much earlier in the document. The clearest iteration that I found was on page 13, the first sentence of section 5.4. It would be helpful for this type of statement to appear in the abstract, and in the introduction”.**

The main objectives of this contribution were already stated in the text. However, clearer sentences explaining the purpose and objectives of this paper are now included in the abstract and the introduction section.

**“For all the discussion of basement, the age, lithology, and metamorphic grade were only briefly discussed, and relatively late in the text. It would be helpful to expand and highlight the section on the basement geology, and specifically previously published geochemistry, instead of the broader regional tectonism. It is particularly confusing because you repeatedly refer to “crystalline basement” but we learn that the basement is composed of Paleozoic slates, phyllites, sandstone, mudstone, limestone, conglomerate, and shale in Figure 11 and at the very end of the background geology, and if these are not the basement rocks then I’m completely lost. This is perhaps relevant because the Sr data is really more about interaction with older rocks with a different radiogenic signature, not rocks that are “crystalline” or not, correct? “**

We expanded the description of basement rocks in the geological setting describing the age, lithology, metamorphic grade and involved tectonic event.

We agree with the reviewer that the Sr data from the basement is likely related to the interaction between vein-forming fluids and older rocks with a higher radiogenic signature. Therefore, we removed the phrase “crystalline rocks” as it was not properly used. Instead, we now refer to “basement rocks”.

**“I would like to see a figure of chemistry/temperature/source and deformation/tectonic events through time, rather than the 3D block diagram. The source and direction of infiltration and upwelling are rather speculative, but putting your observations into a more linear, temporal framework would be really helpful for me (see for instance my quick quick sketch). Similarly, annotating the figures showing geochemistry with some additional information about the inferred timing of cements, or associated structures, would be very helpful.”**

We combined the final 3D diagram with a temporal framework summarizing the tectonic and geochemical evolution of the area through time, similar to the sketch suggested by the reviewer.

All figures showing geochemistry (Fig. 9, 10, 12) have new information about the structure related to each calcite cement. We also added arrows to better observe the relative timing of all cements in the graphs. Therefore, with this new information it is easier to observe the geochemical evolution over time.

**“What you meant by “timing” was a little misleading. At first, I assumed you were talking about relative timing from cross cutting relationships, but then you mention radiogenic ages, but then you acknowledge that you did not get ages... I think it would be better to be more specific, and upfront, about these being relative ages that are broadly linked to specific styles of tectonism”.**

We firstly established the chronological order of the observed structures based on crosscutting relationships of (micro)structures. Then, we attempted to validate our interpretations by means of U/Pb geochronology. However, as we did not obtain absolute ages from U/Pb data, we use relative ages instead of absolute ages for discussion. To better clarify this, we explained in the results section that we did not get absolute ages and therefore, we are discussing with relative ages. In addition, we now use the term “relative timing” throughout the manuscript.

**“This was originally a specific comment, but I think it applies to the whole manuscript: Many hydrothermal systems are ultimately derived from meteoric fluids, and I agree that there is a clear and reasonable distinction between your cooler, younger fluids and hotter fluids, but a short sentence relating the importance of fluid-rock reaction and chemical evolution at higher temperatures and longer times would be helpful, because I think you are really making the point that you can track fluids because of that residence time at depth, not their ultimate source”.**

We added a paragraph at the end of the discussion section 5.3 in which we summarize the geochemical evolution of cements Cc1a to Cc5 and its implication with water-rock interactions and with changes in the fluid regime (upward vs. downward fluid migration). This geochemical evolution through time is clearer in the new final sketch (Fig. 13).

#### **Specific Comments:**

**“Line 13: “timing” is a bit vague here. Because absolute age in faults and fractures is such a hot topic, I think it is important to specifically describe relative ages throughout.”**

Changed. We have specified that we refer to relative timing of fluid migration and vein formation.

**“Lines 17-21: Crystalline basement is vague, especially in light of the abundance of low grade and unmetamorphosed rocks you show in later figures. Also, the distinction between deeply circulated meteoric and hydrothermal fluids... Is this just a matter of temperature or chemical evolution?”**

We removed “crystalline basement rocks” as it was confusing and we now describe only “basement rocks” or “basement lithologies”.

The distinction between deeply circulated meteoric and hydrothermal fluids is based on both, chemical evolution and temperature. For instance, the clearest evidence of the presence of meteoric fluids (which precipitated cements Cc1a and Cc2) comes from the  $\delta^{18}\text{O}_{\text{fluid}}$  (yielding typical meteoric values between -6.4 and -0.3‰SMOW). By contrast, the clearest evidence of the presence of hydrothermal fluids (which precipitated Cc3 and Cc4) comes from the relative high temperatures (up to 208°C) in comparison to the burial depths (probably less than 1 km). In both cases, the high  $^{87}\text{Sr}/^{86}\text{Sr}$  ratios point to deep circulation and interaction with basement lithologies.

**“Line 33: I’m not sure how understanding past fluid flow helps use understand the current configuration of a mountain belt. Perhaps it informs the factors leading to the current configuration? Additionally, I think there is a missing comma after “through time”**

We agree with the reviewer and the paragraph has been changed accordingly. The missing comma has been added.

**“Line 51: You say only a few, but cite 7 papers working on similar topics. Also, “On the other hand” does not seem necessary here.”**

Seven papers work in similar topics in the Pyrenean basement, but all are focused on the same thrust system. This has been specified in the text.

“On the other hand” has been removed.

**“Line 100: These are the crystalline basement rocks? I think the geologic background should be more clear about rock types much earlier.”**

We agree with the reviewer, “crystalline rocks” was incorrectly used and we now use “basement rocks” instead. Also, as said in a previous comment, we expanded the geology of the basement rocks and deleted the word “crystalline” in order to avoid misunderstandings.

**“Line 105: I’d like to see a short description of why samples were selected before launching into all the analysis, i.e. the field methods component, which is well documented in your figures. You include a lot of structural context in “Results” but it is difficult to evaluate whether 35, 12, or 8 samples is enough without some description of the structures that are present.”**

We firstly established the different vein generations observed in all fracture sets and fault-related deformation. Then, we selected representative samples of all these vein generations and related host rocks. This is now explained in the text.

**“Line 121: Extra comma in “then, they”**

The extra comma has been removed.

**“Line 138: Extra comma in “one, keeping”**

The extra comma has been removed.

**“Line 162: First mention of U-Pb geochronology. So is this about absolute age?”**

As said before, we did not get U-Pb data and therefore, our interpretations are based on relative timing. This has been specified in the new manuscript.

**“Line 191: I understand the shorthand for regional foliation being Sr, but it is unfortunate that this paper also discusses strontium. Perhaps use Sr?”**

We do agree with the reviewer and we have changed the shorthand for regional foliation (we now use  $S_1$  instead of Sr).

Also, in order to simplify, we have changed the shorthand for thrust zone foliation affecting the hanging wall and footwall (we now use  $S_2$  instead of  $S_D$  and  $S_{SP}$ ).

**“Line 241: Perhaps “steeply” dipping?”**

Exactly, it has been changed.

**“Line 246: “frequently affect”? Commonly may be a better choice; frequent implies some element of time.”**

Changed. We now use commonly instead of frequently.

**“Lines 225-253: It may be imbedded in the figures, or I may have been tired at this point, but I felt like the cross cutting relations or structural context for sequencing was a bit weak with veins and cements 3-5.”**

Veins V3 to V5 are located in different structural positions (e.g., Fig. 3). Therefore, we could not observe crosscutting relationships between them in the field. However, these veins postdate the thrust-related structures and their formation is compatible with the Neogene extension (as explained in the discussion section). In the case of veins V3 and V4, their related calcite cements Cc3 and Cc4, have a similar geochemistry (Fig. 9 – 12). This supports precipitation of these cements during the same tectonic phase and associated with the same fluid flow event (i.e., although they precipitated in different structures, they are probably contemporaneous). Veins V5, as specified in the text, probably precipitated during the latest stages of extension, when the fluid regime changed from upward fluid migration to downward percolation of fluids, similar to models proposed in similar settings (e.g., Cantarero et al., 2014b).

**“Lines 262-266: This could go in a table.”**

This information is already on table 1. In this part of the text, we describe the isotopic results and the observed isotopic tendencies.

**“Line 301: Oh, there is NOT absolute geochronology. This passage should appear much earlier.”**

This passage has been moved to the results section. There, we also explain that we are dealing with relative timing and not with absolute timing.

**“Line 304: An example of the basement lithologies and ages being clearly and simply defined.”**

As suggested by the reviewer in another comment, we added a similar description in the geological setting in order to better describe the basement geology, linking lithologies, ages and tectonic events.

**“Line 330. Capitalize “Calcite...”**

Done.

**“Lines 355-361: Emphasis on channelized is a little confusing, because you also say that cements in different structural positions precipitated from the same fluids, which then begs the questions How wide are the fluid flow channels? Do you have samples from inside and outside of these channels? I think this invites a lot of extra scrutiny, and as it is written it is too vague.”**

Preferential fluid circulation along the thrust is evidenced by the exclusive presence of calcite cements (Cc1a and Cc2) within the thrust zone. As these cements (Cc1a and Cc2) precipitated during the same tectonic event but in different structural positions within the thrust zone, they likely precipitated from the same fluids, progressively increasing the fluid-rock interaction from the thrust plane (Cc2) towards the hanging wall (Cc1a). We have explained this in the text and the word “channelized” has been removed in order to avoid confusion.

**“Lines 385-390: I think you do a good job defending your interpretation of fluid sources here.”**

We are glad to hear that from the reviewer.

**“Line 393: replace “than” with “as”?**

Replaced.

**“Line 402: Probably the clearest statement of purpose in the manuscript.”**

We added a similar statement of purpose in the abstract and in the introduction. In the 5.4 subsection, we specified that we are assessing the influence of basement rocks on fluid chemistry.

**“Line 464: “Common reservoir” implies a system in hydrologic or pressure communication. I don’t think this is necessarily supported. Rather, you could claim that fluids are sourced or resided in similar basement rocks.”**

We agree! In the new manuscript we state that these fluids are sourced and/or interacted with similar basement rocks.

**“Lines 469-470: Great Basin and Basin and Range Province are not necessarily synonymous, but they are in this case and therefore redundant.”**

Changed. We now use only Great Basin in the text and the two references have been merged.

**“Line 495: Although you do include a caveat, I think the phrase “long-term” implies persistence, which is not necessarily true. I think places in the text that you describe long term fluid flow should be revisited.”**

We removed the term “long-term” as we have no evidence of the persistence of fluid flow. Instead, we state that hydrothermal fluids migrated in Neogene times and in present times and that the circulation of these fluids could be continuous through time or related to different pulses of fluid flow.

**“Line 790 (Table 1): alignment issue after sample C6.II in some columns impacts readability. Also check on reason for differences in significant digits for reported values of the same quantity (for instance, see d18O and d13C columns).”**

The alignment issue has been corrected and the significant digits have been revised.

**“Line 800 (Table 2): check grammar “when is darker”. A scale bar for color might be useful so we know what is considered high or low or how divisions were made (are they quartiles, or relative to some standard?).”**

The grammar has been checked.

In table 2, for each element, the darkest green points qualitatively to the highest concentration and vice versa. This has been explained in the text and a scale bar has been provided.

**“Line 805 (Figure 1): Including generic rock types instead of or in addition to ages would be helpful, see generic comment about describing the lithology of the basement rocks.”**

We added generic rock types in addition to ages of the map performed in the study area.

**“Line 855 (Figure 9): The relative timing of cements can be inferred from their order, but perhaps arrows on the graph showing fluid evolution over time, or some other way to relate these to types of structures or tectonic events would be useful. See general comment about a timeline figure.”**

Arrows have been drawn in the graph to show the geochemical evolution of calcite cements over time. In addition, the structure related to each calcite cement has also been provided.

**“Line 865 (Figure 10): Again, this could be combined with a figure showing fluid evolution in the context of other events or structures, rather than leaving it to the reader to relate samples and setting. Add more text on the graphs to help guide me.”**

A graph showing the structure related to each calcite cement and their evolution over time has also been provided.

**“Line 874 (Figure 11). Shales and mudstones don’t seem particularly “crystalline”, but you refer to crystalline basement a few times in the manuscript. I can understand why dilatant crystalline rocks may be geothermal reservoirs, but why these low grade rocks? Is it just that these rocks exist at deeper, hotter depths? Brown line seems a bit high (it cuts off a few basement values), how it was chosen?”**

As previously stated, the term “crystalline rocks” has been removed, we refer now to “basement rocks”.

The hydrothermal character of the fluids is inferred from their high temperatures (up to 208°C), which are higher than values expected by normal geothermal gradients (if we consider < 1km burial depths, according to Saura, 2004). Therefore, the involved fluids probably warmed at greater depths and then migrated upwards through Neogene faults, flowing fast enough to maintain their high temperatures or at



least, to be in thermal disequilibrium with the surrounding rocks. This has been better explained in the new manuscript.

We selected the limit between basement and cover values taking into account both the previous contributions and our own results. As shown in Fig. 11, all calcite cements precipitated from fluids that have circulated through cover rocks have  $^{87}\text{Sr}/^{86}\text{Sr}$  ratios clearly lower than 0.710. By contrast, all calcite cements precipitated from fluids that have circulated through basement rocks have  $^{87}\text{Sr}/^{86}\text{Sr}$  ratios greater than 0.710 (i.e., these calcites reflect a higher radiogenic signature, similar to that reported for basement rocks). The only exception is observed in reference 14 and reference 16 (Fig. 11). Reference 14 is located in Plan de Larri, at the transition between basement and cover structures. In this location, the lowest  $^{87}\text{Sr}/^{86}\text{Sr}$  values ( $<0.710$ ) are found in relatively undeformed Cretaceous carbonates, which are lithologies widely exposed in the Pyrenean cover (in the Southern Pyrenees). This explains the little overlap between these lowest values and those of the sedimentary cover. On the other hand, as explained in the manuscript, authors from reference 14 (McCaig et al., 1995) used the same limit (i.e.,  $^{87}\text{Sr}/^{86}\text{Sr} = 0.710$ ) to differentiate between values derived from the unaltered limestone protolith and the thrust-related carbonate mylonite affected by a fluid carrying radiogenic Sr. Values of reference 16 belongs to low grade metamorphic rocks. Although the lowest values of this reference overlaps those of the sedimentary cover, no information about synkinematic veins have been provided, which is the focus of the comparison in this contribution.

**“Line 885 (Figure 12). Again, I’d rather follow the changes over time, so instead of looking at changes in Mg, then Fe, then Mn... plot these values in the context of other events and features and then we could see what was happening with Mg when Sr goes up, for instance.”**

We have modified this figure according to the reviewer comment. Now it is easier to follow changes in the elemental composition over time.

**“Line 890 (Figure 13). This is a fine figure, but I don’t know that it adds a great deal to the story, other than showing what you have already described fairly well in the text. If you do keep it, I think showing warmer colors for hotter fluids may be more intuitive.”**

As said before, we added a sketch summarizing both the tectonic and geochemical evolution of the studied area. We also changed colors of the arrows that indicate fluid migration, that is, we now use red and orange colors for warm fluids and green colors for cold fluids.

## Brice Lacroix (Referee 2)

Review of the paper “Influence of basement rocks on fluid evolution during multiphase deformation: the example of the Estamariu thrust in the Pyrenean Axial Zone” by Daniel Muñoz-López, Gemma Alías, David Cruset, Irene Cantarero, Cédric M. Jonh, Anna Travé

“This paper by Munoz-Lopez et al. reports structural and geochemical evidence of several multiphase fluid-flow along the Estamariu thrust located in the Pyrenean Axial Zone combining detailed structural and microstructural observation to O, C, Sr and  $\Delta 47$  isotopes. The techniques employed here are adequate and I’m glad to see application of  $\Delta 47$  thermometry in the Axial zone. The dataset is sound, and the conclusions are reasonable. The authors document a complex fluid-flow history along the thrust during Alpine compression and Neogene extension involving different sources of fluid at different temperatures.

This paper should be published as it is an important regional contribution. As stated by the authors, there is a long list of works studying the fluid-flow along thrust faults affecting the sedimentary cover (e.g. Southern Pyrenean zone), but just a few focuses on the basement from the Axial Zone.”

We thank the referee for his positive comments and detailed reviews.

“Although this work should be published, there are several points that need to be addressed/commented during revision.

1. The structural analysis and description are very detailed but somehow confusing. Here are some suggestions that could clarify the description:

- Adding sub-titles such as 4.1.1. Adding sub-title such as Hanging wall, Main Thrust, and Footwall would help a lot.”

Sub-titles have been added to clarify the text. (i.e., 4.1.1. Hanging wall; 4.1.2. Thrust zone and 4.1.3. Footwall).

- “I would also recommend adding a general schema synthetizing all the relationship between the observed structures and microstructures. The current Figure 3 does that, but it is still confusing.”

As pointed by the reviewer, Fig. 3 represents a general sketch that summarizes the relationships between the observed structures. We have modified this figure in order to avoid confusion. For this, we simplified the terminology used to describe the different structures (see for instance the answer to the following comment) and added arrows to match such structures with their correspondent stereoplots.

- “Also, I found the adopted typologies for structures “Sr, Sm, Ssp, SD, etc...” confusing and did not catch up what the subscript letter (‘r’ and ‘m’) refer to. What about calling these foliations the same way (unless they are associated to different tectonic phases) and just describe them (morphologies, intensity, orientation) in the sub-section. This would simplify understanding of the numerous stereoplots presented in Figure 3. I also noticed that some of these foliation typologies are not called in the text. For example in line 199: “*The foliation within the thrust zone affecting the Devonian hanging wall strikes NW-SE and dips 40 – 50° NE, similar to the regional foliation in the protolith, but it is more closely spaced, generally between 0.2 and 1 cm (Fig. 6A, B).*” Specify in the text if this foliation corresponds to “Sr”. The same comment is applicable for all the section 4.1.”

We changed and simplified the shorthand used to describe the observed structures.

For regional foliation we now use  $S_1$  (instead of Sr).

The foliation associated with the thrust (i.e., the thrust zone foliation) is now called the same way ( $S_2$ ), even if it affects the thrust zone deforming the hanging wall or the footwall (we use  $S_2$  instead of  $S_D$  or  $S_{SP}$ ).

We do not use shorthand for layering magmatic anymore (i.e., we removed the shorthand Sm) because layering magmatic is an inherited fluidal structure that is not discussed in detail.

All foliation typologies are clearer and better described in section 4.1.

- “You mentioned pressure solution surfaces e1 and e2 but it was not clear on which basis they were differentiated. Is there any cross-cutting feature? The orientation of these features (if any) are not presented on stereoplots.”

These stylolites were only observed locally at microscopic scale and therefore, their orientations are given according to more relevant structures (i.e., they trend subparallel to the thrust zone foliation). This is stated in the text.

We could not find crosscutting relationships between these structures, however, we differentiated them according to their spacing and crosscutting relations with veins V1a. Stylolites e1 are less spaced and are always crosscut by veins V1a, whereas, stylolites e2 are more abundant and postdate V1a (as they developed as sutured areas between the host rock and veins V1a). This has been clarified in the new text.

2. “The authors report warm temperature fluid-flow event (up to > 200°C), presumably hydrothermal fluid for the CC3 and CC4 calcite phases. As you know,  $\Delta 47$  composition of carbonate may be altered by  $\Delta 47$ -reordering when carbonate experienced temperature in excess of 200°C (maybe lower temperature). Although, I’m convinced that these hydrothermal events did not alter previous carbonate phases (cc1, cc2), I would like to see the authors discussing potential (or not)  $\Delta 47$ -reordering and how it could be ruled out. Here are some ways to discuss that:

- Is there some metamorphic/Fluid Inclusion/chronology work in the same area reporting temperature-time relationship of this hydrothermal event? If this hydrothermal event is short, the solid-state  $\Delta 47$  probably did not occur;

- Is the thermal history of the area constrained by other studies? If it is the case, the authors could use re-ordering models (e.g. Stolper and Eiler 2015; Lloyd et al., 2017) to see if the  $\Delta 47$  composition of the different calcite phases may experience re-ordering.

- Alternatively, the authors may acknowledge that further re-ordering is possible but unlikely due to the short time.”

We agree that clumped isotopes may potentially be altered due to the relatively high temperatures. However, as suggested by the reviewer, we also consider that this is unlikely because of the relative short time of hydrothermal fluid migration in the study area and because there is no evidence of calcite recrystallization and/or solid-state reactions. We have explained this in the new manuscript, in section 5.3 of discussion.

3. “I have noticed few poorly constructed sentences. I would suggest the English to be checked before re-submission. I won’t make any comment on that as I’m myself always struggling with English.”

The English grammar has been revised and improved.

#### **Minor comments:**

“l. 28: Deformation associated with crustal shortening is mainly accommodated by thrust faulting and related fault zone structures: Add references.”

References added (Mouthereau et al., 2014; Muñoz, 1992a; Sibson, 1994).

“l. 30: “The reactivation of faults may produce changes in the hydraulic....”: Add References.”

References added (Arndt et al., 2014; Barker and Cox, 2011; Cantarero et al., 2018; Cruset et al., 2018a; Lacroix et al., 2018; Travé et al., 2007a).

**“I. 174: Which fractionation curve is used to calculate the oxygen isotope composition of water?”**

The fractionation equation used to calculate the oxygen isotope composition of water is the one from Friedman and O’Neil (1977). This is stated in the new text.

**“I.180 – 181: “The main slip plane is undulose, producing changes in the strike direction and dip, and generates a 2 – 3 m thick thrust zone, which is thicker in the hanging wall, up to 2.5 m thick”: Do you mean the thrust fault consists to a deformation zone affecting both hanging wall and footwall, with deformation zone thicker in the HW?”**

Exactly! The thrust zone affects both the footwall and hanging wall. This has been specified in the new text.

**“I.187: “In the studied outcrops, the Devonian Rueda Formation from the hanging wall is characterized by a well-bedded alternation of dark to light grey limestones with dark grey shales”: Does this refer to S<sub>0</sub>, S<sub>r</sub>, S<sub>d</sub>? Please specify.”**

It refers to S<sub>0</sub> (bedding). It has been better explained in the text.

**“I.190-192: “Deformation in the Devonian protolith (i.e., outside the thrust zone) corresponds to a decametric anticline (Fig. 2B), which has associated an axial plane pervasive regional foliation (S<sub>r</sub>) concentrated in the pelitic intervals (Fig. 5B)”: looking at the stereoplot from Fig. 3, the bedding (S<sub>0</sub>) seems to define a fold oriented E-W (although only based on 3 measurements). In contrast the S<sub>r</sub> does not seem parallel to the axial plane and is more or less oriented N-S (even slightly folded). How can you explain this?”**

As observed in Fig. 2, the fold in the hanging wall corresponds to a tight and SW verging anticline. Looking at the stereoplot (Devonian protolith), the observed planes define the fold limbs, which are approximately oriented WNW-ESE and NE-SW. The intersection between these planes (through the bisector angle) defines the axial surface, which is oriented ~NNW-SSE, similar to the regional foliation. In addition, the geometric relationships between foliation and bedding also constrain the fold type at great scale (Fig. 2B). In the hinge of the anticline, bedding (S<sub>0</sub>) dips towards the SE and forms a high angle with S<sub>1</sub> (Fig. 2B and 5A), whereas in its eastern limb, the regional foliation (S<sub>1</sub>) dips steeper than S<sub>0</sub>. This has been explained in the new text.

**“l. 203-204: “When present, these stylolites are very systematic with densities between 5 and 8 stylolites/cm.” Should the intensity be given in number/cm<sup>2</sup>?”**

This is a rough estimation because stylolites e1 are only locally observed at microscopic scale. Therefore, in the new manuscript, we give the stylolites intensity by means of their spacing, this is, they are 1 – 2 mm spaced (Fig. 6C).

**“l. 201 – 202: “At mesoscale, SD has related shear surfaces (Ci) defining centimetric S-C-type structures, again indicating reverse kinematics (Fig. 6A).”: Do you have a closer view of the C-S relationship?”**

We improved the quality of the picture showing S-C structures. The S-C relationships is better seen now.

**“l.220-222: “The vein cement (Cc2) is milky white in hand sample and consists of up to 3 mm blocky to elongated blocky crystals (Fig. 6G) with a dull to bright orange luminescence (Fig. 6H).”: To me, e2 and V1b are clearly cogenetic as their crosscutting relationship are ambiguous (as stated by the authors). It is also interesting to see that V1b is extensional (Mode I) but also show mode II with conjugate opening (Fig. 6F). In any case all these structures formed under the same field stress and can be assumed contemporaneous.”**

We totally agree with the reviewer and, as it is explained in the text, these observations indicate that these structures developed coevally.

**“l.226: “They are parallel or locally branch off cutting the foliation planes in the subsidiary thrust zone”: What are the textures of these veins? They seem to show interdigitated texture in agreement with extension opening. These are important as they give indication of the opening regime and stress field.”**

As explained in the text, although veins V3 locally branch off, they are mainly parallel to the foliation planes and therefore, we could not observe geometrical features (in the field) indicative of the stress regime. However, the fibrous texture of the calcite crystals, growing perpendicular to the vein walls and to the foliation planes, indicates their extensional character. This extensional opening postdates the thrust zone foliation and is compatible with the Neogene extension. On the other hand, the vein cement (Cc3) has a similar geochemical composition to the cement present in the Neogene normal faults (Cc4). This observation seems to indicate precipitation during the same tectonic event and associated with the same fluid regime. This has been stated in the new text.

**“I.246: You state here v4 for fault. However, you previously used V labels for veins. It is confusing even if we expect slickenside onto these faults.”**

We use V labels (V1 to V5) as a shorthand for calcite veins instead of the related structure type (opening fracture or fault). This has been clarified in the new text.

**“I.252-253: “Shear fractures (V5) are locally mineralized with a greyish microsparite calcite cement (Cc5).”: Any Figure to document?”**

We added two images of these veins, a field image of the vein and a microphotograph of the vein-related cement.

**“I. 400: Huyghe et al. (2018): “Impact of topography, climate and moisture sources on isotopic composition ( $\delta^{18}\text{O}$  &  $\delta\text{D}$ ) of rivers in the Pyrenees: Implications for topographic reconstructions in small orogens” reported new isotope lapse rates for the Pyrenees. This study should be cited here as it supports very well you high elevation hypothesis. The authors could even use these lapse rates to document the paleo-elevation.”**

This reference has been added because, as suggested by the reviewer, this study supports our interpretations.

The paleo-elevation have not been calculated because according to Huyghe et al., 2018 the relationship between the isotopic composition and the elevation is not clear in the Southern Pyrenees. According to these authors, the elevation does not seem to be the only parameter controlling the isotopic composition in this part of the belt.

**“Figure 11: This figure is really good!”**

We are glad that the reviewer likes this figure.

# Influence of basement rocks on fluid evolution during multiphase deformation: the example of the Estamariu thrust in the Pyrenean Axial Zone

5 Daniel Muñoz-López<sup>1</sup>, Gemma Alías<sup>1</sup>, David Cruset<sup>2</sup>, Irene Cantarero<sup>1</sup>, Cédric M. John<sup>3</sup>, Anna Travé<sup>1</sup>

<sup>1</sup>Departament de Mineralogia, Petrologia i Geologia Aplicada. Facultat de Ciències de la Terra, Universitat de Barcelona (UB), C/ Martí i Franquès s/n, 08028 Barcelona, Spain.

<sup>2</sup>[Group of Dynamics of the Lithosphere \(GDL\), Geosciences Barcelona, GEO3BCN-CSIC](#), Lluís Solé i Sabarís s/n, 08028 Barcelona, Spain.

10 <sup>3</sup> Department of Earth Science and Engineering, Imperial College London, London SW7 2BP, UK.

*Correspondence to:* Daniel Muñoz-López (munoz-lopez@ub.edu)

**Abstract.** Calcite veins precipitated in the Estamariu thrust during two tectonic events are studied in order to: (i) decipher the temporal and spatial relationships between deformation and fluid migration in a long-lived thrust and (ii) determine the influence of basement rocks on the fluid chemistry during deformation. Structural and petrological observations constrain the relative timing of fluid migration and vein formation, whilst geochemical analyses ( $\delta^{13}\text{C}$ ,  $\delta^{18}\text{O}$ ,  $^{87}\text{Sr}/^{86}\text{Sr}$ , clumped isotope thermometry and elemental composition) applied to the related calcite cements and host rocks indicate the fluid origin, pathways and extent of fluid-rock interaction. The first tectonic event, recorded by calcite cements Cc1a and Cc2, is related to the Alpine reactivation of the Estamariu thrust, and is characterized by the migration of meteoric fluids, heated at depth at temperatures between 56 and 98 °C, and interacted with basement rocks before upflowing through the thrust zone. During the Neogene extension, the Estamariu thrust was reactivated and normal faults and shear fractures with calcite cements Cc3, Cc4 and Cc5 developed. Calcites Cc3 and Cc4 precipitated from hydrothermal fluids (temperatures between 127 and 208 °C and between 102 and 167 °C, respectively), interacted with basement rocks and expelled through fault zones during deformation. Cc5 precipitated from low temperature meteoric waters percolating from the surface through small shear fractures. The comparison between our results and already published data in other structures from the Southern Pyrenees suggests that regardless of the origin of the fluids and the tectonic context, basement rocks have a significant influence on the fluid chemistry, particularly on the  $^{87}\text{Sr}/^{86}\text{Sr}$  ratio. Accordingly, the cements precipitated from fluids that have interacted with basement rocks have significantly higher  $^{87}\text{Sr}/^{86}\text{Sr}$  ratios (> 0.710) with respect to those precipitated from fluids that have interacted with the sedimentary cover (< 0.710), which involves younger and less radiogenic rocks.

Eliminado: Institut de Ciències de la Terra Jaume Almera, ICTJA-CSIC

Con formato: Inglés (Estados Unidos)

Con formato: Inglés (Estados Unidos)

Con formato: Inglés (Estados Unidos)

Eliminado: of

Eliminado: (

Eliminado: )

Eliminado: crystalline

Eliminado: derived from crystalline

Eliminado:

Eliminado: crystalline



## 1 Introduction

40 Deformation associated with crustal shortening is mainly accommodated by thrust faulting and related fault zone structures (Mouthereau et al., 2014; Muñoz, 1992; Sibson, 1994). Successive faulting may occur and favourably oriented structures may undergo reactivation during different tectonic events in a long-lived orogenic belt (Cochelin et al., 2018; Sibson, 1995). The reactivation of faults may produce changes in the hydraulic behaviour of fault zones as well as in the origin and regime of fluids circulating through them (Arndt et al., 2014; Barker and Cox, 2011; Cantarero et al., 2018; Crusset et al., 2018; Lacroix et al., 2018; Travé et al., 2007). Consequently, constraining the timing of deformation and fluid migration is essential to better understand the main factors leading to the current configuration of a mountain belt, its evolution through time, and the mobilization of different fluids during successive deformation events (Baques et al., 2012; Crespo-Blanc et al., 1995; Fay-Gomord et al., 2018; Fitz-Díaz et al., 2011; Lacroix et al., 2014). Understanding basin-scale fluid flow is of primary importance to reconstruct the diagenetic history of a sedimentary basin, as fluids take part in a wide range of geological processes including precipitation of new mineral phases, dolomitization and petroleum migration, among others (Barker et al., 2009; Foden, 2001; Fontana et al., 2014; Gomez-Rivas et al., 2014; Martín-Martín et al., 2015; Mozafari et al., 2019; Piessens et al., 2002). Due to the economic interest of these processes, in particular related to oil and ore deposits exploration, CO<sub>2</sub> sequestration, seismic activity and water management, many researchers have addressed the study of the relationship between deformation and fluid migration (Beaudoin et al., 2014; Breesch et al., 2009; Cox, 2007; Dewever et al., 2013; Gasparrini et al., 2013; Suchy et al., 2000; Travé et al., 2009; Voicu et al., 2000; Warren et al., 2014).

In the Pyrenees, the basement rocks from the Axial Zone are affected by numerous fault systems considered Variscan in age but reactivated during the Pyrenean compression (Cochelin et al., 2018; Poblet, 1991). However, no real consensus exists about the influence of the Alpine deformation on the basement rocks and the age of basement-involved structures is still debated (Cochelin et al., 2018; García-Sansegundo et al., 2011). As a consequence, the relationships between deformation and fluid flow have been widely focused on structures from the Mesozoic and Cenozoic cover (Beaudoin et al., 2015; Crognier et al., 2018; Crusset et al., 2016, 2018, 2020a; Lacroix et al., 2011, 2014; Martínez Casas et al., 2019; Nardini et al., 2019; Travé et al., 1998, 2000, 1997), where the timing of deformation and thrust emplacement is well-constrained (Crusset et al., 2020b; Vergés, 1993; Vergés and Muñoz, 1990). Contrarily, less contributions, only concentrated along the Gavarnie thrust system, have tackled the relationships between deformation and fluid migration in the Paleozoic basement (Banks et al., 1991; Grant et al., 1990; Henderson and McCaig, 1996; McCaig et al., 2000a, 1995; Rye and Bradbury, 1988; Trincal et al., 2017). Another important aspect of studying the fault-fluid system is related to the heat flow and the influence of faults on the development of geothermal systems (Faulds et al., 2010; Grasby and Hutcheon, 2001; Liotta et al., 2010; Rowland and Sibson, 2004). Particularly, in the NE part of the Iberian Peninsula (including the Pyrenees and the Catalan Coastal Ranges), the presence of high-permeability Neogene extensional faults, acting as conduits for upward migration, provide efficient pathways for hydrothermal fluids to flow from deeper to shallower crustal levels (Carmona et al., 2000; Fernández and Banda, 1990;

Código de campo cambiado

Eliminado: crystalline

Eliminado: only a few

Eliminado: this topic

Eliminado: involving crystalline rocks

Eliminado: On the other hand, a

Eliminado: focused

Taillefer et al., 2017, 2018). In this sense, understanding the fault-fluid system evolution and the **relative** timing of hydrothermal fluid migration is of great importance to characterize the potential geothermal resources of this area.

In this contribution, we report the temporal and spatial relationships between deformation and fluid migration in a long-lived Variscan thrust deforming basement rocks in the Pyrenean Axial Zone. For this purpose, we combine structural, petrological and geochemical analyses of calcite veins precipitated in the Estamariu thrust during two **reactivation** episodes **related to the** Pyrenean compression and **the** Neogene extension. Structural and petrological observations allow us to unravel the **relative** timing of fluid migration and vein formation in relation to the involved tectonic events. The geochemistry of the vein cements and related host rocks provides information on the fluid origin, pathways and extent of fluid-rock interaction during deformation. **Therefore, the main objectives of this paper are:** (i) to constrain the **relative** timing of vein formation and fluid migration; (ii) to determine the fluid origin and pathways during successive compressional and extensional deformation phases; (iii) to assess the influence of basement rocks on the chemistry of fluids circulating during deformation; and (iv) to provide insights into the fluid flow at regional scale in the NE part of the Iberian Peninsula, where the presence of hydrothermal fluids has been reported from Neogene times to present.

**Eliminado:** of regional tectonic activity (

**Eliminado:** )

**Eliminado:** The integration of all these data within the studied geological setting in the Pyrenean basement will allow us

## 90 2 Geological setting

The Pyrenees constitute an asymmetric and doubly verging orogenic belt developed from the Late Cretaceous to Oligocene, **resulting from** the Alpine convergence between the Iberian and European plates (Choukroune, 1989; Muñoz, 1992; Roure et al., 1989; Sibuet et al., 2004; Srivastava et al., 1990; Vergés and Fernández, 2012). The Pyrenean structure consists of a central antiformal stack of basement-involved rocks from the Axial Zone, flanked by two oppositely verging fold-and-thrust belts and their associated foreland basins (Muñoz, 1992; Muñoz et al., 1986) (Fig. 1A). The Axial Zone represents a fragment of the European Variscan orogen, **incorporated into the Pyrenean belt during the Alpine convergence** (Matte, 1991). It consists of a duplex of three south-directed basement thrust sheets (from upper to lower: Noguères, Orri and Rialp), involving Cambrian to Carboniferous rocks deformed by the Variscan compressional events, and an Upper Carboniferous to Triassic post-Variscan cover (Poblet, 1991; Saura, 2004; Saura and Teixell, 2006).

**Eliminado:** in relation to

**Con formato:** Español (España)

**Eliminado:** y

100 During the Neogene tectonic evolution of the eastern Axial Pyrenees, a horst and basin system bounded by E-W to ENE-WSW faults developed (Roca, 1996; Roca and Guimerà, 1992). The most important fault, La Tet fault (roughly striking N60°E and dipping around 60°N) has associated a set of E-W extensional basins such as La Cerdanya, Conflent, La Seu d'Urgell and Cerc basins (Cabrera et al., 1988; Roca, 1996). The Cerc basin consists of a Stephano-Permian accumulation of volcanic rocks discordantly overlying Cambro-Ordovician materials from the Orri thrust sheet. This basin is thrust in its eastern limit by the Estamariu thrust, whereas the northern and southern boundaries correspond to two Neogene extensional faults, La Seu d'Urgell fault and the Ortedó fault, respectively (Hartevelt, 1970; Roca, 1996; Saura, 2004) (Fig. 1B, C). In the NW part of the basin, the limit between the Stephano-Permian unit and the Upper Ordovician sequence corresponds to a Stephano-Permian

extensional fault formed coevally with the deposition of the volcanic sequence (Saura, 2004). This fault was reactivated during the latest stages of the Neogene extension (Saura, 2004) and is here referred as the Sant Antoni fault (Fig. 1C).

The Estamariu thrust is a basement-involved reverse fault originated during the Variscan orogeny with a minimum displacement of 27 km (Poblet, 1991). However, in its southwestern termination, it juxtaposes the Devonian Rueda Formation against the Stephano-Permian Erill Castell Formation. The Erill Castell Formation developed during the late to post-orogenic collapse of the Variscan belt (Lago et al., 2004; Martí, 1991, 1996; Ziegler, 1988), evidencing the reactivation of the Estamariu thrust during the Alpine Orogeny (Poblet, 1991; Saura, 2004).

Rocks cropping out around the Estamariu thrust and the Cerc basin range from Upper Ordovician to Miocene (Fig. 1C) and are deformed by successive Variscan, Alpine and Neogene phases (Saura and Teixell, 2006). Due to such a complex structural setting, the stratigraphic record is discontinuous and only Upper Ordovician, Devonian, Stephano-Permian and Neogene rocks are present in the study area. The basement lithologies consists of Upper Ordovician and Devonian metasedimentary rocks affected by multiscale folds and related pervasive axial plane regional foliation (Bons, 1988; Casas et al., 1989; Cochelin et al., 2018; Zwart, 1986). This deformation is linked to low-grade metamorphic conditions developed during the Variscan orogeny (Hartevelt, 1970; Poblet, 1991; Saura, 2004). The Upper Ordovician succession basically includes a centimetric to metric alternation of shales, sandstones, conglomerates, quartzites and phyllites and the Devonian sequence consists of a centimetric to decimetric alternation of limestones and black slates (Rueda Formation) (Mey, 1967). The Stephano-Permian sequence developed during the late to post-orogenic extensional collapse of the Variscan belt and in the study area is represented by a volcanic and volcanoclastic unit (the Erill Castell Formation) (Martí, 1991; Mey et al., 1968), involving tuffs and ignimbrites at the base and andesites in the upper part (Martí, 1996; Saura and Teixell, 2006). Finally, the Neogene sequence is constituted of detrital and poorly lithified sediments, mainly shales, sandstones and conglomerates deposited during the Neogene tectonic extension associated with the opening of the NW Mediterranean Sea (Roca, 1996).

### 3 Methods

This study integrates a field compilation of structural data and samples and petrological and geochemical analyses of calcite cements and related host rocks. The structural data includes bedding, foliation strike and fracture orientation, type, crosscutting relationships and kinematics. Such data were plotted in equal-area lower-hemisphere projections and different fracture sets were established according to their type, strike, mineral infillings, and relative age deduced from crosscutting relationships. All these data were integrated in a schematic map and a cross-section of the Estamariu thrust and the Cerc basin (Fig. 2A, B and 3). Samples considered representative of the involved host rocks and all calcite vein generations observed in the different fracture sets and fault-related structures were selected for petrological and geochemical analyses. Thin sections of these samples were prepared and studied under a Zeiss Axiophot optical microscope and a Cold cathodoluminescence (CL) microscope model 8200 Mk5-1 operating between 16–19 kV and 350 µA gun current.

**Eliminado:** Rocks cropping out around the Estamariu thrust and the Cerc basin range from Upper Ordovician to Miocene (Fig. 1C) and are deformed by successive Variscan, Alpine and Neogene phases (Saura and Teixell, 2006). Due to such a complex structural setting, the stratigraphic record is discontinuous and only Upper Ordovician, Devonian, Stephano-Permian and Neogene successions are present in the study area. The Upper Ordovician consists mainly of a detrital sedimentary sequence affected by a low-graded metamorphism (Hartevelt, 1970; Poblet, 1991; Saura, 2004). This succession basically includes a centimetric to metric alternation of shales, sandstones, conglomerates, quartzites and phyllites. The Devonian succession consists of a centimetric to decimetric alternation of limestones and black slates (Rueda Formation) (Mey, 1967). The Stephano-Permian sequence is represented by a volcanic and volcanoclastic unit (the Erill Castell Formation) (Mey et al., 1968), involving tuffs and ignimbrites at the base and andesites in the upper part (Martí, 1996; Saura and Teixell, 2006). Finally, the Neogene sequence is constituted of detrital and poorly lithified sediments, mainly shales, sandstones and conglomerates (Roca, 1996).<sup>†</sup>

**Eliminado:** and

**Eliminado:** Host rocks and calcite cements were sampled

**Eliminado:** were

**Con formato:** Color de fuente: Texto 1

170 Thirty-five representative samples of the different generations of calcite cements and the carbonate portion of the Devonian rocks were sampled for carbon and oxygen isotopy. Sampling was carried out with a 500  $\mu\text{m}$ -diameter microdrill. 50-100  $\mu\text{g}$  of powdered samples were reacted with 100% phosphoric acid during two minutes at 70  $^{\circ}\text{C}$ . The resultant  $\text{CO}_2$  was analyzed with an automated Kiel Carbonate Device attached to a Thermal Ionization Mass Spectrometer Thermo Electron MAT-252 (Thermo Fisher Scientific) according to the method of (McCrea, 1950). For calibration, the International Standard NBS-18 and the internal standard RC-1, traceable to the International Standard NBS-19, were used. The standard deviation is  $\pm 0.03\%$  for  $\delta^{13}\text{C}$  and  $\pm 0.05\%$  for  $\delta^{18}\text{O}$  expressed with respect to the VPDB standard (Vienna Pee Dee Belemnite).

175 The elemental composition of twelve samples of calcite cements and related host rocks were analyzed using a high resolution inductively coupled plasma-mass spectrometry (HR-ICP-MS, model Element XR, Thermo Fisher Scientific). 100 mg of powdered samples were dried at 40  $^{\circ}\text{C}$  during 24 h and then, they were acid digested in closed polytetrafluoroethylene (PTFE) vessels with a combination of  $\text{HNO}_3 + \text{HF} + \text{HClO}_4$  (2.5 mL: 5 mL: 2.5 mL v/v). The samples were evaporated and 1 mL of  $\text{HNO}_3$  was added to make a double evaporation. Finally, the samples were re-dissolved and diluted with MilliQ water (18.2  $\text{M}\Omega\text{ cm}^{-1}$ ) and 1 mL of  $\text{HNO}_3$  in a 100 mL volume flask. A tuning solution containing 1  $\text{g L}^{-1}$  Li, B, Na, K, Sc, Fe, Co, Cu, Ga, Y, Rh, In, Ba, Tl, U was used in order to improve the sensitivity of the ICP-MS, and as internal standard, 20  $\text{mg L}^{-1}$  of a monoelemental solution of  $^{115}\text{In}$ . Reference materials are the BCS-CRM n $^{\circ}$ 393 (ECRM 752-1) limestone, JA-2 Andesite and JB-3 Basalt. The precision of the results was expressed in terms of two standard deviations of a set of eight reference materials measurements (reference material JA-2), whereas accuracy (%) was calculated using the absolute value of the difference between the measured values obtained during the analysis and the certified values of a set of eight reference material analysis (reference material BCS-CRM n $^{\circ}$ 393 for major oxides and JA-2 for trace elements). The detection limit (DL) was calculated as three times the standard deviation of the average of ten blanks.

185 The  $^{87}\text{Sr}/^{86}\text{Sr}$  ratio was analyzed for eight representative samples of calcite cements and host rocks. Powdered samples were dissolved in 5 mL of 10% acetic acid. After centrifugation, the supernatant was dried and dissolved in 1 mL of 1M  $\text{HNO}_3$ . The solid residue generated after evaporation was diluted in 3 mL of 3M  $\text{HNO}_3$  and loaded into chromatographic columns to separate the Rb-free Sr fraction, using SrResinTM (crown-ether (4,4'(5')-di-t-butylcyclohexano-18-crown-6)) and 0.05M  $\text{HNO}_3$  as eluent. After evaporation, samples were loaded onto a Re filament along with 1  $\mu\text{L}$  of 1 M phosphoric acid and 2  $\mu\text{L}$  of  $\text{Ta}_2\text{O}_5$ . Isotopic analyses were carried out in a TIMS-Phoenix mass spectrometer performing a dynamic multicollection method, during 10 blocks of 16 cycles each one, keeping a  $^{88}\text{Sr}$  beam intensity of 3-V. Possible  $^{87}\text{Rb}$  interferences and possible mass fractionation during sample loading and analysis were corrected and normalized with the reference value of  $^{88}\text{Sr}/^{86}\text{Sr} = 0.1194$ . The isotopic standard NBS-987 was analyzed six times during sample analysis, yielding an average value of  $0.710243 \pm 0.000009$  (standard deviation,  $2\sigma$ ). NBS 987 data have been used to correct the sample ratios for standard drift from the certified value. The analytical error in the  $^{87}\text{Sr}/^{86}\text{Sr}$  ratio, referred to two standard deviations, was 0.01%, whereas the internal precision is 0.000003. Sr procedural blanks were always below 0.5 ng.

190 The  $^{143}\text{Nd}/^{144}\text{Nd}$  ratios were analyzed in seven samples of calcite cements and host rocks. Samples were weighted in Teflon $^{\circledR}$  vessels, with enriched spike solution ( $^{149}\text{Sm}$ - $^{150}\text{Nd}$  - Oak Ridge) and dissolved in 5 mL of ultrapure HF and 3 mL of ultrapure

Eliminado: .

Eliminado: .

Eliminado: .

HNO<sub>3</sub> (Merck-Suprapur™). The PFA-vessels were placed 65 hours at 120 °C into an oven. After that, cold vials were evaporated at 120 °C on a heat plate. 4 mL of 6N distilled HCL were added to the dried samples and placed at 120 °C in an oven overnight. The solid residue generated after evaporation was dissolved in 3 mL of distilled and titrated 2.5 N HCl. Samples were centrifuged at 4000 rpm for 10 minutes to separate the possible dissolved fraction from the residue. Chromatographic separation of the whole group of REE was performed with a previously calibrated cation exchange resin DOWEX 50W-X8 200-400 mesh. After that, recovered REE fractions were dried and again dissolved in 200 µL HCl 0.18N. Such solutions were passed in a new chromatographic step (Ln-resin). The result is a complete separation between the Nd and the Sm fractions, using 0.3N HCl and 0.4N HCl as eluent, respectively. Dried Sm and Nd samples dissolved with 2 µL of 0.05M phosphoric acid were loaded onto a side Rhenium (Re) filament of a triple Re filament arrangement. Nd ratios were analysed in a mass spectrometer TIMS-Phoenix®, using a dynamic multicollection method, through 160 cycles at a stable intensity of 1V for the <sup>144</sup>Nd mass. In turn, Sm ratios were analysed in the same spectrometer, using a single static method through 112 cycles keeping 1V intensity for the <sup>149</sup>Sm mass. Nd analyses were corrected for <sup>142</sup>Ce and <sup>144</sup>Sm interferences, if any, and normalized to a ratio of <sup>146</sup>Nd/<sup>144</sup>Nd = 0.7219 to correct the possible mass fractionation during the processes of loading and analysing at the TIMS. Nd isotopic standard JNdi-1 was checked to correct the sample ratios for standard drift from the certified value. The analytical error (2STD) was 0.1% in the <sup>147</sup>Sm/<sup>144</sup>Nd ratio and 0.006% in the <sup>143</sup>Nd/<sup>144</sup>Nd ratio. Procedural blanks were always below 0.1 ng.

U-Pb geochronology of the calcite cements Cc1a to Cc5 was accomplished at FIERCE (Frankfurt Isotope and Element Research Center, Goethe University) using a laser ablation inductively coupled plasma mass spectrometry (LA-ICPMS). Clumped isotope thermometry of the calcite cements was carried out in order to determine the temperature and composition ( $\delta^{18}\text{O}_{\text{fluid}}$ ) of the vein-forming fluids. 2–3 mg aliquots from cements were measured with an automated line, the Imperial Batch Extraction system (IBEX), developed at Imperial College. Samples were dropped in 105% phosphoric acid at 90 °C and reacted during 30 min. The reactant CO<sub>2</sub> was separated with a poropak-Q column and transferred into the bellows of a Thermo Scientific MAT 253 mass spectrometer. The characterization of a replicate consisted of 8 acquisitions in dual inlet mode with 7 cycles per acquisition. The post-acquisition processing was completed with Easotope, a software for clumped isotope analyses (John and Bowen, 2016). During phosphoric acid digestion,  $\Delta_{47}$  values were corrected for isotope fractionation using a phosphoric acid correction of 0.069‰ at 90 °C for calcite (Guo et al., 2009). The data were also corrected for non-linearity applying the heated gas method (Huntington et al., 2009) and projected into the reference frame of (Dennis et al., 2011). Carbonate  $\delta^{18}\text{O}$  values were calculated with the acid fractionation factors of (Kim and O'Neil, 1997). Results were converted to temperatures applying the calibration method of (Kluge et al., 2015). Calculated  $\delta^{18}\text{O}_{\text{fluid}}$  values are expressed in ‰ with respect to the Vienna Standard Mean Ocean Water (VSMOW).

## 4 Results

### 235 4.1 Structure and associated calcite cements

The Estamariu thrust strikes N-S to NW-SE and dips between 40 and 70° towards the NE. It has a displacement of a few hundred meters and juxtaposes a Devonian alternation of limestones and shales in the hanging wall against Stephano-Permian andesites in the footwall (Poblet, 1991) (Fig. 2-4). The main slip plane is undulose and generates a 2 – 3 m thick thrust zone affecting both the hanging wall and footwall, but it is thicker in the hanging wall, up to 2.5 m thick. In the footwall, the thrust zone is less than 1 m thick and has associated minor restricted thrust zones developed as subsidiary accommodation structures related to the main thrust fault (Fig. 2A, B). All kinematic indicators, including S-C structures and slickenlines, indicate reverse displacement towards the west.

The mesostructures and microstructures observed in the study area are described below according to their structural position in relation to the Estamariu thrust, that is, hanging wall, thrust zone and footwall (Fig. 3, 4). U-Pb dating of the vein cements failed due to their high lead contents and low uranium contents and therefore, the relative timing of the different mesostructures and microstructures has been determined by means of crosscutting relationships and microstructural analysis.

#### 4.1.1 Hanging wall

In the studied outcrops, the Devonian Rueda Formation is characterized by a well-bedded alternation of dark to light grey limestones with subordinated dark grey shales ( $S_0$ ) (Fig. 5A). Limestones are made up of encrinites, which consist of a bioclastic packstone formed essentially of crinoid stems (Fig. 5B). Under cathodoluminescence, encrinites show dark to bright orange colors (Fig. 5C). Devonian rocks form a decametric anticline oriented NW-SE with a well-developed axial plane foliation ( $S_1$ ) concentrated in the pelitic intervals.  $S_1$ , which is oriented NNW-SSE, is a pervasive regional foliation dipping 30 to 55° towards the E and NE and is generally between 2 and 5 cm spaced. In the hinge of the anticline, bedding ( $S_0$ ) dips towards the SE and forms a high angle with  $S_1$  (Fig. 2B and 5A), whereas in its eastern limb, the regional foliation ( $S_1$ ) dips steeper than  $S_0$ . These geometric relationships between bedding and foliation have been used to determine the fold type at great scale (i.e., as it is shown in Fig. 2B).

#### 4.1.2 Thrust zone

The thrust zone consists of a deformation zone affecting both the hanging wall and the footwall. Within the hanging wall, the Devonian host rocks are still recognizable, but the intensity of deformation progressively increases towards the main thrust plane. This deformation consists of a penetrative thrust zone foliation ( $S_2$ ), two generations of stylolites (e1, e2) and three generations of calcite veins (V0, V1a and V1b) (Fig. 3, 6). These structures are described below in chronological order.

The foliation within the thrust zone affecting the Devonian hanging wall ( $S_2$ ) strikes NW-SE and dips 40 – 50° NE, similar to the regional foliation ( $S_1$ ), but it is more closely spaced, generally between 0.2 and 1 cm (Fig. 6A, B). This observation points

Eliminado: , producing changes in the strike direction and dip,

Eliminado: , which

Movido (inserción)[1]

Eliminado: calcite

Eliminado: Cc1a to Cc5

Eliminado: ur

Eliminado: ¶

Con formato: Título 3

Con formato: Color de fuente: Automático

Eliminado: from the hanging wall

Con formato: Fuente: 8 pto

Eliminado: (

Eliminado: are more abundant and

Con formato: Fuente: 10 pto

Eliminado: Deformation in the Devonian protolith (i.e., outside the thrust zone) corresponds to a decametric anticline (Fig. 2B), which has associated an axial plane pervasive regional foliation ( $S_r$ ) concentrated in the pelitic intervals (Fig. 5B). The  $S_r$  has a NW-SE mean orientation, dips 30 to 55° towards the E and NE and is generally between 2 and 5 cm spaced. The angular relationship between the Devonian bedding strike and the regional foliation is oblique and changes to nearly perpendicular when approaching the thrust zone (Fig. 2B).

Con formato: Título 3

Con formato: Inglés (Reino Unido)

Eliminado: the thrust zone affecting

Eliminado: intensity

Eliminado: ( $S_D$ )

Eliminado: in the protolith

out to a progressive transposition of the regional foliation within the thrust zone during thrusting. At mesoscale,  $S_2$  has related shear surfaces (Ci) defining centimetric S-C-type structures, indicating again reverse kinematics (Fig. 6A).

Stylolites e1 have a wave-like shape and trend subparallel to the thrust zone foliation ( $S_2$ ) (Fig. 6B, C). When present, these stylolites are very systematic exhibiting a spacing of 1 – 2 mm (Fig. 6C).

290 The first calcite vein generation (V0), only observed at microscopic scale (Fig. 6B, C), corresponds to up to 1 cm long and less than 1 mm thick veins cemented by blocky to elongated blocky calcite crystals featuring a dark-brown luminescence (cement Cc0). Veins V0 and stylolites e1 are perpendicular between them and show ambiguous crosscutting relationships. These microstructures are concentrated into discontinuous fragments of the Devonian host rocks within the thrust zone. Calcite veins V1a crosscut the previous vein generation (V0) as well as the stylolites e1 and are developed within  $S_2$  surfaces (Fig. 3, 6D).

295 These veins are the most abundant, exhibit a white to brownish color in hand sample and are up to 10 cm long and 1 cm thick. The vein cement (Cc1a) is formed of up to 3-4 mm in size anhedral crystals displaying a blocky texture and a dark brown luminescence (Fig. 6E).

Stylolites e2, more abundant than stylolites e1, are up to 10 cm long and show spacing between 0.5 and 2 cm (Fig. 6D, F). These stylolites mainly correspond to sutured areas developed between the host rock and the calcite veins V1a and between foliation surfaces  $S_2$ .

300 Calcite veins V1b, up to 1 cm long and less than one mm thick, were also identified at microscopic scale (Fig. 6D, F). The vein cement (Cc1b) consists of up to 0.1 mm calcite crystals with a blocky texture and a bright yellow luminescence. These veins postdate the previous V0 and V1a generations and trend perpendicular to stylolites e2.

305 Towards the fault plane, the thrust zone foliation  $S_2$  is progressively more closely-spaced and stylolites e2 become more abundant (showing mm spacing) and exhibit ambiguous cross-cutting relationships with veins V1b (Fig. 6F). The main slip surface corresponds to a discrete plane that contains calcite slickensides (veins V2). The vein cement (Cc2) is milky white in hand sample and consists of up to 3 mm blocky to elongated blocky crystals (Fig. 6G) with a dull to bright orange luminescence (Fig. 6H).

310 Deformation in the footwall is concentrated within the main thrust zone and subsidiary thrust zones and corresponds to the thrust zone foliation ( $S_2$ ) and calcite veins V3 (Fig. 3). This foliation ( $S_2$ ) strikes NW-SE, dips towards the NE and is mm to cm spaced (Fig. 7A). Calcite veins V3 are generally 1 – 2 cm thick and strike NW-SE. They are parallel or locally branch off cutting the  $S_2$  planes in the subsidiary thrust zone (Fig. 7A, B). Outside the thrust zone, veins V3 are locally present but have a NE-SW strike. These veins are mostly less than 1 m long and are spaced between a few cm and 50 cm. The vein cement (Cc3) is made up of a milky white calcite characterized by up to 3 mm long fibrous crystals oriented perpendicular to the vein walls (Fig. 7C). Locally, anhedral blocky crystals ranging in size from 0.1 to 1 mm are also present. This cement displays a bright yellow to bright orange luminescence (Fig. 7D).

Eliminado: D

Eliminado: again

Eliminado: with densities between 5 and 8 stylolites/cm.

Eliminado: D

Eliminado: a

Eliminado: ( $S_{SP}$ )

Eliminado: ¶

Eliminado: e

Eliminado: foliation

### 4.1.3 Footwall

In the footwall, the Stephano-Permian Erill Castell Formation comprises massive, dark-greenish andesitic levels showing a rhythmic magmatic layering (Fig. 7E), which corresponds to a fluidal structure of the host rock. The local presence of pyroclastic and brecciated volcanoclastic levels is also ubiquitous mainly in the lower part of this sequence. Andesites are characterized by a porphyritic texture defined by a dark fine-grained spherulitic matrix partially devitrified and large zoned crystals of plagioclase (Fig. 7F), up to 2 – 3 cm long, and less abundant biotite and hornblende. These mafic phenocrystals are systematically pseudomorphosed by clay minerals and frequently show evidence of oxidation and chloritization. Andesites are affected by E-W striking open joints (J1) dipping indistinctively towards the north and south (Fig. 7E). These joints locally trend parallel to the magmatic layering (Fig. 3).

Finally, as described above, the northern and southern limits of both the Cerc basin and the Estamariu thrust correspond to two Neogene extensional faults, La Seu d'Urgell and the Ortedó fault systems (Fig 1C). These faults are subvertical or steeply dip towards the north. In the northern part, the slip plane of La Seu d'Urgell fault has not been observed and the limit between the Stephano-Permian rocks and the Neogene deposits is not well constrained due to the poor quality of the Neogene outcrops and the presence of Quaternary deposits. In the southern part, the Ortedó fault generates a several meter-thick dark greyish to brown fault zone, characterized by the presence of clay-rich incohesive fault rocks developed at the contact between Stephano-Permian and Upper Ordovician rocks. Related to these main fault systems, mesoscale normal faults commonly affect the andesites within the Cerc basin. These faults are mainly E-W and locally NE-SW, are subvertical and dip indistinctly towards the N and S. Fault planes are locally mineralized with calcite cement (veins V4) and exhibit two striae set generations indicating dip-slip and strike-slip movements (Fig. 8A). The calcite cement (Cc4) consists of up to 2 mm blocky to elongated blocky crystals (Fig. 8B) with a homogeneous dark orange luminescence (Fig. 8C). On the other hand, the main Estamariu thrust zone is locally displaced by shear fractures (Fig. 8D) and a later set of shear bands (Cn) (Fig. 8E), both having an overall NNW-SSE to NNE-SSW strike (Fig. 3) that indicate a minor normal displacement. Shear fractures are locally mineralized with calcite (veins V5). The vein cement consists of a greyish microsparite calcite cement (Cc5) (Fig. 8F-G).

### 4.2 Geochemistry of calcite cements and host rocks

The geochemistry ( $\delta^{18}\text{O}$ ,  $\delta^{13}\text{C}$ ,  $\delta^{18}\text{O}_{\text{fluid}}$ ,  $^{87}\text{Sr}/^{86}\text{Sr}$ ,  $^{143}\text{Nd}/^{144}\text{Nd}$  and elemental composition) and the calculated temperature of precipitation of the different calcite cements Cc1a to Cc5 are described below. Veins V0 and V1b were only observed at microscopic scale and their calcite cement Cc0 and Cc1b could not be sampled to perform these geochemical analyses.

The  $\delta^{18}\text{O}$  and  $\delta^{13}\text{C}$  isotopic composition of the carbonate fraction of the Devonian hanging wall and the different calcite cements (Cc1a to Cc5) are summarized in Table 1 and represented in Fig. 9. The micritic matrix of the Devonian packstone ranges in  $\delta^{18}\text{O}$  values between -10.5 and -8.4 ‰ VPDB and in  $\delta^{13}\text{C}$  values between +1.5 and +2.8 ‰ VPDB, whereas the calcite cements have a broader range of values depending on the cement generation (Fig. 9).

Con formato: Título 3

Con formato: Color de fuente: Automático, Inglés (Reino Unido)

Eliminado: (Sm)

Eliminado: greatly

Eliminado: (V4)

Eliminado: are also frequent affecting

Eliminado: (V5)

Eliminado: (V5)



Calcite cement Cc1a has  $\delta^{18}\text{O}$  values between -11.3 and -10.3 ‰VPDB and  $\delta^{13}\text{C}$  values between +0.8 and +2.1 ‰VPDB. Cc2 is characterized by  $\delta^{18}\text{O}$  values between -14.9 and -12.9 ‰VPDB and  $\delta^{13}\text{C}$  values between -1.2 and +1.5 ‰VPDB. Cc3 has  $\delta^{18}\text{O}$  values between -14.3 and -13.4 ‰VPDB and  $\delta^{13}\text{C}$  values between -9.3 and -6.9 ‰VPDB. Cc4 exhibits  $\delta^{18}\text{O}$  values between -13.8 and -13.4 ‰VPDB and  $\delta^{13}\text{C}$  values between -7.4 and -7.2 ‰VPDB and Cc5 ranges in  $\delta^{18}\text{O}$  between -8.1 and -5.7 ‰VPDB and in  $\delta^{13}\text{C}$  between -8.2 and -3.8 ‰VPDB. The calcite cement Cc1a, precipitated in the fault zone affecting the Devonian hanging wall, has enriched  $\delta^{13}\text{C}$  values, whilst the calcite cement within the fault plane (Cc2) exhibits either negative or positive  $\delta^{13}\text{C}$  values and the calcite cements hosted in the Stephano-Permian andesites (Cc3 to Cc5) have more depleted  $\delta^{13}\text{C}$  values (Fig. 9). In addition, calcite cements show a progressive depletion in  $\delta^{18}\text{O}$  from Cc1a to Cc4, whereas Cc5 displays more enriched  $\delta^{18}\text{O}$  values.

The obtained  $\Delta_{47}$  values from clumped isotope thermometry were converted into temperatures and  $\delta^{18}\text{O}_{\text{fluid}}$  (Table 1 and Fig. 10) using the equation of (Kluge et al., 2015) and (Friedman and O'Neil, 1977), respectively. Cc2 has a  $\Delta_{47}$  of 0.567, which translates into a temperature between 56 and 98 °C and a  $\delta^{18}\text{O}_{\text{fluid}}$  between -6.4 and -0.3 ‰VSMOW. For Cc3,  $\Delta_{47}$  is 0.045 and the calculated T and  $\delta^{18}\text{O}_{\text{fluid}}$  are 127 to 208 °C and +4.3 to +12.1 ‰VSMOW, respectively.  $\Delta_{47}$  for Cc4 is 0.48, which translates into a T and a  $\delta^{18}\text{O}_{\text{fluid}}$  between 102 to 167 °C and +0.9 to +8.1 ‰VSMOW, respectively. For Cc5 the  $\Delta_{47}$  is 0.77 and the calculated T and a  $\delta^{18}\text{O}_{\text{fluid}}$  are between -5 and +3 °C and between -12.4 and -10.1 ‰VSMOW, respectively.

The  $^{87}\text{Sr}/^{86}\text{Sr}$  ratio of calcite cements Cc1a to Cc5 and host rocks are reported in Table 1 and Fig. 11. Devonian limestones from the hanging wall have a  $^{87}\text{Sr}/^{86}\text{Sr}$  ratio of 0.710663, whilst the Stephano-Permian andesites in the footwall exhibit a more radiogenic  $^{87}\text{Sr}/^{86}\text{Sr}$  ratio of 0.743983. The calcite cements have more radiogenic  $^{87}\text{Sr}/^{86}\text{Sr}$  ratios than the Devonian limestones but less radiogenic values than the Stephano-Permian andesites. This ratio ranges from 0.713018 to 0.714092 in Cc1a, is 0.718294 for Cc2, 0.714619 for Cc3, 0.717706 for Cc4 and 0.716923 for Cc5. These results are compared with already published data from synkinematic veins and deformed rocks in other Pyrenean structures developed in the basement and in the sedimentary cover during the Pyrenean compression (Fig. 11). This comparison shows that values obtained in this study are: 1) significantly more radiogenic than the values of marine carbonates and synkinematic veins precipitated in the sedimentary cover (i.e., in the South Pyrenean fault and thrust belt); and, 2) within the same range of values of synkinematic veins and deformed rocks in the Pyrenean basement (Axial Zone).

The analyzed samples for  $^{143}\text{Nd}/^{144}\text{Nd}$  ratios in calcite cements and host rocks are reported in Table 1. However, due to the general low Nd concentrations in most of the analyzed calcite cements and the limited amount of powdered samples that were available, only calcite cement Cc5 and the andesite host rock (footwall) could be measured. Cc5 has a  $^{143}\text{Nd}/^{144}\text{Nd}$  ratio of 0.512178, which is similar to the one of its footwall host rocks, which is 0.512196.

The obtained elemental composition broadly varies among the different calcite cements and related host rocks (Table 2 and Fig. 12). In the thrust zone affecting the hanging wall, calcite cement Cc1a shows a similar trend to that of the Devonian limestones, both having high Sr, intermediate-high Mg and Fe and low Mn contents (Fig. 12). In the main thrust plane, calcite cement Cc2 has low Mg and Fe and intermediate Mn and Sr contents with respect to the other cements. In the footwall, Cc3 and Cc4 have similar elemental composition, characterized by high Mn, intermediate-high Sr, intermediate-low Fe and low

Mg contents. Finally, calcite cement Cc5 follows a similar trend to that of the Stephano-Permian andesites, both having the highest Fe and Mg and the lowest Sr and Mn contents with respect to the other cements and host rocks.

## 5 Discussion

### 400 5.1 Chronology of the observed structures

The Estamariu thrust, affecting basement rocks in the Axial Pyrenees, resulted from a long-lived tectonic history that lasted from Variscan to Neogene times.

The Paleozoic metasedimentary rocks from the Pyrenean basement are broadly affected by multiscale folds and axial plane regional foliation, developed during the main Variscan deformation phase (Bons, 1988; Cochelin et al., 2018; Zwart, 1986).

405 Similar structures, a decametric-scale anticline and pervasive axial plane foliation ( $S_1$ ), are found in the Devonian sequence located in the thrust hanging wall (Fig. 2B) and therefore, we consider them to be developed during the Variscan compression, contemporaneous with the main activity of the Estamariu thrust. Veins V0 are perpendicular to stylolites e1 and show ambiguous crosscutting relationships between them. Thus, they are interpreted as originated coevally. Both microstructures are concentrated into discontinuous fragments of the Devonian host rocks and are therefore considered inherited microstructures likely developed in Variscan times. However, as pointed above, in the study area the Estamariu thrust affects late- to post-Variscan Stephano-Permian andesites, confirming thus its reactivation during the Alpine orogeny. Accordingly, the structures that are strictly attributed to the Alpine reactivation of the thrust are those structures indicating reverse kinematics or associated with a compressional stress, which are found within the thrust zone deformation, at the contact between Devonian and Stephano-Permian units. Contrarily, the magmatic layering and joints J1 are broadly present in the andesitic footwall, outside the thrust zone, and in other Stephano-Permian basins, and are therefore considered inherited fluidal and cooling structures, respectively. For this reason, the calcite veins V1a and V2 (and related cements Cc1a and Cc2), exclusively occurring within the thrust zone, have been associated with the reactivation of the Estamariu thrust. During this period, and associated with ongoing deformation and progressive shortening, stylolites e2 developed as sutured areas between host rock and veins V1a and between foliation surfaces, coevally with the development of veins V1b, as denoted by their crosscutting relationships and orientations.

420 Other structures present in the study area, such as veins V3 to V5 and related cements Cc3 to Cc5, are attributed to the Neogene extension. Veins V3 precipitated in the subsidiary thrust zone developed in the footwall of the Estamariu thrust. These veins strike parallel to the thrust zone foliation ( $S_2$ ) (Fig 7A, B) but are characterized by calcite fibers growing perpendicular to the vein walls and to the foliation surfaces (Fig. 7C), thus evidencing their extensional character. The presence of extensional calcite veins opened along previously formed foliation surfaces in a thrust zone has been reported in other structures in the Pyrenees and has been considered to postdate the thrust activity (Lacroix et al., 2011, 2014). Veins V4 precipitated in subvertical and E-W mesoscale faults affecting the Stephano-Permian andesites (Fig. 8), outside the thrust zone (Fig. 3). The fault orientation and dip and the two striae set generations observed on the fault planes are compatible with the Neogene

**Movido hacia arriba[1]:** U-Pb dating of calcite cements Cc1a to Cc5 failed due to their high lead contents and low uranium contents and therefore, the timing of the different mesostructures and microstructures has been determined by means of crosscutting relationships and microstructural analysis.

**Eliminado:** n.

435 extensional faults that bound the Cerc basin and postdate the Estamariu thrust (Cabrera et al., 1988; Roca, 1996; Saura, 2004).  
440 Calcite cements Cc3 and Cc4, occluding veins V3 and V4, have a similar geochemical composition (Fig. 9 – 12), supporting  
that their precipitation occurred during the same tectonic event and associated with a similar fluid regime (i.e., although these  
cements precipitated in different structures, they are likely contemporaneous). Finally, veins V5 (and related cement Cc5)  
precipitated locally in shear fractures crosscutting and postdating the thrust-related deformation (Fig. 3, 4 and 8D). These veins  
strike parallel to the shear bands (Cn) located in the main thrust zone (Fig. 8E), exhibiting normal slip kinematics, postdating  
the reverse structures and therefore indicating reactivation of the Estamariu thrust during the Neogene extension.

## 5.2 Fluid system during the Alpine reactivation of the Estamariu thrust

As veins V1a and V2 developed during the Alpine reactivation of the Estamariu thrust, the geochemistry of their related calcite  
cements Cc1a and Cc2 record the fluid system during this tectonic event.

445 Calcite cements Cc1a and Cc2 are characterized by high  $^{87}\text{Sr}/^{86}\text{Sr}$  ratios (from 0.713 to 0.714 for Cc1a and 0.718 for Cc2),  
significantly more radiogenic than ratios of Phanerozoic seawater (between 0.7070 and 0.7090) (McArthur et al., 2012). This  
may reflect the incorporation of radiogenic Sr from a fluid derived or interacted with Rb-rich and/or Sr-rich basement rocks  
such as those underlying the Estamariu thrust. Previous studies in the Pyrenees reported similar  $^{87}\text{Sr}/^{86}\text{Sr}$  ratios in Paleozoic  
rocks and in related synkinematic veins (Wayne and McCaig, 1998; McCaig et al., 1995; Banks et al., 1991; Bickle et al.,  
450 1988) (Fig. 11). Contrarily, rocks from the Mesozoic-Cenozoic cover in the Southern Pyrenean fold and thrust belt have similar  
or slightly higher  $^{87}\text{Sr}/^{86}\text{Sr}$  ratios with respect to Phanerozoic seawater (Fig. 11). On the other hand, Cc1a has a narrow range  
of  $\delta^{13}\text{C}$ , between +0.91 and +2 ‰VPDB, consistent with values of the Devonian marine limestones from the hanging wall  
(between +1.54 and +2.75 ‰VPDB) and within the range of Devonian marine carbonate values (Veizer et al., 1999). Likewise,  
the elemental composition of Cc1a follows a similar trend to that of its Devonian host, both having high Mg and Sr and low  
455 Mn contents with respect to the other calcite cements (Fig. 12). These geochemical similarities indicate high fluid-rock  
interaction and buffering of the carbon and elemental composition of the precipitating fluid by the Devonian carbonates  
(Marshall, 1992). Calcite cement Cc2 has slightly lower  $\delta^{13}\text{C}$ , lower Mg and Sr and higher Mn contents with respect to both  
Cc1a and the Devonian host. On the other hand, the temperature and the  $\delta^{18}\text{O}$  composition of the vein-forming fluids, calculated  
from clumped isotope thermometry of Cc2, range between 56 °C and 96 °C and between -6.4 and -0.3 ‰SMOW, respectively.  
460 These values are interpreted as the involvement of heated meteoric fluids. These fluids, which probably heated at depth and  
were enriched in radiogenic Sr during their flow and interaction with basement rocks, flowed preferentially along the thrust  
zone (Fig. 13A), as evidenced by the exclusive presence of calcite in this area, due to the enhanced permeability associated  
with the thrust discontinuity (McCaig et al., 1995; Trinca et al., 2017). As Cc1a and Cc2 precipitated during the same tectonic  
event but in different structural positions within the thrust zone, they likely precipitated from the same fluids, progressively  
465 increasing the fluid-rock interaction from the thrust plane (Cc2) towards the hanging wall (Cc1a). Previous studies already  
reported syntectonic migration of fluids that had interacted at depth with basement rocks before upflowing along thrust zones

Eliminado: c

Eliminado: crystalline

Eliminado: crystalline rocks

Eliminado: developed in the Pyrenean basement

Eliminado: trend

Eliminado: through

Eliminado: crystalline

Eliminado: channelized

Eliminado: channelized

Eliminado: fluid

Eliminado: the

in other structures from the Pyrenean basement, such as the Gavarnie thrust and the related Pic-de-Port-Vieux thrust (McCaig et al., 1995).

### 480 5.3 Fluid system during the Neogene extension

Calcite veins V3 to V5 are attributed to the Neogene extension and the geochemistry of their related calcite cements Cc3 to Cc5 characterize the fluid system during this period.

Cc3 and Cc4 have considerably high  $^{87}\text{Sr}/^{86}\text{Sr}$  ratios (0.714619 and 0.717706, respectively), similar to the ones reported for Cc1a and Cc2 (Fig. 11), indicating interaction with basement rocks. The  $\delta^{18}\text{O}_{\text{fluid}}$  calculated from clumped isotopes, between 485 +4.3 and +12.1 ‰SMOW for Cc3 and between +0.9 and +8.1 ‰SMOW for Cc4, falls within the range of metamorphic and/or formation brines (Taylor, 1987). The  $\delta^{18}\text{O}$ -depleted values of these cements (around -14 ‰VPDB) are due to the high temperatures of the fluids (between 127 °C and 208 °C for Cc3 and between 102 °C and 167 °C for Cc4). Assuming a normal geothermal gradient of 30 °C, these temperatures would have been reached at a minimum depth of 3 – 5 km. However, these veins have never reached such a burial depth, since during the Neogene extension the studied structure acquired its current configuration (Saura, 2004) and was only buried under the Devonian sequence (hanging wall), which has a maximum thickness of several hundred meters (Mey, 1967). This assumption evidences the hydrothermal character of the circulating fluids, which probably migrated rapid enough through normal faults to maintain their high temperatures and to be in thermal disequilibrium with the surrounding rocks. Similarly, the high Mn content of Cc3 and Cc4 (around 7700-8300 and 4000 ppm, respectively), responsible of their bright luminescence (Fig. 7D, 8C), is consistent with hydrothermal waters (Pfeifer et al., 1988; Pomerol, 1983; Pratt et al., 1991). On the other hand, the  $\delta^{13}\text{C}$ -depleted values of these cements are indicative of the influence of organic derived carbon (Cerling, 1984; Vilasi et al., 2006). The most probable source for these low  $\delta^{13}\text{C}$  values is the Silurian black shales that do not crop out in the study area but acted as the main detachment level during the Variscan compression, and locally during the Alpine compression, in the Pyrenean Axial Zone (Mey, 1967). These black shales have significant organic carbon contents (TOC around 2.3%), and around the Gavarnie thrust, they exhibit syntectonic carbonate veins yielding  $\delta^{13}\text{C}$  values between -2 and -8 ‰VPDB (McCaig et al., 1995). Thus, cements Cc3 and Cc4 precipitated from hydrothermal fluids derived and/or equilibrated with basement rocks and expelled through newly formed and reactivated fault zones during deformation (Fig. 13B). The hydrothermal character of the fluids involved in this deformation event, and their relative high temperatures (up to 200°C) could have altered the clumped isotope composition of the previous calcite cement generations (Cc1a and Cc2). Clumped isotopes may be reset by recrystallization and by solid-state isotopic exchange reactions and diffusion within the mineral lattice (Shenton et al., 2015; Stolper and Eiler, 2015). However, in the studied vein samples, there is no evidence of calcite recrystallization (for instance, grain coarsening linked to grain boundary migration). Additionally, this hydrothermal event probably took place during a relatively short period of time (during precipitation of cements Cc3 and Cc4). Solid-state reordering needs temperatures in excess of 120°C during a period of at least 10 Ma, and probably longer (Henkes et al., 2014). Therefore, we conclude that although it is possible, there is little chance for crumpled isotopes of cements Cc1a and Cc2 to have been reset during precipitation of Cc3 and Cc4.

Eliminado: ,

Eliminado: these shales

Eliminado: have

Eliminado: crystalline

515

Finally, the isotopic signature of Cc5, ranging between -8.1 and -5.7 ‰VPDB for  $\delta^{18}\text{O}$  and between -8.2 and -3.8 ‰VPDB for  $\delta^{13}\text{C}$ , indicates a meteoric origin. The similar tendency in the elemental composition of this cement and the Stephano-Permian volcanic rocks, both having the highest Mg and Fe and the lowest Mn and Sr contents with respect to the other cements and host rocks, reveals high fluid-rock interaction with the footwall rocks. The significant water-rock interaction is also demonstrated by the Nd isotopic composition of Cc5 (0.512178), yielding to values of the volcanic host (0.512196). This fact, together with the scarcity and small size of Cc5 veins, indicate that this cement precipitated from percolation of meteoric fluids, which geochemistry was controlled by its volcanic host rock. The  $\delta^{18}\text{O}_{\text{fluid}}$  and the temperature of precipitation calculated from clumped isotopes, ranging between -12.4 and -10.1 ‰SMOW and between -5 and 3°C, respectively. These values corroborate

Con formato: Inglés (Reino Unido)

520

the meteoric origin and may be indicative of high latitude and/or high altitude conditions (Dansgaard, 1964), because the  $\delta^{18}\text{O}_{\text{fluid}}$  and the temperature decrease with elevation (Huyghe et al., 2018). During the Neogene, the study area was approximately at the same latitude as today (Smith, 1996). Studies focused on infiltration of meteoric fluids and subsequent upflowing along La Tet fault during the Neogene extension, have shown that meteoric waters in the area infiltrate at high altitudes, around 2000 m, and low temperatures, around 5°C (Krimissa et al., 1994; Taillefer et al., 2018). On the other hand, the widespread presence of glacial and fluvio-glacial deposits has been reported unconformably overlying the Neogene basin infill and the Variscan rocks from the eastern Axial Pyrenees (Roca, 1996; Turu i Michels and Peña Monné, 2006). These deposits reflect several Quaternary glacial periods in the area, which in turn could have contributed to the low temperature and low  $\delta^{18}\text{O}_{\text{fluid}}$  (Gregory et al., 1989). In any case, precipitation of Cc5 probably took place during the latest stages of extension, after the fluid regime changed from upward fluid migration to percolation of cold meteoric waters, as also occurred in the Barcelona Plain (Catalan Coastal Ranges) (Cantarero et al., 2014).

Eliminado: .

525

Eliminado: than

530

535

In conclusion, the high  $^{87}\text{Sr}/^{86}\text{Sr}$  ratios of the different calcite cements (Cc1a to Cc5) evidence the interaction between the vein-forming fluids and Paleozoic basement rocks with higher radiogenic signature than those of the Mesozoic sedimentary cover (located in the Southern Pyrenees). The geochemical evolution of these cement generations also highlights the progressive change in the fluid regime and composition during successive compressional and extensional tectonic events (Fig. 13). The continuous increase in precipitation temperatures and enrichment in  $\delta^{18}\text{O}_{\text{fluid}}$  from calcite cements Cc1a and Cc2 (Alpine) to cements Cc3 and Cc4 (Neogene) is probably linked to higher extent of fluid-rock interaction with basement rocks. By contrast, during the latest stages of extension, the fluids responsible for precipitation of Cc5 are characterized by lower precipitation temperatures and lighter  $\delta^{18}\text{O}_{\text{fluid}}$ , evidencing a more significant change in the fluid regime and the infiltration of cold meteoric fluids (Fig. 13).

Con formato: No ajustar espacio entre texto latino y asiático, No ajustar espacio entre texto asiático y números

Con formato: Fuente: 10 pto

540

#### 5.4 Influence of Paleozoic basement rocks on fluid chemistry during deformation

Con formato: Fuente: (Predeterminada) Times, Inglés (Reino Unido)

Eliminado: crystalline

545

In this section, we assess the influence of basement rocks on the chemistry of fluids during deformation. As pointed above, previous studies constrained the relationships between deformation and fluid migration in other structures from the Mesozoic and Cenozoic cover (Cruset et al., 2016, 2018; Travé et al., 1997, 2000), and to a lesser extent, from the Paleozoic basement

Eliminado: The aim of this study was to provide insights into the behavior and evolution of fluids circulating through a long-lived thrust, and to determine

Eliminado: fluid

555 (Banks et al., 1991; McCaig et al., 1995, 2000b; Wayne and McCaig, 1998). The comparison between these studies and the new data provided in this contribution evidences that fluids migrating through basement or cover units have a different geochemical signature. This signature is recorded in the vein cements, particularly in their  $^{87}\text{Sr}/^{86}\text{Sr}$  ratios. Accordingly, the high  $^{87}\text{Sr}/^{86}\text{Sr}$  ratios (0.713 to 0.718) of the analyzed calcite cements, originated during successive compressional and extensional tectonic events, indicate that regardless of the origin of the fluids and the tectonic context, basement rocks have a significant influence on the fluid chemistry. This implies that cements precipitated from fluids that have circulated through basement rocks have significantly high  $^{87}\text{Sr}/^{86}\text{Sr}$  ratios ( $> 0.710$ ) (Fig. 11), reflecting the interaction between the vein-forming fluids and rocks with a high radiogenic signature. Similar high radiogenic  $^{87}\text{Sr}/^{86}\text{Sr}$  ratios have also been attributed to basement-derived fluids in the Glarus nappe (Swiss Alps) (Burkhard et al., 1992). By contrast, vein cements precipitated from fluids that have circulated through the Mesozoic-Cenozoic sedimentary cover in the Pyrenees (i.e., through younger rocks with a different radiogenic signature) have significantly lower  $^{87}\text{Sr}/^{86}\text{Sr}$  ratios ( $< 0.710$ ). Such lower values may be similar to Phanerozoic seawater values, evidencing interaction between the vein-forming fluids and marine carbonate units, or higher, evidencing interaction with siliciclastic rocks (Cruset et al., 2018; Travé et al., 2007). A previous study, focused on fluid flow along the Gavarnie thrust in the central-western Axial Pyrenees, used this limit value ( $^{87}\text{Sr}/^{86}\text{Sr} = 0.710$ ) to differentiate between the unaltered limestone protolith and the Cretaceous thrust-related carbonate mylonite affected by fluids carrying radiogenic Sr (McCaig et al., 1995).

Eliminado: means

Eliminado: crystalline

Eliminado: with Rb-rich source

### 5.5 Fluid flow at regional scale: the NE part of the Iberian Peninsula during the Neogene extension

During the late Oligocene to middle Miocene, the opening of the NW Mediterranean Sea was responsible for the development of a complex ENE-WSW to NE-SW extensional fault system in the NE part of the Iberian Peninsula (Roca, 1996; Roca and Guimerà, 1992; Vergés et al., 2002). In the eastern Axial Pyrenees, La Tet fault is the main Neogene structure and has associated major E-W extensional faults, such as the Ortedó and La Seu d'Urgell faults, which crosscut the Alpine structures (e.g., the reactivation of the Estamariu thrust) and delimitate the Cerc basin (Fig. 1). Within this basin, E-W mesoscale normal faults (and related veins V4) also developed during this period and previously formed weakness surfaces were reopened (i.e., the thrust zone foliation associated with the Estamariu thrust, veins V3). During this episode, calcite cements Cc3 and Cc4 precipitated from hydrothermal fluids (temperatures between 102 and 208 °C) that interacted at depth with basement rocks before ascending through newly formed fault zones and reactivated structures. These interpretations are consistent with the presence of several hydrothermal springs (temperatures of 29 °C to 73 °C) currently upwelling aligned along La Tet fault and related Neogene deformation in the Pyrenean Axial Zone (Krimissa et al., 1994; Taillefer et al., 2017, 2018). Several studies indicate the origin of these hot water springs as meteoric fluids, infiltrated at high-elevated reliefs, above 2000 m, warmed at great depths by normal geothermal gradients, and migrated upwards along permeability anisotropies related to fault zones (Taillefer et al., 2017, 2018). The geochemical analysis of these springs, and in particular their high radiogenic  $^{87}\text{Sr}/^{86}\text{Sr}$  ratios, ranging between 0.715 and 0.730, according to French Geological Survey reports (Caballero et al., 2012), are within the range of values obtained in this study and also accounts for interaction between circulating fluids and basement lithologies. Studies

Eliminado: derived

Eliminado: crystalline

Eliminado: crystalline

Eliminado: rocks

595 based on numerical models suggest that La Tet fault and the involved **basement** rocks are still permeable down to 3 km depth (Taillefer et al., 2017, 2018), although the fault has been dormant since the Mio-Pliocene (Goula et al., 1999). These authors also suggest that the footwall topography is the major factor controlling the infiltration of meteoric fluids and the recharge of the hydrothermal system. The topography, which induces high hydraulic gradients and produces fluid advection, controls the circulation depth and therefore, the maximum temperature reached by the migrating fluids (Taillefer et al., 2017).

Eliminado: crystalline

600 A similar geological context and fluid regime evolution to that explained above is found in the Barcelona Plain and the Vallès Basin, located in the northeast part of the Catalan Coastal Ranges (CCR) (Fig. 1A). Consequently, the comparison between both geological contexts allows us to give insights into the fluid circulation in extensional basins at regional scale (in the NE part of Iberia). In these locations of the CCR, the main fault system associated with the Neogene extension acted as conduits for hydrothermal fluid circulation at temperatures between 130 and 150 °C during synkinematic periods (Cantarero et al., 2014; Cardellach et al., 2003), and is also responsible for the present-day circulation of hot water springs up to 70 °C (Carmona et al., 2000; Fernández and Banda, 1990). In both cases, fluids would have been topographically driven from elevated areas to great depths (Cantarero et al., 2014), where they circulated through **basement** rocks, acquiring high  $^{87}\text{Sr}/^{86}\text{Sr}$  ratios ( $> 0.712$ ) and high temperatures (Cardellach et al., 2003) before ascending through fault discontinuities. However, in the Penedès basin,

Eliminado: crystalline

610 which corresponds to the southwestern termination of the Neogene structure in the CCR, **basement lithologies** do not crop out and the extensional faults only involve Neogene deposits filling the basin and a Mesozoic sedimentary substrate. In this location, the main fault system acted as conduits for several episodes of meteoric fluids percolation during the Neogene extension and evidence of hydrothermal fluid circulation has not been reported in the area (Travé and Calvet, 2001; Travé et al., 1998; Baqués et al., 2012, 2010). This fact agrees with previous studies that highlight that hydrothermal activity, and in particular the occurrence of hot water springs in the Pyrenees and in the CCR, is preferably concentrated in basement rocks, which constitute the elevated footwall of the main extensional fault systems (Taillefer et al., 2017; Carmona et al., 2000).

Eliminado: crystalline

Eliminado: rocks

615 All these observations indicate that the fluids responsible for precipitation of synkinematic cements during Neogene times in the eastern Axial Pyrenees and in the northeast part of the CCR, and fluids currently flowing through Neogene extensional faults in both places are hydrothermal and **are sourced and/or interacted with similar basement rocks**. This evidences an open fluid system in the NE part of the Iberian Peninsula associated with the Neogene extensional deformation. Accordingly, this extensional fault system has acted as a conduit for **circulation of hot fluids in Neogene times and in the present**. This fault-controlled fluid flow could have been continuous through time or could be related to intermittent pulses. Fault control on upflowing of hot fluids along fault systems is a common process in different geological settings and has been reported in the Great Basin, USA (Faulds et al., 2010; Nelson et al., 2006), in the Western Turkey (Faulds et al., 2010), in the Southern Canadian Cordillera (Grasby and Hutcheon, 2001) **and in the southern Tuscany, Italy (Liotta et al., 2010)**.

Eliminado:

Eliminado: have crystalline basement rocks as a common reservoir

Eliminado: long-term

Eliminado: from

Eliminado: to

Eliminado: long-term

Eliminado: , in the Basin and Range Province (Nelson et al., 2006)

## 6 Conclusions

The Estamariu thrust, in the Pyrenean Axial Zone, resulted from a multistage Variscan to Neogene tectonic evolution. Our data, combining structural and petrological observations with geochemical analyses of synkinematic calcite veins and host rocks, provide a structural and diagenetic framework that constrains the fault-fluid system evolution and assesses the relationships between deformation and fluid migration in the Paleozoic Pyrenean basement. In the study area, the Variscan Estamariu thrust places a Devonian pre-Variscan unit against a Stephano-Permian late to post-Variscan sequence and therefore, the structures present within the thrust zone, affecting both sequences, are attributed to the Alpine and subsequent Neogene reactivation of the thrust. During the Alpine compression, the reactivation of the thrust resulted in the transposition of the Variscan regional foliation within the thrust zone and in the formation of a subsidiary thrust zone affecting the andesites in the footwall. During this period, meteoric fluids interacted with basement rocks and migrated upwards along the thrust and related structures at temperatures between 56 and 98 °C. These fluids progressively increased the fluid-rock interaction from the thrust plane towards the hanging wall. During the Neogene extension, the Estamariu thrust was reactivated and normal faults and shear fractures were formed. These structures allowed basement-derived fluids to flow upwards through reactivated and newly formed fault zones at temperatures up to 208 °C. Finally, during the latest to post stages of extension and uplift of the structure, the fluid regime changed to percolation of low temperature meteoric fluids that were buffered by the volcanic host rocks.

The comparison between our results and previously published data allows us to provide insights into the fluid characteristics and fluid regime at regional scale. On the one hand, the influence of basement rocks on the fluid chemistry during deformation in the Pyrenees has been assessed. In this sense, regardless the fluid origin and the tectonic context, the fluids that have interacted with basement rocks have a significantly higher  $^{87}\text{Sr}/^{86}\text{Sr}$  ratio ( $> 0.710$ ) with respect to those that have circulated through the sedimentary cover ( $< 0.710$ ). On the other hand, a similar fluid regime associated with the Neogene extension in the NE part of the Iberian Peninsula (including the eastern Pyrenees and the northeastern part of the Catalan Coastal Ranges) has been observed. In both settings, the extensional deformation structures have acted as conduits for fluid migration in Neogene times and in the present. Fluids migrating during this period are hydrothermal and have interacted with basement rocks before ascending through fault zones and related structures.

### Data availability

The data used in this study is included within the manuscript.

### Author contributions

Conceptualization, DM-L,GA, DC, IC; AT; data curation, DM-L; formal analysis, all authors; funding acquisition, AT; investigation and methodology, all authors; writing-original draft preparation, DM-L; writing-review and editing, all authors.

Eliminado: the crystalline

Eliminado: crystalline

Eliminado: long-term

Eliminado: from

Eliminado: to

Eliminado: M

Eliminado: fluids

Eliminado: crystalline

Con formato: Normal



### **Competing interest**

The authors declare that they have no conflict of interest.

Con formato: Normal

### **Acknowledgments**

We acknowledge the constructive comments from Owen Callahan and Brice Lacroix, who helped to improve the quality of the manuscript, as well as the editorial guidance of Randolph Williams. We also thank Josep Maria Casas, from the Universitat de Barcelona, for showing us the location of the studied outcrops. Carbon and oxygen isotopic analyses were carried out at “Centre Científics i Tecnològics” of the Universitat de Barcelona. Strontium and Neodymium analyses were performed at the “CAI de Geocronología y Geoquímica Isotópica” of the Universidad Complutense de Madrid. The Elemental composition was analysed at the Geochemistry Facility of labGEOTOP of Geosciences Barcelona (GEO3BCN-CSIC). Clumped isotope thermometry was carried out at the Imperial College London. This research was carried out within the framework of DGICYT Spanish Project PGC2018-093903-B-C22 (Ministerio de Ciencia, Innovación y Universidades / Agencia Estatal de Investigación / Fondo Europeo de Desarrollo Regional, Unión Europea) and the Grup Consolidat de Recerca “Geologia Sedimentària” (2017-SGR- 824). The PhD research of DM-L is supported by the FPI2016 (BES-2016-077214) Spanish program from MINECO.

Eliminado: the Institute of Earth Sciences Jaume Almera

Eliminado: ICTJA

Con formato: Español (España)

### **References**

- Arndt, M., Virgo, S., Cox, S. F. and Urai, J. L.: Changes in fluid pathways in a calcite vein mesh (Natih Formation, Oman Mountains): insights from stable isotopes, *Geofluids*, 14(4), 391–418, doi:10.1111/gfl.12083, 2014.
- Banks, D., Da Vies, G., Yardley, B. W., McCaig, A. and Grant, N.: The chemistry of brines from an Alpine thrust system in the Central Pyrenees: An application of fluid inclusion analysis to the study of fluid behaviour in orogenesis, *Geochim. Cosmochim. Acta*, 55(4), 1021–1030, doi:10.1016/0016-7037(91)90160-7, 1991.
- Baques, V., Trave, A., Roca, E., Marin, M. and Cantarero, I.: Geofluid behaviour in successive extensional and compressional events: a case study from the southwestern end of the Valles-Penedes Fault (Catalan Coastal Ranges, NE Spain), *Pet. Geosci.*, 18(1), 17–31, doi:10.1144/1354-079311-017, 2012.
- Barker, S. L. L. and Cox, S. F.: Evolution of fluid chemistry and fluid-flow pathways during folding and faulting: an example from Taemas, NSW, Australia, *Geol. Soc. London, Spec. Publ.*, 359(1), 203–227, doi:10.1144/SP359.12, 2011.
- Barker, S. L. L., Bennett, V. C., Cox, S. F., Norman, M. D. and Gagan, M. K.: Sm–Nd, Sr, C and O isotope systematics in hydrothermal calcite–fluorite veins: Implications for fluid–rock reaction and geochronology, *Chem. Geol.*, 268(1–2), 58–66, doi:10.1016/j.chemgeo.2009.07.009, 2009.
- Beaudoin, N., Bellahsen, N., Lacombe, O., Emmanuel, L. and Pironon, J.: Crustal-scale fluid flow during the tectonic evolution

- 705 of the Bighorn Basin (Wyoming, USA), *Basin Res.*, 26(3), 403–435, doi:10.1111/bre.12032, 2014.
- Beaudoin, N., Huyghe, D., Bellahsen, N., Lacombe, O., Emmanuel, L., Mouthereau, F. and Ouahnon, L.: Fluid systems and fracture development during syn-depositional fold growth: An example from the Pico del Aguila anticline, Sierras Exteriores, southern Pyrenees, Spain, *J. Struct. Geol.*, 70, 23–38, doi:10.1016/j.jsg.2014.11.003, 2015.
- Bickle, M. J., Wickham, S. M., Chapman, H. J. and Taylor, H. P.: A strontium, neodymium and oxygen isotope study of hydrothermal metamorphism and crustal anatexis in the Trois Seigneurs Massif, Pyrenees, France, *Contrib. to Mineral. Petrol.*, 100(4), 399–417, doi:10.1007/BF00371371, 1988.
- Bons, A.: Intracrystalline deformation and slaty cleavage development in very low-grade slates from the Central Pyrenees, *Geol. Ultraiectina*, 1988.
- Breesch, L., Swennen, R. and Vincent, B.: Fluid flow reconstruction in hanging and footwall carbonates: Compartmentalization by Cenozoic reverse faulting in the Northern Oman Mountains (UAE), *Mar. Pet. Geol.*, 26(1), 113–128, doi:10.1016/j.marpetgeo.2007.10.004, 2009.
- Burkhard, M., Kerrich, R., Maas, R. and Fyfe, W. S.: Stable and Sr-isotope evidence for fluid advection during thrusting of the glarus nappe (swiss alps), *Contrib. to Mineral. Petrol.*, 112(2–3), 293–311, doi:10.1007/BF00310462, 1992.
- Caballero, Y., Gironde, C. and Le Goff, E.: Ressource en eau thermale de la station d' Amélie-les-Bains. Etat des lieux. Rapport BRGM/RP-60618-FR., 2012.
- Cabrera, L., Roca, E. and Santanach, P.: Basin formation at the end of a strike-slip fault: the Cerdanya Basin (eastern Pyrenees), *J. Geol. Soc. London.*, 145(2), 261–268, doi:10.1144/gsjgs.145.2.0261, 1988.
- Cantarero, I., Travé, A., Alías, G. and Baqués, V.: Polyphasic hydrothermal and meteoric fluid regimes during the growth of a segmented fault involving crystalline and carbonate rocks (Barcelona Plain, NE Spain), *Geofluids*, 14(1), 20–44, doi:10.1111/gfl.12021, 2014.
- 725 Cantarero, I., Alías, G., Cruset, D., Carola, E., Lanari, P. and Travé, A.: Fluid composition changes in crystalline basement rocks from ductile to brittle regimes, *Glob. Planet. Change*, 171(March), 273–292, doi:10.1016/j.gloplacha.2018.03.002, 2018.
- Cardellach, E., Canals, À. and Grandia, F.: Recurrent hydrothermal activity induced by successive extensional episodes: the case of the Berta F–(Pb–Zn) vein system (NE Spain), *Ore Geol. Rev.*, 22(1–2), 133–141, doi:10.1016/S0169-1368(02)00112-9, 2003.
- 730 Carmona, J. M., Bitzer, K., López, E. and Bouazza, M.: Isotopic composition and origin of geothermal waters at Caldetes (Maresme-Barcelona), *J. Geochemical Explor.*, 69–70, 441–447, doi:10.1016/S0375-6742(00)00127-8, 2000.
- Casas, J. M., Domingo, F., Poblet, J. and Soler, A.: On the role of the Hercynian and Alpine thrusts in the Upper Paleozoic rocks of the Central and Eastern Pyrenees, *Geodin. Acta*, 3(2), 135–147, doi:10.1080/09853111.1989.11105181, 1989.
- 735 Cerling, T. E.: The stable isotopic composition of modern soil carbonate and its relationship to climate, *Earth Planet. Sci. Lett.*, doi:10.1016/0012-821X(84)90089-X, 1984.
- Choukroune, P.: The Eors Pyrenean deep seismic profile reflection data and the overall structure of an orogenic belt, *Tectonics*, doi:10.1029/TC008i001p00023, 1989.

- Cochelin, B., Lemirre, B., Denèle, Y., de Saint Blanquat, M., Lahfid, A. and Duchêne, S.: Structural inheritance in the Central Pyrenees: the Variscan to Alpine tectonometamorphic evolution of the Axial Zone, *J. Geol. Soc. London.*, 175(2), 336–351, doi:10.1144/jgs2017-066, 2018.
- Cox, S. F.: Structural and isotopic constraints on fluid flow regimes and fluid pathways during upper crustal deformation: An example from the Taemas area of the Lachlan Orogen, SE Australia, *J. Geophys. Res.*, 112(B8), B08208, doi:10.1029/2006JB004734, 2007.
- Crespo-Blanc, A., Masson, H., Sharp, Z., Cosca, M. and Hunziker, J.: A stable and  $40\text{Ar}/39\text{Ar}$  isotope study of a major thrust in the Helvetic nappes (Swiss Alps): Evidence for fluid flow and constraints on nappe kinematics, *Geol. Soc. Am. Bull.*, 107(10), 1129–1144, doi:10.1130/0016-7606(1995)107<1129:ASAAA1>2.3.CO;2, 1995.
- Crognier, N., Hoareau, G., Aubourg, C., Dubois, M., Lacroix, B., Branellec, M., Callot, J. P. and Vennemann, T.: Syn-orogenic fluid flow in the Jaca basin (south Pyrenean fold and thrust belt) from fracture and vein analyses, *Basin Res.*, 30(2), 187–216, doi:10.1111/bre.12249, 2018.
- Cruset, D.: Sequential fluid migration along a fold and thrust belt SE pyrenees from late Cretaceous to Oligocene, PhD thesis, Universitat de Barcelona., 2019.
- Cruset, D., Cantarero, I., Travé, A., Vergés, J. and John, C. M.: Crestal graben fluid evolution during growth of the Puig-reig anticline (South Pyrenean fold and thrust belt), *J. Geodyn.*, 101, 30–50, doi:10.1016/j.jog.2016.05.004, 2016.
- Cruset, D., Cantarero, I., Vergés, J., John, C. M., Muñoz-López, D. and Travé, A.: Changes in fluid regime in syn-orogenic sediments during the growth of the south Pyrenean fold and thrust belt, *Glob. Planet. Change*, 171(October 2017), 207–224, doi:10.1016/j.gloplacha.2017.11.001, 2018.
- Cruset, D., Cantarero, I., Benedicto, A., John, C. M., Vergés, J., Albert, R., Gerdes, A. and Travé, A.: From hydroplastic to brittle deformation: Controls on fluid flow in fold and thrust belts. Insights from the Lower Pedraforca thrust sheet (SE Pyrenees), *Mar. Pet. Geol.*, 120, 104517, doi:10.1016/j.marpetgeo.2020.104517, 2020a.
- Cruset, D., Vergés, J., Albert, R., Gerdes, A., Benedicto, A., Cantarero, I. and Travé, A.: Quantifying deformation processes in the SE Pyrenees using U-Pb dating of fracture-filling calcites, *J. Geol. Soc. London.*, (August), jgs2020-014, doi:10.1144/jgs2020-014, 2020b.
- Dansgaard, W.: Stable isotopes in precipitation, *Tellus*, doi:10.3402/tellusa.v16i4.8993, 1964.
- Dennis, K. J., Affek, H. P., Passey, B. H., Schrag, D. P. and Eiler, J. M.: Defining an absolute reference frame for ‘clumped’ isotope studies of  $\text{CO}_2$ , *Geochim. Cosmochim. Acta*, 75(22), 7117–7131, doi:10.1016/j.gca.2011.09.025, 2011.
- Dewever, B., Swennen, R. and Breesch, L.: Fluid flow compartmentalization in the Sicilian fold and thrust belt: Implications for the regional aqueous fluid flow and oil migration history, *Tectonophysics*, 591, 194–209, doi:10.1016/j.tecto.2011.08.009, 2013.
- Faulds, J., Coolbaugh, M., Bouchot, V., Moeck, I., Oğuz, K. and Cedex, O.: Characterizing Structural Controls of Geothermal Reservoirs in the Great Basin , USA , and Western Turkey : Developing Successful Exploration Strategies in Extended Terranes, *World, C(2010)*, 25–29, 2010.

- Fay-Gomord, O., Allanic, C., Verbiest, M., Honlet, R., Champenois, F., Bonifacie, M., Chaduteau, C., Wouters, S., Muchez, P., Lasseur, E. and Swennen, R.: Understanding Fluid Flow during Tectonic Reactivation: An Example from the Flamborough Head Chalk Outcrop (UK), *Geofluids*, 2018, 1–17, doi:10.1155/2018/9352143, 2018.
- 775 Fernández, M. and Banda, E.: Geothermal anomalies in the Valles-Penedes Graben Master Fault: Convection through the Horst as a possible mechanism, *J. Geophys. Res.*, 95(B4), 4887, doi:10.1029/JB095iB04p04887, 1990.
- Fitz-Diaz, E., Hudleston, P., Siebenaller, L., Kirschner, D., Camprubi, A., Tolson, G. and Puig, T. P.: Insights into fluid flow and water-rock interaction during deformation of carbonate sequences in the Mexican fold-thrust belt, *J. Struct. Geol.*, 33(8), 1237–1253, doi:10.1016/j.jsg.2011.05.009, 2011.
- 780 Foden, J.: Sr-isotopic evidence for Late Neoproterozoic rifting in the Adelaide Geosyncline at 586 Ma: implications for a Cu ore forming fluid flux, *Precambrian Res.*, 106(3–4), 291–308, doi:10.1016/S0301-9268(00)00132-7, 2001.
- Fontana, S., Nader, F. H., Morad, S., Ceriani, A., Al-Aasm, I. S., Daniel, J. M. and Mengus, J. M.: Fluid-rock interactions associated with regional tectonics and basin evolution, *Sedimentology*, 61(3), 660–690, doi:10.1111/sed.12073, 2014.
- 785 Friedman, I. and O’Neil, J. R.: Compilation of stable isotope fractionation factors of geochemical interest, in *Professional Papers.*, 1977.
- García-Sansegundo, J., Poblet, J., Alonso, J. L. and Clariana, P.: Hinterland-foreland zonation of the Variscan orogen in the Central Pyrenees: comparison with the northern part of the Iberian Variscan Massif, *Geol. Soc. London, Spec. Publ.*, 349(1), 169–184, doi:10.1144/SP349.9, 2011.
- 790 Gasparrini, M., Ruggieri, G. and Brogi, A.: Diagenesis versus hydrothermalism and fluid-rock interaction within the Tuscan Nappe of the Monte Amiata CO<sub>2</sub>-rich geothermal area (Italy), *Geofluids*, 13(2), 159–179, doi:10.1111/gfl.12025, 2013.
- Gomez-Rivas, E., Bons, P. D., Koehn, D., Urai, J. L., Arndt, M., Virgo, S., Laurich, B., Zeeb, C., Stark, L. and Blum, P.: The Jabal Akhdar dome in the Oman Mountains: Evolution of a dynamic fracture system, *Am. J. Sci.*, 314(7), 1104–1139, doi:10.2475/07.2014.02, 2014.
- 795 Goula, X., Olivera, C., Fleta, J., Grellet, B., Lindo, R., Rivera, L. A., Cisternas, A. and Carbon, D.: Present and recent stress regime in the eastern part of the Pyrenees, *Tectonophysics*, doi:10.1016/S0040-1951(99)00120-1, 1999.
- Grant, N. T., Banks, D. A., McCaig, A. M. and Yardley, B. W. D.: Chemistry, source, and behavior of fluids involved in alpine thrusting of the Central Pyrenees, *J. Geophys. Res.*, 95(B6), 9123, doi:10.1029/JB095iB06p09123, 1990.
- Grasby, S. E. and Hutcheon, I.: Controls on the distribution of thermal springs in the southern Canadian Cordillera, *Can. J. Earth Sci.*, 38(3), 427–440, doi:10.1139/cjes-38-3-427, 2001.
- 800 Gregory, R. T., Douthitt, C. B., Duddy, I. R., Rich, P. V. and Rich, T. H.: Oxygen isotopic composition of carbonate concretions from the lower Cretaceous of Victoria, Australia: implications for the evolution of meteoric waters on the Australian continent in a paleopolar environment, *Earth Planet. Sci. Lett.*, 92(1), 27–42, doi:10.1016/0012-821X(89)90018-6, 1989.
- Guo, W., Mosenfelder, J. L., Goddard, W. A. and Eiler, J. M.: Isotopic fractionations associated with phosphoric acid digestion of carbonate minerals: Insights from first-principles theoretical modeling and clumped isotope measurements, *Geochim. Cosmochim. Acta*, 73(24), 7203–7225, doi:10.1016/j.gca.2009.05.071, 2009.
- 805

- Hartevelt, J. J. A.: Geology of the Upper Segre and Valira Valleys, Central Pyrenees, Andorra, Spain, Geological Institute, Leiden University, Leiden, 1970.
- Henderson, I. H. C. and McCaig, A. M.: Fluid pressure and salinity variations in shear zone-related veins, central Pyrenees, France: Implications for the fault-valve model, *Tectonophysics*, 262(1–4), 321–348, doi:10.1016/0040-1951(96)00018-2, 1996.
- Henkes, G. A., Passey, B. H., Grossman, E. L., Shenton, B. J., Pérez-Huerta, A. and Yancey, T. E.: Temperature limits for preservation of primary calcite clumped isotope paleotemperatures, *Geochim. Cosmochim. Acta*, 139, 362–382, doi:10.1016/j.gca.2014.04.040, 2014.
- 815 Huntington, K. W., Eiler, J. M., Affek, H. P., Guo, W., Bonifacie, M., Yeung, L. Y., Thiagarajan, N., Passey, B., Tripathi, A., Daëron, M. and Came, R.: Methods and limitations of “clumped” CO<sub>2</sub> isotope ( $\Delta_{47}$ ) analysis by gas-source isotope ratiomass spectrometry, *J. Mass Spectrom.*, 44(9), 1318–1329, doi:10.1002/jms.1614, 2009.
- Huyghe, D., Mouthereau, F., Sébilo, M., Vacherat, A., Ségalen, L., Richard, P., Biron, P. and Bariac, T.: Impact of topography, climate and moisture sources on isotopic composition ( $\delta^{18}\text{O}$  &  $\delta\text{D}$ ) of rivers in the Pyrenees: Implications for topographic reconstructions in small orogens, *Earth Planet. Sci. Lett.*, 484(January), 370–384, doi:10.1016/j.epsl.2017.12.035, 2018.
- 820 John, C. M. and Bowen, D.: Community software for challenging isotope analysis: First applications of ‘Easotope’ to clumped isotopes, *Rapid Commun. Mass Spectrom.*, 30(21), 2285–2300, doi:10.1002/rcm.7720, 2016.
- Kim, S.-T. and O’Neil, J. R.: Equilibrium and nonequilibrium oxygen isotope effects in synthetic carbonates, *Geochim. Cosmochim. Acta*, 61(16), 3461–3475, doi:10.1016/S0016-7037(97)00169-5, 1997.
- 825 Kluge, T., John, C. M., Jourdan, A.-L., Davis, S. and Crawshaw, J.: Laboratory calibration of the calcium carbonate clumped isotope thermometer in the 25–250 °C temperature range, *Geochim. Cosmochim. Acta*, 157, 213–227, doi:10.1016/j.gca.2015.02.028, 2015.
- Krimissa, M., Chery, L., Fouillac, C. and Michelot, J. L.: Origin and Recharge Altitude of the Thermo-Mineral Waters of the Eastern Pyrenees, *Isot. Isot. Environ. Heal. Stud.*, 30(4), 317–331, doi:10.1080/00211919408046747, 1994.
- 830 Lacroix, B., Buatier, M., Labaume, P., Travé, A., Dubois, M., Charpentier, D., Ventalon, S. and Convert-Gaubier, D.: Microtectonic and geochemical characterization of thrusting in a foreland basin: Example of the South-Pyrenean orogenic wedge (Spain), *J. Struct. Geol.*, 33(9), 1359–1377, doi:10.1016/j.jsg.2011.06.006, 2011.
- Lacroix, B., Travé, A., Buatier, M., Labaume, P., Vennemann, T. and Dubois, M.: Syntectonic fluid-flow along thrust faults: Example of the South-Pyrenean fold-and-thrust belt, *Mar. Pet. Geol.*, 49, 84–98, doi:10.1016/j.marpetgeo.2013.09.005, 2014.
- 835 Lacroix, B., Baumgartner, L. P., Bouvier, A.-S., Kempton, P. D. and Vennemann, T.: Multi fluid-flow record during episodic mode I opening: A microstructural and SIMS study (Cotiella Thrust Fault, Pyrenees), *Earth Planet. Sci. Lett.*, 503, 37–46, doi:10.1016/j.epsl.2018.09.016, 2018.
- Lago, M., Arranz, E., Pocoví, A., Galé, C. and Gil-Imaz, A.: Permian magmatism and basin dynamics in the southern Pyrenees: a record of the transition from late Variscan transtension to early Alpine extension, *Geol. Soc. London, Spec. Publ.*, 223(1), 439–464, doi:10.1144/GSL.SP.2004.223.01.19, 2004.
- 840

- Liotta, D., Ruggieri, G., Brogi, A., Fulignati, P., Dini, A. and Nardini, I.: Migration of geothermal fluids in extensional terrains: the ore deposits of the Boccheggiano-Montieri area (southern Tuscany, Italy), *Int. J. Earth Sci.*, 99(3), 623–644, doi:10.1007/s00531-008-0411-3, 2010.
- Marshall, J. D.: Climatic and oceanographic isotopic signals from the carbonate rock record and their preservation, *Geol. Mag.*,  
845 doi:10.1017/S0016756800008244, 1992.
- Martí, J.: Caldera-like structures related to Permo-Carboniferous volcanism of the Catalan Pyrenees (NE Spain), *J. Volcanol. Geotherm. Res.*, 45(3–4), 173–186, doi:10.1016/0377-0273(91)90057-7, 1991.
- Martí, J.: Genesis of crystal-rich volcanoclastic facies in the Permian red beds of the Central Pyrenees (NE Spain), *Sediment. Geol.*, 106(1–2), 1–19, doi:10.1016/0037-0738(95)00143-3, 1996.
- 850 Martín-Martín, J. D., Travé, A., Gomez-Rivas, E., Salas, R., Sizun, J. P., Vergés, J., Corbella, M., Stafford, S. L. and Alfonso, P.: Fault-controlled and stratobound dolostones in the Late Aptian-earliest Albian Benassal Formation (Maestrat Basin, E Spain): Petrology and geochemistry constrains, *Mar. Pet. Geol.*, 65, doi:10.1016/j.marpetgeo.2015.03.019, 2015.
- Martínez Casas, L. F., Travé, A., Cruset, D. and Muñoz-López, D.: The Montagut Fault System: Geometry and Fluid Flow Analysis (Southern Pyrennes, Spain), in *Petrogenesis and Exploration of the Earth's Interior. Proceedings of the 1st Springer*  
855 *Conference of the Arabian Journal of Geosciences (CAJG-1), Tunisia 2018*, pp. 211–214., 2019.
- Matte, P.: Accretionary history and crustal evolution of the Variscan belt in Western Europe, *Tectonophysics*, doi:10.1016/0040-1951(91)90328-P, 1991.
- McArthur, J. M., Howarth, R. J. and Shields, G. A.: Strontium Isotope Stratigraphy, in *The Geologic Time Scale*, vol. 1–2, pp. 127–144, Elsevier., 2012.
- 860 McCaig, A. ., Tritlla, J. and Banks, D. .: Fluid mixing and recycling during Pyrenean thrusting: evidence from fluid inclusion halogen ratios, *Geochim. Cosmochim. Acta*, 64(19), 3395–3412, doi:10.1016/S0016-7037(00)00437-3, 2000a.
- McCaig, A. M., Wayne, D. M., Marshall, J. D., Banks, D. and Henderson, I.: Isotopic and fluid inclusion studies of fluid movement along the Gavarnie Thrust, central Pyrenees; reaction fronts in carbonate mylonites, *Am. J. Sci.*, 295(3), 309–343, doi:10.2475/ajs.295.3.309, 1995.
- 865 McCaig, A. M., Wayne, D. M. and Rosenbaum, J. M.: Fluid expulsion and dilatancy pumping during thrusting in the Pyrenees: Pb and Sr isotope evidence, *Geol. Soc. Am. Bull.*, 112(8), 1199–1208, doi:10.1130/0016-7606(2000)112<1199:FEADPD>2.0.CO;2, 2000b.
- McCrea, J. M.: On the isotopic chemistry of carbonates and a paleotemperature scale, *J. Chem. Phys.*, doi:10.1063/1.1747785, 1950.
- 870 Mey, P. H. W.: The geology of the upper Ribagorzana and Baliera Valleys, Central Pyrenees, Spain, *Leidse Geol. Meded.*, 41, 153–220, 1967.
- Mey, P. H. W., Nagtegaal, P. J. C., Roberti, K. J. and Hartevelt, J. J. A.: Lithostratigraphic subdivision of Post-Hercynian deposits in the South-Central Pyrenees, Spain, *Leidse Geol. Meded.*, 41(1), 221–228, 1968.
- Mouthereau, F., Filleaudeau, P. Y., Vacherat, A., Pik, R., Lacombe, O., Fellin, M. G., Castellort, S., Christophoul, F. and

- 875 Masini, E.: Placing limits to shortening evolution in the Pyrenees: Role of margin architecture and implications for the Iberia/Europe convergence, *Tectonics*, 33(12), 2283–2314, doi:10.1002/2014TC003663, 2014.
- Mozafari, M., Swennen, R., Balsamo, F., El Desouky, H., Storti, F. and Taberner, C.: Fault-controlled dolomitization in the Montagna dei Fiori Anticline (Central Apennines, Italy): record of a dominantly pre-orogenic fluid migration, *Solid Earth*, 10(4), 1355–1383, doi:10.5194/se-10-1355-2019, 2019.
- 880 Muñoz, J. A.: Evolution of a continental collision belt: ECORS-Pyrenees crustal balanced cross-section, in *Thrust Tectonics*, pp. 235–246, Springer Netherlands, Dordrecht., 1992.
- Muñoz, J. A.: Fault-related folds in the southern Pyrenees, *Am. Assoc. Pet. Geol. Bull.*, 101(04), 579–587, doi:10.1306/011817DIG17037, 2017.
- Muñoz, J. A., Martínez, A. and Verges, J.: Thrust sequences in the eastern Spanish Pyrenees, *J. Struct. Geol.*, 8, 399–405, 885 1986.
- Nardini, N., Muñoz-López, D., Cruset, D., Cantarero, I., Martín-Martín, J., Benedicto, A., Gomez-Rivas, E., John, C. and Travé, A.: From Early Contraction to Post-Folding Fluid Evolution in the Frontal Part of the Bóixols Thrust Sheet (Southern Pyrenees) as Revealed by the Texture and Geochemistry of Calcite Cements, *Minerals*, 9(2), 117, doi:10.3390/min9020117, 2019.
- 890 Nelson, S. T., Mayo, A. L., Gilfillan, S., Dutson, S. J., Harris, R. A., Shipton, Z. K. and Tingey, D. G.: Enhanced fracture permeability and accompanying fluid flow in the footwall of a normal fault: The Hurricane fault at Pah Tempe hot springs, Washington County, Utah, *Geol. Soc. Am. Bull.*, preprint(2008), 1, doi:10.1130/B26285.1, 2006.
- Pfeifer, H.-R., Oberhänsli, H. and Epprecht, W.: Geochemical evidence for a synsedimentary hydrothermal origin of Jurassic iron-manganese deposits at Gonzen (Sargans, Helvetic Alps, Switzerland), *Mar. Geol.*, 84(3–4), 257–272, doi:10.1016/0025- 895 3227(88)90105-3, 1988.
- Piessens, K., Muechez, P., Dewaele, S., Boyce, A., De Vos, W., Sintubin, M., Debacker, T. N., Burke, E. A. J. and Viaene, W.: Fluid flow, alteration and polysulphide mineralisation associated with a low-angle reverse shear zone in the Lower Palaeozoic of the Anglo-Brabant fold belt, Belgium, *Tectonophysics*, doi:10.1016/S0040-1951(01)00250-5, 2002.
- Poblet, J.: Estructura herciniana i alpina del vessant sud de la zona axial del Pirineu centra, PhD thesis, Universitat de 900 barcelona., 1991.
- Pomerol, B.: Geochemistry of the late Cenomanian-early Turonian chalks of the Paris Basin: Manganese and carbon isotopes in carbonates as paleoceanographic indicators, *Cretac. Res.*, 4(1), 85–93, doi:10.1016/0195-6671(83)90025-3, 1983.
- Pratt, L. M., Force, E. R. and Pomerol, B.: Coupled manganese and carbon-isotopic events in marine carbonates at the Cenomanian-Turonian boundary, *J. Sediment. Petrol.*, doi:10.1306/D4267717-2B26-11D7-8648000102C1865D, 1991.
- 905 Roca, E.: The Neogene Cerdanya and Seu d'Urgell intramontane basins (Eastern Pyrenees), in *Tertiary basins of Spain*, edited by P. F. Friend and C. J. Dabrio, pp. 114–119, Cambridge University Press, Cambridge., 1996.
- Roca, E. and Guimerà, J.: The Neogene structure of the eastern Iberian margin: Structural constraints on the crustal evolution of the Valencia trough (western Mediterranean), *Tectonophysics*, 203(1–4), 203–218, doi:10.1016/0040-1951(92)90224-T,

Con formato: Español (España)

1992.

910 Roure, F., Choukroune, P., Berastegui, X., Munoz, J. a., Villien, a., Matheron, P., Bareyt, M., Seguret, M., Camara, P. and Deramond, J.: Ecors deep seismic data and balanced cross sections: Geometric constraints on the evolution of the Pyrenees, *Tectonics*, 8, 41-50, doi:10.1029/TC008i001p00041, 1989.

Rowland, J. V. and Sibson, R. H.: Structural controls on hydrothermal flow in a segmented rift system, Taupo Volcanic Zone, New Zealand, *Geofluids*, 4(4), 259–283, doi:10.1111/j.1468-8123.2004.00091.x, 2004.

915 Rye, D. M. and Bradbury, H. J.: Fluid flow in the crust; an example from a Pyrenean thrust ramp, *Am. J. Sci.*, 288(3), 197–235, doi:10.2475/ajs.288.3.197, 1988.

Saura, E.: *Análisis estructural de la Zona de les Nogueres (Pirineus Centrals)*, PhD thesis, Universitat de Barcelona., 2004.

Saura, E. and Teixell, A.: Inversion of small basins: effects on structural variations at the leading edge of the Axial Zone antiformal stack (Southern Pyrenees, Spain), *J. Struct. Geol.*, 28(11), 1909–1920, doi:10.1016/j.jsg.2006.06.005, 2006.

920 Shenton, B. J., Grossman, E. L., Passey, B. H., Henkes, G. A., Becker, T. P., Laya, J. C., Perez-Huerta, A., Becker, S. P. and Lawson, M.: Clumped isotope thermometry in deeply buried sedimentary carbonates: The effects of bond reordering and recrystallization, *Geol. Soc. Am. Bull.*, 127(7–8), B31169.1, doi:10.1130/B31169.1, 2015.

Sibson, R. H.: Crustal stress, faulting and fluid flow, *Geol. Soc. London, Spec. Publ.*, 78(1), 69–84, doi:10.1144/GSL.SP.1994.078.01.07, 1994.

925 Sibson, R. H.: Selective fault reactivation during basin inversion: potential for fluid redistribution through fault-valve action, *Geol. Soc. London, Spec. Publ.*, 88(1), 3–19, doi:10.1144/GSL.SP.1995.088.01.02, 1995.

Sibuet, J. C., Srivastava, S. P. and Spakman, W.: Pyrenean orogeny and plate kinematics, *J. Geophys. Res. B Solid Earth*, 109(8), 1–18, doi:10.1029/2003JB002514, 2004.

930 Srivastava, S. P., Schouten, H., Roest, W. R., Klitgord, K. D., Kovacs, L. C., Verhoef, J. and Macnab, R.: Iberian plate kinematics: A jumping plate boundary between Eurasia and Africa, *Nature*, doi:10.1038/344756a0, 1990.

Stolper, D. A. and Eiler, J. M.: The kinetics of solid-state isotope-exchange reactions for clumped isotopes: A study of inorganic calcites and apatites from natural and experimental samples, *Am. J. Sci.*, 315(5), 363–411, doi:10.2475/05.2015.01, 2015.

935 Suchy, V., Heijlen, W., Sykorova, I., Muechez, P., Dobes, P., Hladikova, J., Jackova, I., Safanda, J. and Zeman, A.: Geochemical study of calcite veins in the Silurian and Devonian of the Barrandian Basin (Czech Republic): evidence for widespread post-Variscan fluid flow in the central part of the Bohemian Massif, *Sediment. Geol.*, 131(3–4), 201–219, doi:10.1016/S0037-0738(99)00136-0, 2000.

940 Taillefer, A., Soliva, R., Guillou-Frottier, L., Le Goff, E., Martin, G. and Seranne, M.: Fault-Related Controls on Upward Hydrothermal Flow: An Integrated Geological Study of the Têt Fault System, Eastern Pyrénées (France), *Geofluids*, 2017, 1–19, doi:10.1155/2017/8190109, 2017.

Taillefer, A., Guillou-Frottier, L., Soliva, R., Magri, F., Lopez, S., Courrioux, G., Millot, R., Ladouche, B. and Le Goff, E.: Topographic and Faults Control of Hydrothermal Circulation Along Dormant Faults in an Orogen, *Geochemistry, Geophys.*

Con formato: Español (España)



Geosystems, 19(12), 4972–4995, doi:10.1029/2018GC007965, 2018.

Taylor, B. D.: Stable isotope geochemistry of ore-forming fluids, in Short Course Handbook., 1987.

- 945 Travé, A., Labaume, P., Calvet, F. and Soler, A.: Sediment dewatering and pore fluid migration along thrust faults in a foreland basin inferred from isotopic and elemental geochemical analyses (Eocene southern Pyrenees, Spain), *Tectonophysics*, 282(1–4), 375–398, doi:10.1016/S0040-1951(97)00225-4, 1997.

- Travé, A., Labaume, P., Calvet, F., Soler, A., Tritlla, J., Buatier, M., Potdevin, J.-L., Séguret, M., Raynaud, S. and Briquieu, L.: Fluid migration during Eocene thrust emplacement in the south Pyrenean foreland basin (Spain): an integrated structural, mineralogical and geochemical approach, *Geol. Soc. London, Spec. Publ.*, 134(1), 163–188, doi:10.1144/GSL.SP.1998.134.01.08, 1998.

- 950 Travé, A., Calvet, F., Sans, M., Vergés, J. and Thirlwall, M.: Fluid history related to the Alpine compression at the margin of the south-Pyrenean Foreland basin: the El Guix anticline, *Tectonophysics*, 321(1), 73–102, doi:10.1016/S0040-1951(00)00090-1, 2000.

- 955 Travé, A., Labaume, P. and Vergés, J.: Fluid Systems in Foreland Fold-and-Thrust Belts: An Overview from the Southern Pyrenees, in *Thrust Belts and Foreland Basins*, edited by O. Lacombe, F. Roure, J. Lavé, and J. Vergés, pp. 93–115, Springer Berlin Heidelberg, Berlin, Heidelberg., 2007.

- Travé, A., Roca, E., Playà, E., Parcerisa, D., Gómez-Gras, D. and Martín-Martín, J. D.: Migration of Mn-rich fluids through normal faults and fine-grained terrigenous sediments during early development of the Neogene Vallès-Penedès half-graben (NE Spain), *Geofluids*, 9(4), 303–320, doi:10.1111/j.1468-8123.2009.00258.x, 2009.

- 960 Trincal, V., Buatier, M., Charpentier, D., Lacroix, B., Lanari, P., Labaume, P., Lahfid, A. and Vennemann, T.: Fluid–rock interactions related to metamorphic reducing fluid flow in meta-sediments: example of the Pic-de-Port-Vieux thrust (Pyrenees, Spain), *Contrib. to Mineral. Petrol.*, 172(9), 78, doi:10.1007/s00410-017-1394-5, 2017.

- 965 Turu i Michels, V. and Peña Monné, J. L.: Las terrazas fluviales del sistema Segre-Valira (Andorra- La Seu d'Urgell-Organyà, Pirineos Orientales): relación con el glaciario y la tectónica activa., *Geomorfol. y Territ. IX Reun. Nac. Geomorfología*, (January 2006), 113–128, 2006.

- Veizer, J., Ala, D., Azmy, K., Bruckschen, P., Buhl, D., Bruhn, F., Carden, G. A. F., Diener, A., Ebner, S., Godderis, Y., Jasper, T., Korte, C., Pawellek, F., Podlaha, O. G. and Strauss, H.:  $^{87}\text{Sr}/^{86}\text{Sr}$ ,  $\delta^{13}\text{C}$  and  $\delta^{18}\text{O}$  evolution of Phanerozoic seawater, *Chem. Geol.*, 161(1–3), 59–88, doi:10.1016/S0009-2541(99)00081-9, 1999.

- 970 Vergés, J.: Estudi geològic del vessant Sud del Pirineu Oriental i Central: Evolució cinemàtica en 3D. PhD thesis, University of Barcelona, Barcelona., 1993.

Vergés, J. and Fernández, M.: Tethys–Atlantic interaction along the Iberia–Africa plate boundary: The Betic–Rif orogenic system, *Tectonophysics*, 579, 144–172, doi:10.1016/j.tecto.2012.08.032, 2012.

Vergés, J. and Muñoz, J. A.: Thrust sequences in the southern central Pyrenees, *Bull. French Geol. Soc.*, 2, 265–271, 1990.

- 975 Vergés, J., Fernández, M. and Martínez, A.: The Pyrenean orogen: pre-, syn-, and post-collisional evolution, *J. Virtual Explor.*, 08(January 2002), doi:10.3809/jvirtex.2002.00058, 2002.

Con formato: Español (España)

Con formato: Español (España)

Vilasi, N., Swennen, R. and Roure, F.: Diagenesis and fracturing of Paleocene-Eocene carbonate turbidite systems in the Ionian Basin: The example of the Kelçyra area (Albania), *J. Geochemical Explor.*, 89(1-3 SPEC. ISS.), 409–413, doi:10.1016/j.gexplo.2005.11.018, 2006.

980 Voicu, G., Bardoux, M., Stevenson, R. and Jébrak, M.: Nd and Sr isotope study of hydrothermal scheelite and host rocks at Omai, Guiana Shield: implications for ore fluid source and flow path during the formation of orogenic gold deposits, *Miner. Depos.*, 35(4), 302–314, doi:10.1007/s001260050243, 2000.

Warren, J., Morley, C. K., Charoentitirat, T., Cartwright, I., Ampaiwan, P., Khositichaisri, P., Mirzaloo, M. and Yingyuen, J.: Structural and fluid evolution of Saraburi Group sedimentary carbonates, central Thailand: A tectonically driven fluid system, 985 *Mar. Pet. Geol.*, 55, 100–121, doi:10.1016/j.marpetgeo.2013.12.019, 2014.

Wayne, D. M. and McCaig, A. M.: Dating fluid flow in shear zones: Rb-Sr and U-Pb studies of syntectonic veins in the Néouvielle Massif, Pyrenees, *Geol. Soc. London, Spec. Publ.*, 144(1), 129–135, doi:10.1144/GSL.SP.1998.144.01.09, 1998.

Ziegler, P. A.: Evolution of the Arctic-North Atlantic and the Western Tethys, in *AAPG Memoir Volume 43: Evolution of the Arctic-North Atlantic and the Western Tethys.*, 1988.

990 Zwart, H. J.: The variscan geology of the Pyrenees, *Tectonophysics*, 129(1–4), 9–27, doi:10.1016/0040-1951(86)90243-X, 1986.

995

1000

1005

1010

**Table 1.  $\delta^{18}\text{O}$ ,  $\delta^{13}\text{C}$ ,  $^{87}\text{Sr}/^{86}\text{Sr}$  and  $^{143}\text{Nd}/^{144}\text{Nd}$  ratios of the calcite cements and related host rocks. The calculated precipitation temperature and the  $\delta^{18}\text{O}_{\text{fluid}}$  of the parent fluids are also indicated. NR indicates analyzed samples in which no result was obtained.**

Sample	Vein	Cement	$\delta^{18}\text{O}$ ‰VPDB	$\delta^{13}\text{C}$ ‰VPDB	$^{87}\text{Sr}/^{86}\text{Sr}$	$^{143}\text{Nd}/^{144}\text{Nd}$	$\Delta_{47}$	T (°C)	$\delta^{18}\text{O}_{\text{fluid}}$ ‰SMOW
C9	V1a	Cc1a	-11.2	+0.91					
C8B	V1a	Cc1a	-10.7	+2					
C8A.I	V1a	Cc1a	-10.4	+2					
C8A.II	V1a	Cc1a	-10.96	+1.3	0.713018	NR			
C8A.III	V1a	Cc1a	-10.9	+1.2					
C7.I	V1a	Cc1a	-10.9	+2.1					
C7.II	V1a	Cc1a	-10.8	+0.8					
C7.III	V1a	Cc1a	-10.4	+1.96					
C4B	V1a	Cc1a	-10.3	+1.9	0.714092	NR			
C3A.I	V1a	Cc1a	-11.2	+1.9					
C3A.II	V1a	Cc1a	-11.3	+1.7					
C3A.III	V1a	Cc1a	-10.5	+1.98					
C15.I	V2	Cc2	-14.9	-1.2	0.718294	NR	0.567	56 to 98	-0.3 to -6.4
C15.II	V2	Cc2	-13.3	+0.5					
C15.III	V2	Cc2	-12.91	+1.54					
C13	V3	Cc3	-13.8	-7.1	0.714619	NR	0.445	127 to 208	+4.3 to +12.1
C12.II	V3	Cc3	-14.3	-7.3					
C10	V3	Cc3	-14.2	-9.3					
C11A	V3	Cc3	-14.2	-8.7					
C13.II	V3	Cc3	-13.6	-7.2					
C14.I	V3	Cc3	-13.4	-6.9					
C14.II	V3	Cc3	-13.7	-7.4					
C16A	V3	Cc3	-13.8	-7.2					
C16B	V3	Cc3	-14	-7					
C16C	V3	Cc3	-14.1	-6.9					
C18.I	V4	Cc4	-13.4	-7.2	0.717706		0.48	102 to 167	+0.9 to +8.1
C18.II	V4	Cc4	-13.8	-7.4					
C12.I	V5	Cc5	-8.1	-7.8	0.716923	0.512178			
C6.I	V5	Cc5	-6.7	-8.2					
C6.II	V5	Cc5	-7.4	-7.4					
C11B	V5	Cc5	-5.7	-3.8					
C3A.HR	Devonian		-9.5	+2.4	0.710663	NR	0.77	-5 to +3	-12.4 to -10.1
C17.HR	carbonates		-10.5	+1.5					
C4.HR			-8.4	+2.7					
C11.HR	Andesites		-	-	0.743983	0.512196			

1020

Table 2: Elemental composition (Ca, Mg, Fe, Mn, Sr) of the calcite cements Cc1a to Cc5 and host rocks from the hanging wall (HW) and footwall (FW). The **qualitative** scale in greens indicates **different contents (for each element, the darkest green points to the highest concentration and vice versa)**.

Sample	Ca ppm	Mg ppm	Fe ppm	Mn ppm	Sr ppm
Cc1a	391618	1335.9	5603.5	1243.7	543.7
Cc1a	349063	1548.6	4121.3	781.6	460.2
Cc1a	351134	1231.8	5205.4	810.3	545.5
Cc1a	337588	1126.6	3914.9	680.7	704.0
Cc2	328169	501.2	1061.4	3629.3	248.5
Cc3	364995	331.9	1647.8	8277.9	122.3
Cc3	333123	909.5	5545.9	7695.5	424.9
Cc4	333563	624.4	3814.9	4034.6	72.2
Cc5	233784	2260.0	8656.6	161.4	72.1
Cc5	281741	1626.2	4078.0	138.8	25.3
HW	320038	2752.6	6289.0	621.1	449.4
FW	4234	12830.5	43107.1	466.6	18.6

Higher content		Lower content
----------------	--	---------------

Eliminado: higher concentrations when is darker.

1025

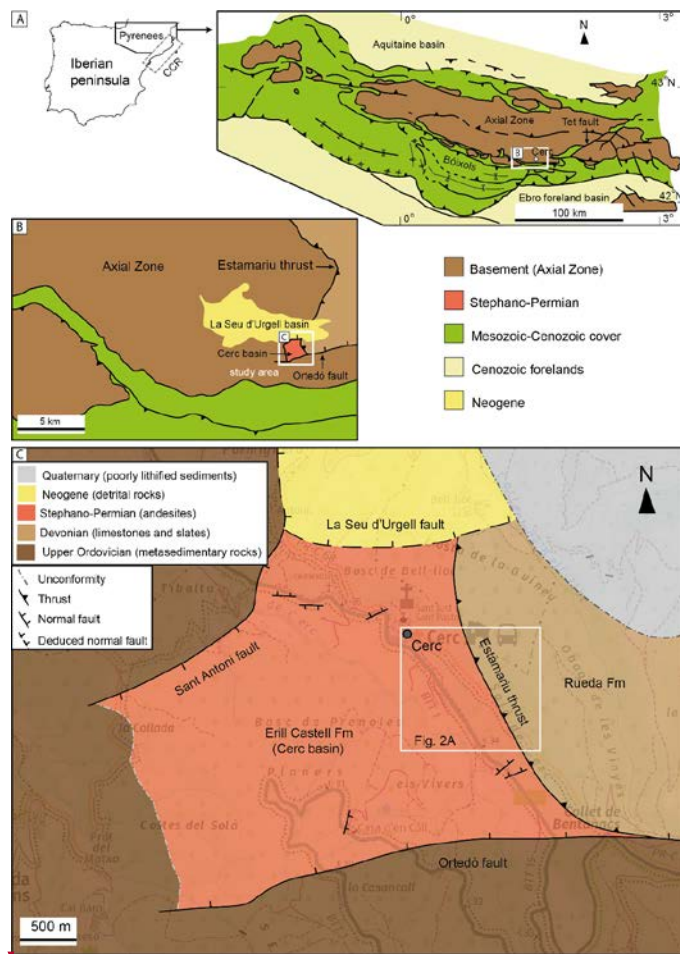
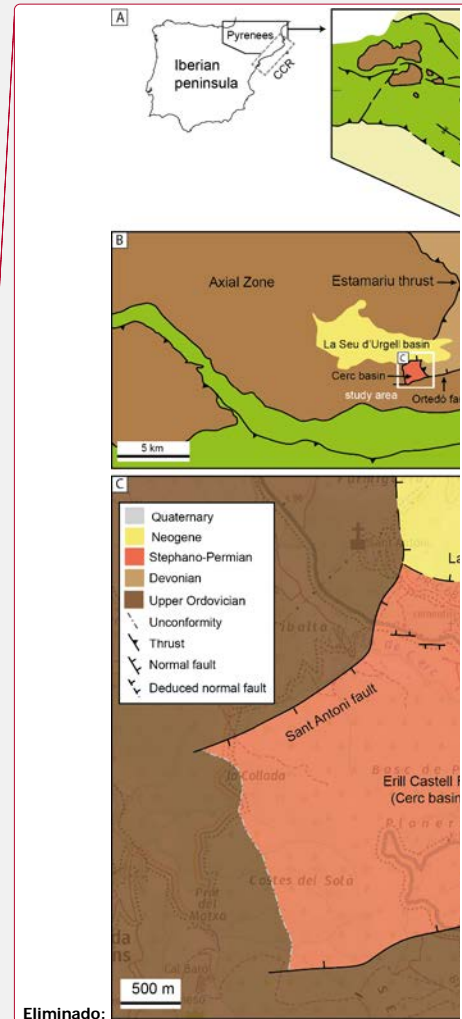
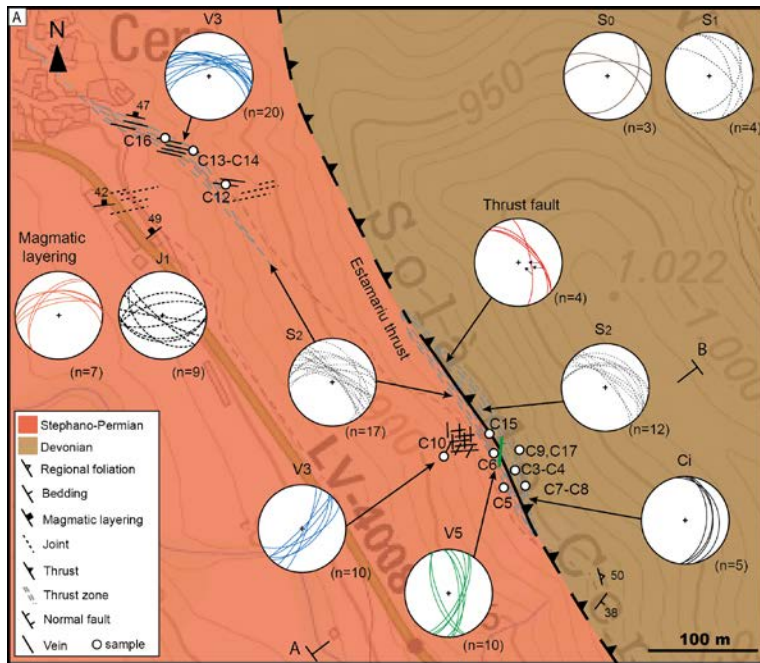


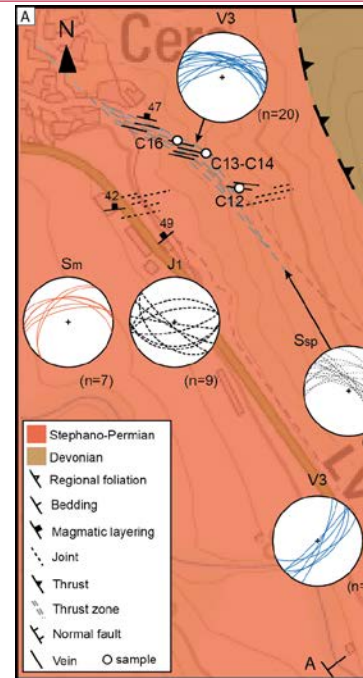
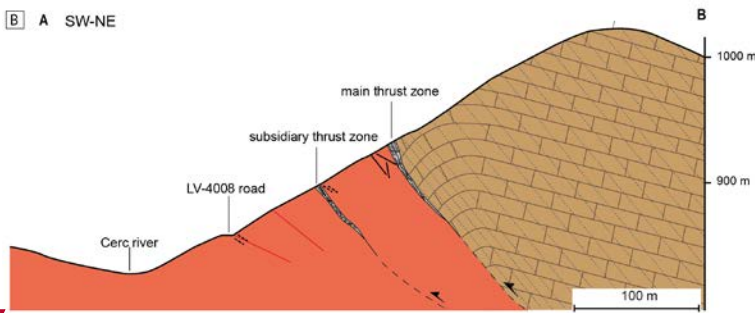
Figure 1: (A) Simplified geological map of the Pyrenees modified from (Muñoz, 2017) and its location in the Iberian Peninsula (location of the Catalan Coastal Range, CCR, is also shown). (B) Detail of the study area located within the Pyrenean Axial zone. (C) Geological map of the Cerc basin (using data from Saura (2004) and our own data) with the Estamariu thrust located in its eastern termination and the Neogene extensional faults in the northern and southern limits. The white square indicates the location of the main outcrop (Fig. 2A).



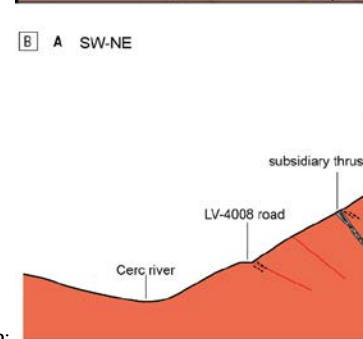
Eliminado:



B A SW-NE



B A SW-NE



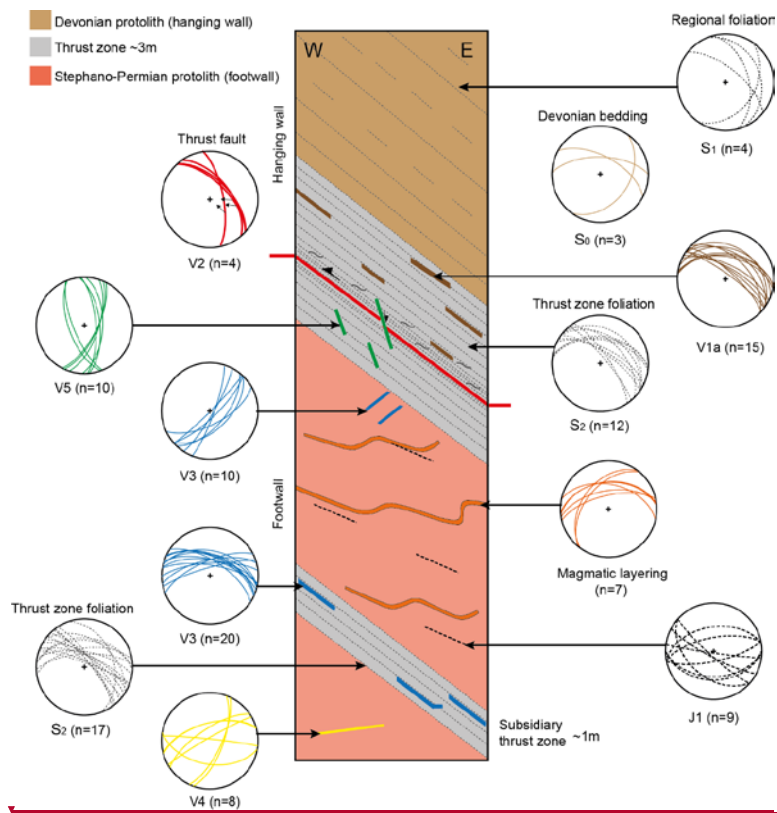
Eliminado:

Eliminado: Sr

Eliminado: (SD) ...nd footwall (S<sub>2</sub>SP..., magmatic layering (Sm)

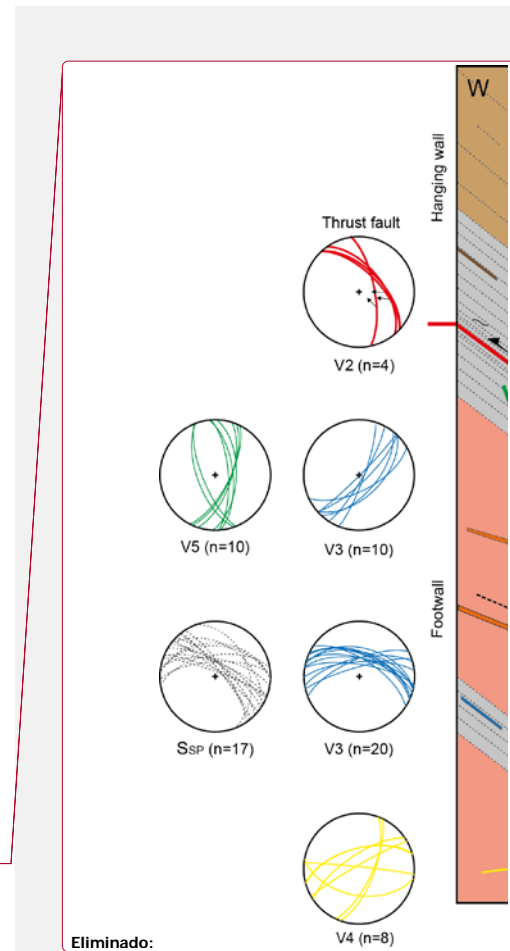
Con formato: Subindice

1035 Figure 2: (A) Geological map and (B) cross-section of the Estamariu thrust, which juxtaposes a Devonian unit against a Stephano-Permian sequence (H=V, no vertical exaggeration). Lower-hemisphere equal-area stereoplots of the Devonian bedding (S<sub>0</sub>), regional foliation (S<sub>1</sub>), thrust zone foliation affecting the hanging wall and footwall (S<sub>2</sub>), magmatic layering and the different faults and veins observed in the study area are also included. Location in Fig. 1B.



1050

Figure 3: Sketch showing the spatial distribution of mesoscale structures within the main outcrop and lower-hemisphere equal-area stereoplots of the different mesostructures.



Eliminado:



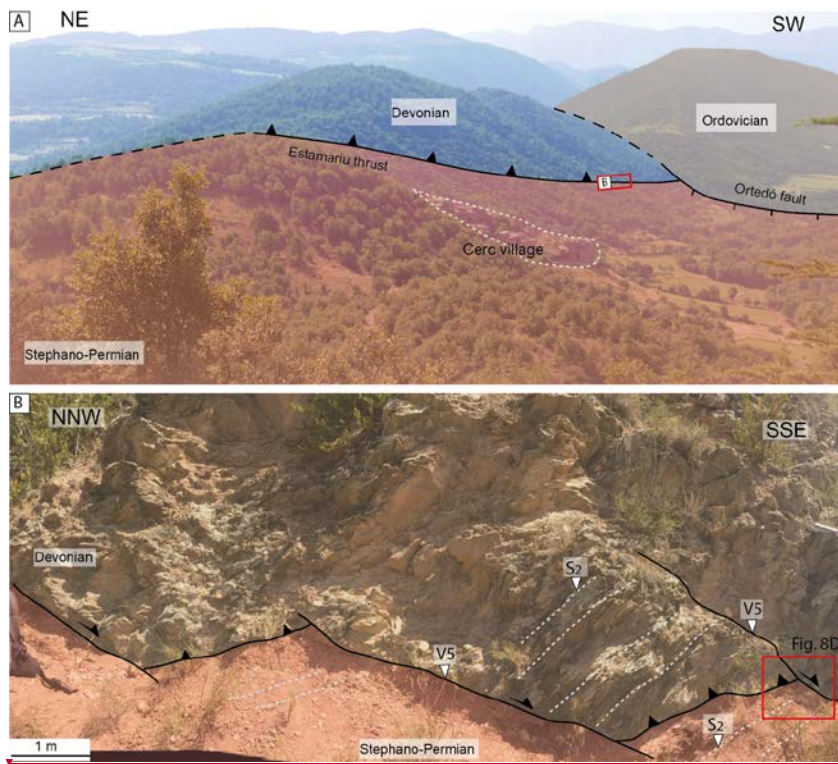


Figure 4: Main outcrop of the Estamariu thrust. A) Panoramic view from the Sant Antoni hill showing the extensional Ortedó fault postdating the Estamariu thrust. B) Main outcrop showing the Estamariu thrust and the related thrust zone foliation developed in the Devonian hanging wall and in the Stephano-Permian footwall (S<sub>2</sub>). The thrust is displaced by later shear fractures locally mineralized with calcite (V5).

Eliminado: (SD)  
 Eliminado: SP

1055



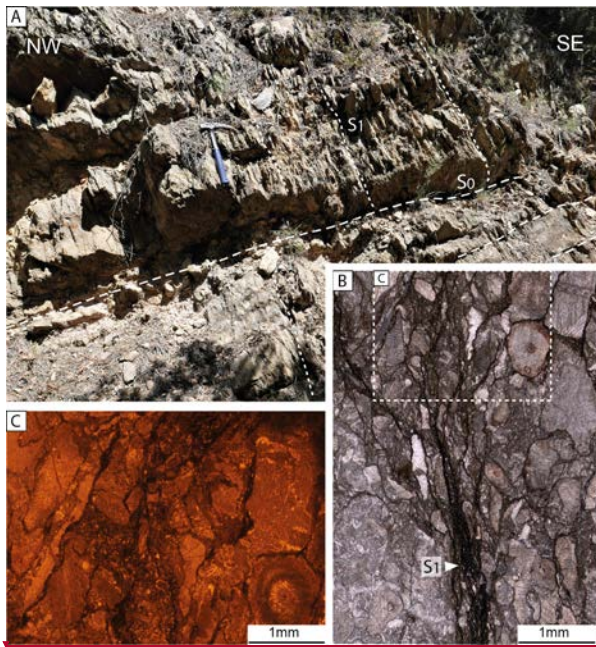
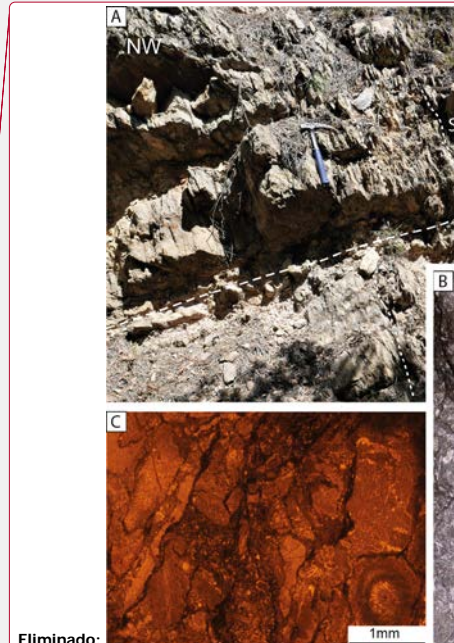


Figure 5: Devonian protolith. A) Field image showing the relationship between bedding ( $S_0$ ) and regional foliation ( $S_1$ ). B) Plane polarized light and C) Cathodoluminescence microphotographs of the encrinites alternating with pelitic rich bands, where the  $S_1$  is concentrated.



Eliminado: r

Eliminado: r

Eliminado: r

065

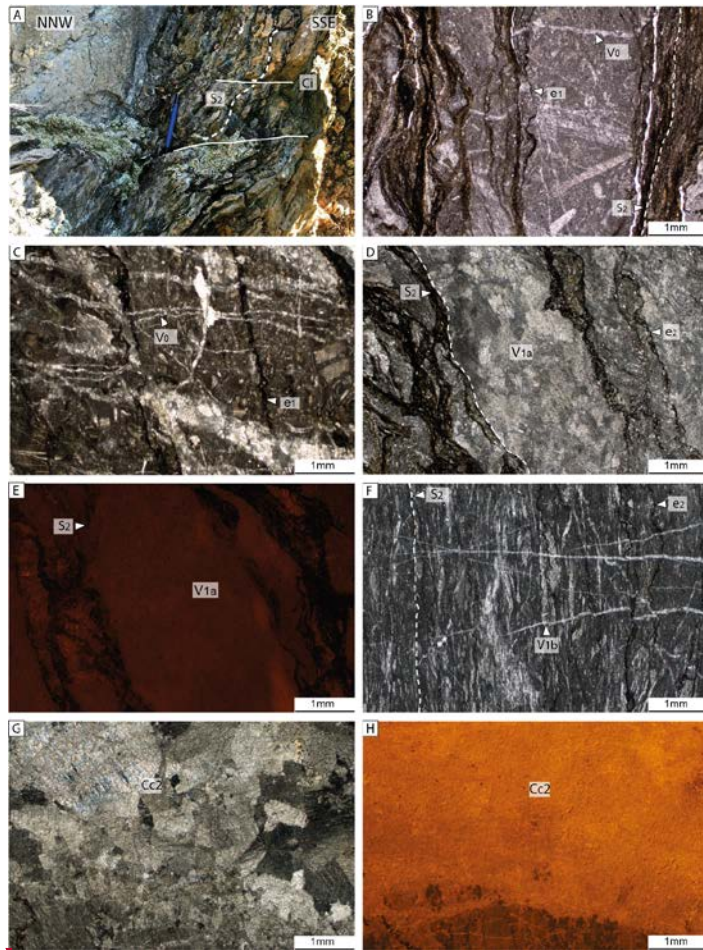
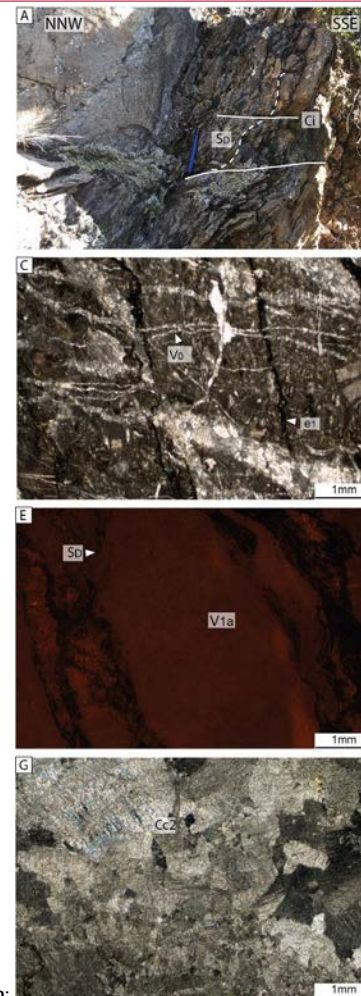


Figure 6: Mesostructures and microstructures found within the thrust zone affecting the hanging wall. A) Outcrop image of the thrust zone foliation ( $S_2$ ) and related C planes indicating reverse kinematics ( $C_1$ ). Microphotographs of B) thrust zone foliation ( $S_2$ ), C) stylolites e1 and veins V0 affecting the Devonian encrinites, D) Crossed polarized light and E) cathodoluminescence microphotographs of veins V1a concentrated between foliation surfaces. F) Thrust zone foliation ( $S_2$ ) near the fault plane and ambiguous and perpendicular relationships between V1b and e2. G) Crossed polarized light and H) cathodoluminescence microphotographs of calcite cement Cc2 located on the main thrust plane (V2).



Eliminado:

Eliminado: D

Eliminado: D



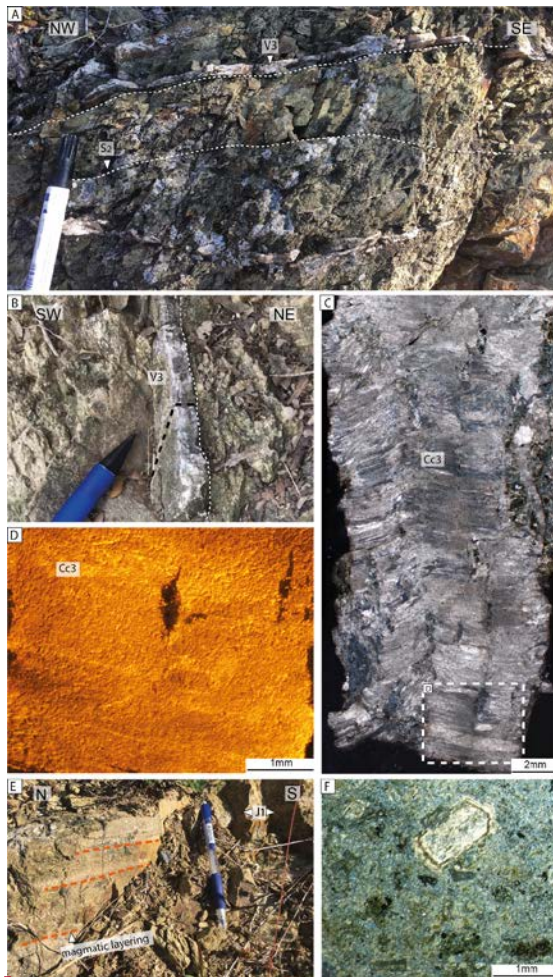
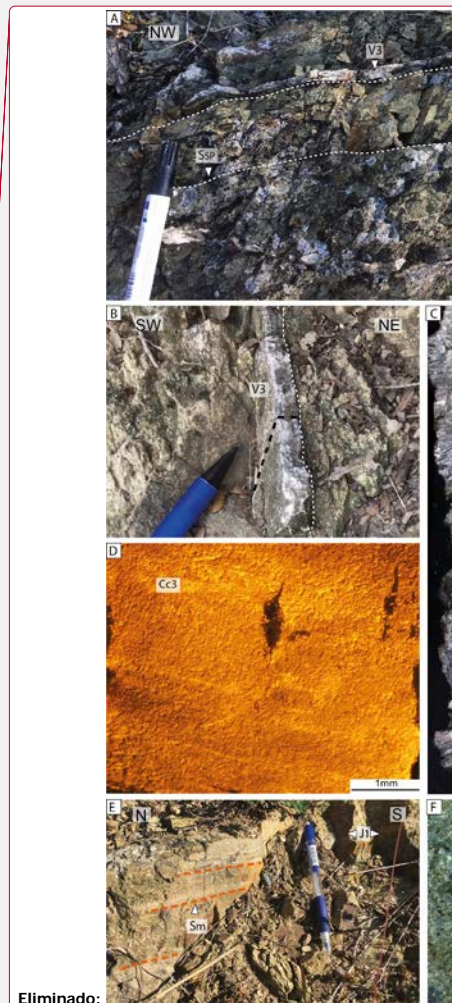


Figure 7: Mesostructures and microstructures present in the Stephano-Permian volcanic footwall. A) Field image of the subsidiary thrust zone in the footwall showing the thrust zone foliation (S) and the veins V3. B) Detail of veins V3 also in the subsidiary thrust zone. The black dashed line indicates the original position of the thin section observed in C. C) Crossed polarized light and D) Cathodoluminescence microphotographs of veins V3, characterized by calcite fibers growing perpendicular to the vein walls (Cc3). E) Field image of the footwall andesites showing the magmatic layering and joints Jl. F) Plane polarized light microphotograph of the volcanic andesites exhibiting a porphyritic texture with a large plagioclase crystal.

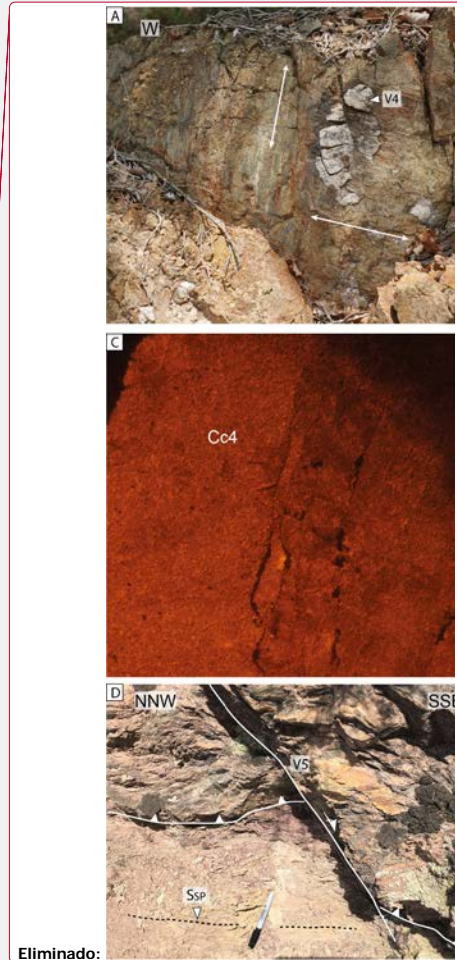
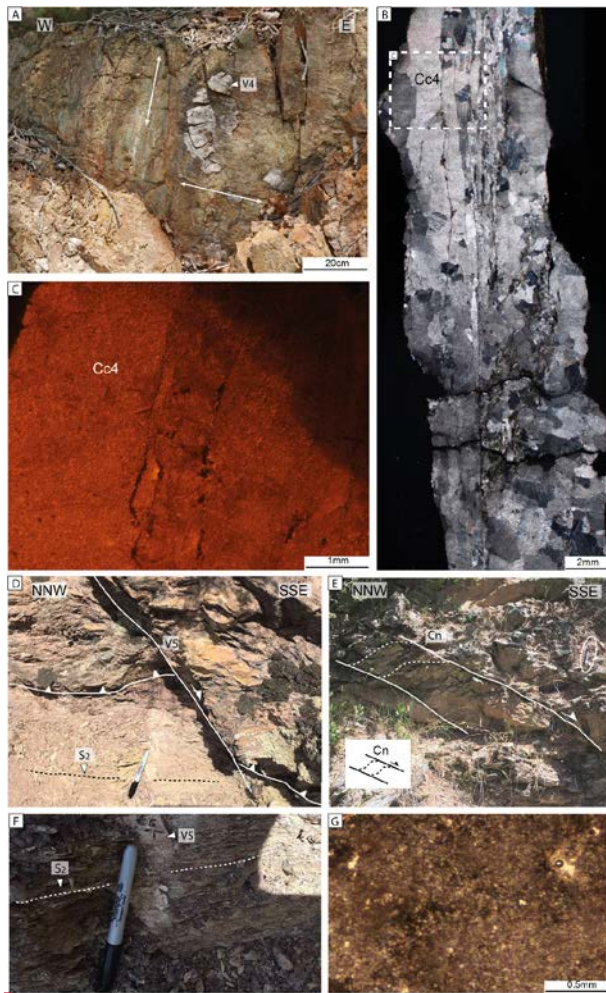


Eliminado:

Eliminado: SsP

Eliminado: c

Eliminado: (Sm)



Eliminado:

Figure 8: A) Field image of a subvertical and E-W fault plane mineralized with calcite (veins V4) and showing two striae set generations (white arrows) indicating dip-slip and strike-slip kinematics. B) Crossed polarized light and C) cathodoluminescence microphotographs of the vein-related calcite cement (Cc4). D) Shear fracture postdating the thrust zone foliation, locally mineralized with calcite veins V5. E) Shear bands (Cn) with normal kinematics located in the main thrust zone, indicating a later reactivation of the Estamariu thrust. **F) Field image of a calcite vein V5 and G) Plane polarized light of the vein-related cement (Cc5).**

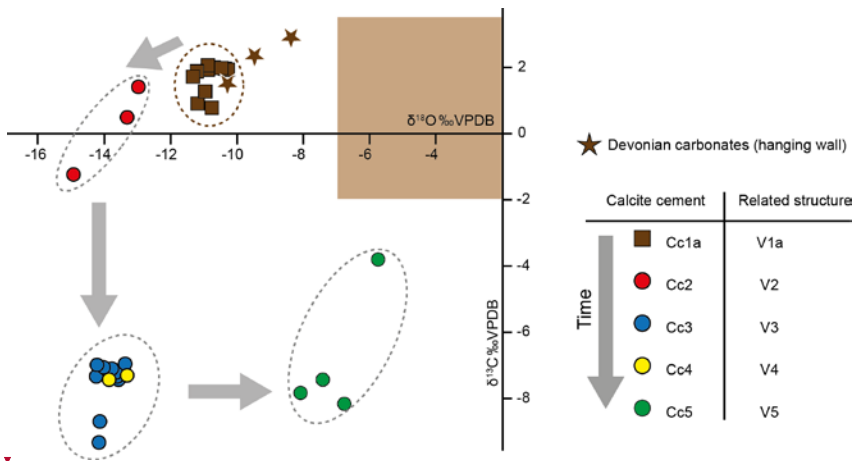
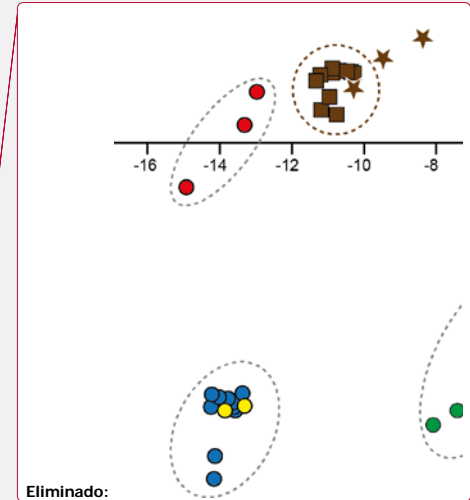


Figure 9:  $\delta^{18}\text{O}$  and  $\delta^{13}\text{C}$  values of calcite cements Cc1a to Cc5 and the Devonian carbonates from the hanging wall. Arrows indicate evolution over time according to the inferred relative timing of cements. The brown box refers to typical values of Devonian marine carbonates (Veizer et al., 1999).



1105

1110

1115

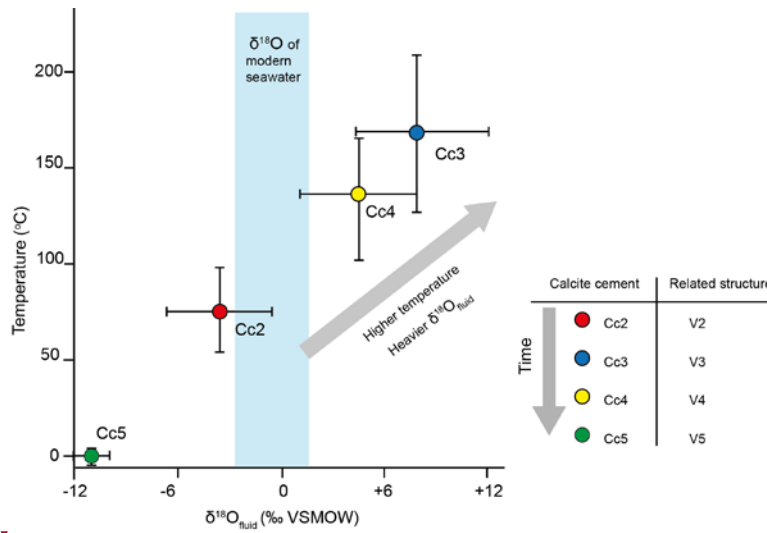
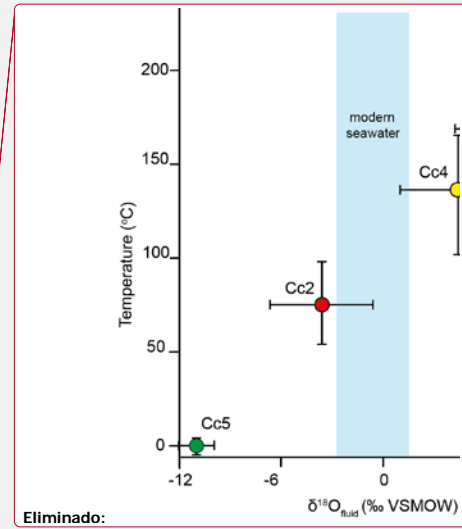


Figure 10: Temperatures (°C) vs  $\delta^{18}\text{O}_{\text{fluid}}$  calculated for cements Cc2 to Cc5. The typical  $\delta^{18}\text{O}$  values for modern seawater (blue band) are from (Veizer et al., 1999).



Eliminado:



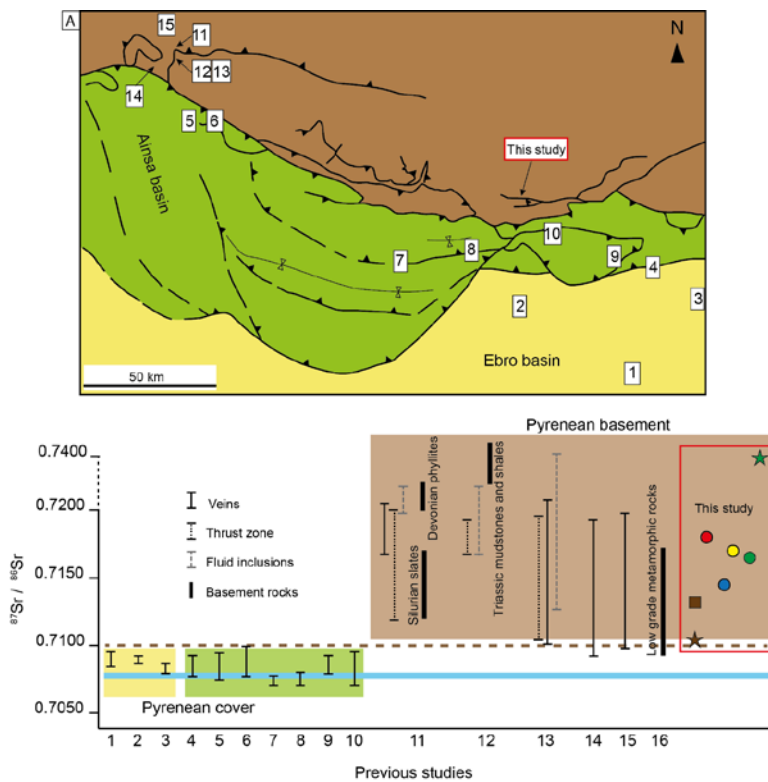


Figure 11: Simplified geological map of the south-central Pyrenees showing the location of structures where  $^{87}\text{Sr}/^{86}\text{Sr}$  analysis have been carried out. Below,  $^{87}\text{Sr}/^{86}\text{Sr}$  ratios from this study compared to results from other structures involving either cover units (1-10) or basement rocks (11-16). The blue thick line refers to the  $^{87}\text{Sr}/^{86}\text{Sr}$  range of Phanerozoic seawater and the dashed brown line represents the  $^{87}\text{Sr}/^{86}\text{Sr}$  limit value between basement and cover structures. 1. El Guix anticline (Travé et al., 2000), 2. Puig Reig anticline (Cruset et al., 2016), 3. L'Escala thrust (Cruset et al., 2018), 4. Valfogona thrust (Cruset et al., 2018), 5. Ainsa basin (Travé et al., 1997), 6. Ainsa-Bielsa area (McCaig et al., 1995), 7. Minor Bóixols thrust (Muñoz-López et al., under review), 8. Bóixols anticline (Nardini et al., 2019), 9. Lower Pedraforca thrust (Cruset et al., 2020a), 10. Upper Pedraforca thrust (Cruset, 2019), 11. Gavarnie thrust (McCaig et al., 1995), 12. Pic de Port Vieux thrust (Banks et al., 1991), 13. Pic de Port Vieux thrust (McCaig et al., 2000b), 14. Plan de Larri thrust (McCaig et al., 1995), 15. La Glere shear zone (Wayne and McCaig, 1998), 16. Trois Seigneurs Massif (not in the map) (Bickle et al., 1988).

Con formato: Español (España)

Código de campo cambiado

Con formato: Español (España)

Código de campo cambiado

Con formato: Español (España)

Código de campo cambiado

Con formato: Español (España)

Con formato: Español (España)

Código de campo cambiado

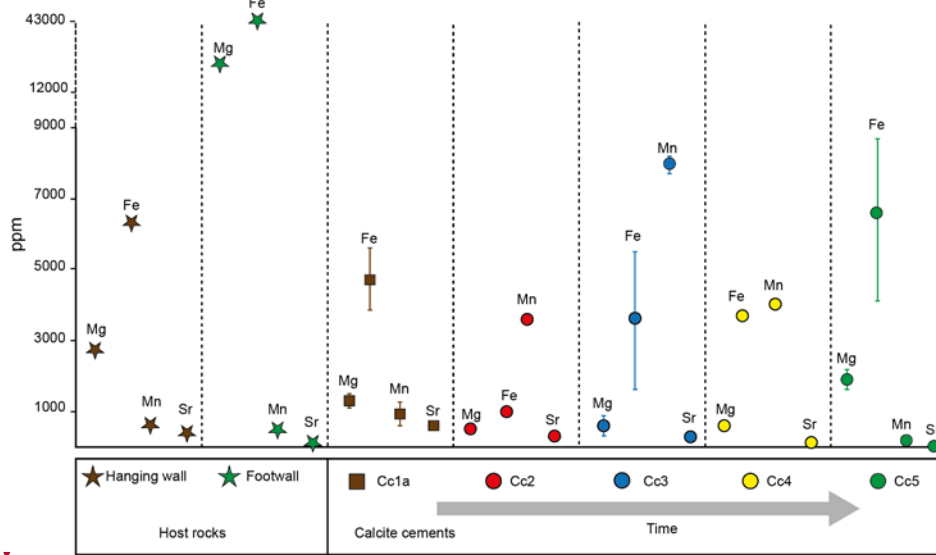
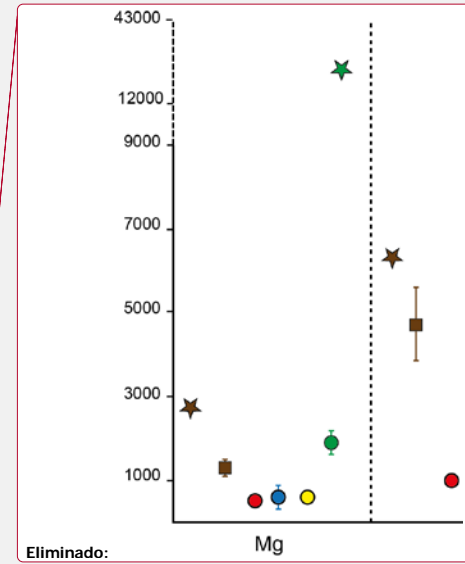


Figure 12: Elemental composition (including Mg, Fe, Mn and Sr) in ppm of the different calcite cements and host rocks. Bars indicate maximum, minimum and average composition.



Eliminado:

Mg

Eliminado: <objeto>

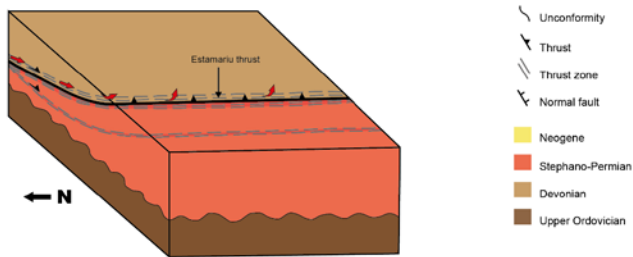
1140

1145



**A Alpine compression**

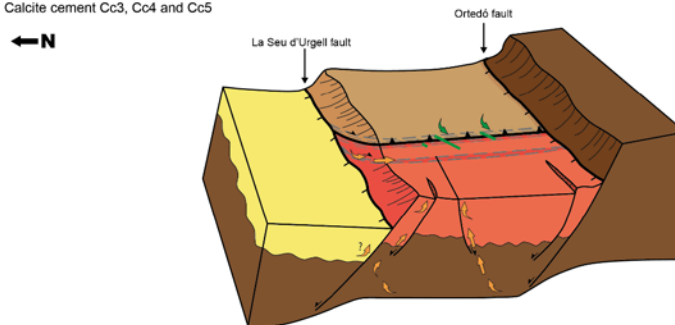
Reactivation of the Estamaru thrust. Calcite cements Cc1a and Cc2



Regional tectonism	A	Alpine compression		B			Neogene extension
Calcite cement		Cc1a	Cc2	Cc3	Cc4	Cc5	
Related structure		V1a	V2	V3	V4	V5	
Geochemistry	$\delta^{13}C_{calcite}$						
	$\delta^{18}O_{calcite}$						
	$^{87}Sr / ^{86}Sr$						
	Mg						
	Fe						
	Mn						
	Sr						
$\delta^{18}O_{fluid}$							
Temperature							
Fluid source		Upward meteoric fluid		Upward hydrothermal fluid		Downward meteoric fluid	
Implications		Change in the fluid regime. Increasing extent of fluid-rock interaction			Main change in the fluid regime		

**B Neogene extension**

Reactivation of the Estamaru thrust and development of normal faults  
Calcite cement Cc3, Cc4 and Cc5



155 | **Figure 13: Tectonic and geochemical evolution of the study area (not to scale) and relationships with the evolution of the fluid system. A) During the Alpine reactivation of the Estamariu thrust, a meteoric fluid (red arrows) interacted at depth with basement rocks and then migrated along the fault plane towards the hanging wall, precipitating cements Cc1a and Cc2. B) During the Neogene extension, basement-derived hydrothermal fluids (orange arrows) flowed upwards through newly formed and reactivated fault zones. This fluid precipitated calcite cements Cc3 and Cc4. Finally, during ongoing deformation, meteoric fluids (green arrows) percolated in the system and precipitated Cc5, revealing a main change in the fluid regime.**

Eliminado: yellow

Eliminado: channelized

Eliminado: blu

Eliminado: e

# Influence of basement rocks on fluid evolution during multiphase deformation: the example of the Estamariu thrust in the Pyrenean Axial Zone

Daniel Muñoz-López<sup>1</sup>, Gemma Alías<sup>1</sup>, David Cruset<sup>2</sup>, Irene Cantarero<sup>1</sup>, Cédric M. John<sup>3</sup>, Anna Travé<sup>1</sup>

<sup>1</sup>Department de Mineralogia, Petrologia i Geologia Aplicada. Facultat de Ciències de la Terra, Universitat de Barcelona (UB), C/ Martí i Franquès s/n, 08028 Barcelona, Spain.

<sup>2</sup>Group of Dynamics of the Lithosphere (GDL), Geosciences Barcelona, GEO3BCN-CSIC, Lluís Solé i Sabarís s/n, 08028 Barcelona, Spain.

<sup>3</sup> Department of Earth Science and Engineering, Imperial College London, London SW7 2BP, UK.

Correspondence to: Daniel Muñoz-López (munoz-lopez@ub.edu)

**Abstract.** Calcite veins precipitated in the Estamariu thrust during two tectonic events are studied in order to: (i) decipher the temporal and spatial relationships between deformation and fluid migration in a long-lived thrust and, (ii) determine the influence of basement rocks on the fluid chemistry during deformation. Structural and petrological observations constrain the influence of basement rocks on the fluid chemistry during deformation. Structural and petrological observations constrain the relative timing of fluid migration and vein formation, whilst geochemical analyses ( $\delta^{13}\text{C}$ ,  $\delta^{18}\text{O}$ ,  $^{87}\text{Sr}/^{86}\text{Sr}$ , clumped isotope thermometry and elemental composition) applied to the related calcite cements and host rocks indicate the fluid origin, pathways and extent of fluid-rock interaction. The first tectonic event, recorded by calcite cements Cc1a and Cc2, is related to the Alpine reactivation of the Estamariu thrust, and is characterized by the migration of meteoric fluids, heated at depth at temperatures between 56 and 98 °C, and interacted with basement rocks before upflowing through the thrust zone. During the Neogene extension, the Estamariu thrust was reactivated and normal faults and shear fractures with calcite cements Cc3, Cc4 and Cc5 developed. Calcites Cc3 and Cc4 precipitated from hydrothermal fluids (temperatures between 127 and 208 °C and between 102 and 167 °C, respectively), interacted with basement rocks and expelled through fault zones during deformation. Cc5 precipitated from low temperature meteoric waters percolating from the surface through small shear fractures. The comparison between our results and already published data in other structures from the Southern Pyrenees suggests that regardless of the origin of the fluids and the tectonic context, basement rocks have a significant influence on the fluid chemistry, particularly on the  $^{87}\text{Sr}/^{86}\text{Sr}$  ratio. Accordingly, the cements precipitated from fluids that have interacted with basement rocks have significantly higher  $^{87}\text{Sr}/^{86}\text{Sr}$  ratios ( $> 0.710$ ) with respect to those precipitated from fluids that have interacted with the sedimentary cover ( $< 0.710$ ), which involves younger and less radiogenic rocks.

Eliminado: Institut de Ciències de la Terra Jaume Almera, ICTJA-CSIC

Con formato: Inglés (Estados Unidos)

Con formato: Inglés (Estados Unidos)

Con formato: Inglés (Estados Unidos)

Eliminado: of

Eliminado: (

Eliminado: )

Eliminado: crystalline

Eliminado: derived from crystalline

Eliminado:

Eliminado: crystalline

## 1 Introduction

40 Deformation associated with crustal shortening is mainly accommodated by thrust faulting and related fault zone structures (Mouthereau et al., 2014; Muñoz, 1992; Sibson, 1994). Successive faulting may occur and favourably oriented structures may undergo reactivation during different tectonic events in a long-lived orogenic belt (Cochelin et al., 2018; Sibson, 1995). The reactivation of faults may produce changes in the hydraulic behaviour of fault zones as well as in the origin and regime of fluids circulating through them (Arndt et al., 2014; Barker and Cox, 2011; Cantarero et al., 2018; Crusset et al., 2018; Lacroix et al., 2018; Travé et al., 2007). Consequently, constraining the timing of deformation and fluid migration is essential to better

45 understand the main factors leading to the current configuration of a mountain belt, its evolution through time, and the mobilization of different fluids during successive deformation events (Baques et al., 2012; Crespo-Blanc et al., 1995; Fay-Gomord et al., 2018; Fitz-Diaz et al., 2011; Lacroix et al., 2014). Understanding basin-scale fluid flow is of primary importance to reconstruct the diagenetic history of a sedimentary basin, as fluids take part in a wide range of geological processes including precipitation of new mineral phases, dolomitization and petroleum migration, among others (Barker et al., 2009; Foden, 2001; Fontana et al., 2014; Gomez-Rivas et al., 2014; Martín-Martín et al., 2015; Mozafari et al., 2019; Piessens et al., 2002). Due to the economic interest of these processes, in particular related to oil and ore deposits exploration, CO<sub>2</sub> sequestration, seismic activity and water management, many researchers have addressed the study of the relationship between deformation and fluid migration (Beaudoin et al., 2014; Breesch et al., 2009; Cox, 2007; Dewever et al., 2013; Gasparrini et al., 2013; Suchy et al., 2000; Travé et al., 2009; Voicu et al., 2000; Warren et al., 2014).

55 In the Pyrenees, the basement rocks from the Axial Zone are affected by numerous fault systems considered Variscan in age but reactivated during the Pyrenean compression (Cochelin et al., 2018; Poblet, 1991). However, no real consensus exists about the influence of the Alpine deformation on the basement rocks and the age of basement-involved structures is still debated (Cochelin et al., 2018; García-Sansegundo et al., 2011). As a consequence, the relationships between deformation and fluid flow have been widely focused on structures from the Mesozoic and Cenozoic cover (Beaudoin et al., 2015; Crognier et al., 2018; Crusset et al., 2016, 2018, 2020a; Lacroix et al., 2011, 2014; Martinez Casas et al., 2019; Nardini et al., 2019; Travé et al., 1998, 2000, 1997), where the timing of deformation and thrust emplacement is well-constrained (Crusset et al., 2020b; Vergés, 1993; Vergés and Muñoz, 1990). Contrarily, less contributions, only concentrated along the Gavarnie thrust system, have tackled the relationships between deformation and fluid migration in the Paleozoic basement (Banks et al., 1991; Grant et al., 1990; Henderson and McCaig, 1996; McCaig et al., 2000a, 1995; Rye and Bradbury, 1988; Trincal et al., 2017). Another important aspect of studying the fault-fluid system is related to the heat flow and the influence of faults on the development of geothermal systems (Faulds et al., 2010; Grasby and Hutcheon, 2001; Liotta et al., 2010; Rowland and Sibson, 2004). Particularly, in the NE part of the Iberian Peninsula (including the Pyrenees and the Catalan Coastal Ranges), the presence of high-permeability Neogene extensional faults, acting as conduits for upward migration, provide efficient pathways for hydrothermal fluids to flow from deeper to shallower crustal levels (Carmona et al., 2000; Fernández and Banda, 1990;

60

65

Código de campo cambiado

Eliminado: crystalline

Eliminado: only a few

Eliminado: this topic

Eliminado: involving crystalline rocks

Eliminado: On the other hand, a

Eliminado: focused

Taillefer et al., 2017, 2018). In this sense, understanding the fault-fluid system evolution and the **relative** timing of hydrothermal fluid migration is of great importance to characterize the potential geothermal resources of this area.

In this contribution, we report the temporal and spatial relationships between deformation and fluid migration in a long-lived Variscan thrust deforming basement rocks in the Pyrenean Axial Zone. For this purpose, we combine structural, petrological

80 and geochemical analyses of calcite veins precipitated in the Estamariu thrust during two **reactivation** episodes **related to the** Pyrenean compression and **the** Neogene extension. Structural and petrological observations allow us to unravel the **relative** timing of fluid migration and vein formation in relation to the involved tectonic events. The geochemistry of the vein cements and related host rocks provides information on the fluid origin, pathways and extent of fluid-rock interaction during deformation. **Therefore, the main objectives of this paper are:** (i) to constrain the **relative** timing of vein formation and fluid  
85 migration; (ii) to determine the fluid origin and pathways during successive compressional and extensional deformation phases; (iii) to assess the influence of basement rocks on the chemistry of fluids circulating during deformation; and (iv) to provide insights into the fluid flow at regional scale in the NE part of the Iberian Peninsula, where the presence of hydrothermal fluids has been reported from Neogene times to present.

## 2 Geological setting

90 The Pyrenees constitute an asymmetric and doubly verging orogenic belt developed from the Late Cretaceous to Oligocene, **resulting from** the Alpine convergence between the Iberian and European plates (Choukroune, 1989; Muñoz, 1992; Roure et al., 1989; Sibuet et al., 2004; Srivastava et al., 1990; Vergés and Fernández, 2012). The Pyrenean structure consists of a central antiformal stack of basement-involved rocks from the Axial Zone, flanked by two oppositely verging fold-and-thrust belts and their associated foreland basins (Muñoz, 1992; Muñoz et al., 1986) (Fig. 1A). The Axial Zone represents a fragment of the  
95 European Variscan orogen, **incorporated into the Pyrenean belt during the Alpine convergence** (Matte, 1991). It consists of a duplex of three south-directed basement thrust sheets (from upper to lower: Noguères, Orri and Rialp), involving Cambrian to Carboniferous rocks deformed by the Variscan compressional events, and an Upper Carboniferous to Triassic post-Variscan cover (Poblet, 1991; Saura, 2004; Saura and Teixell, 2006).

During the Neogene tectonic evolution of the eastern Axial Pyrenees, a horst and basin system bounded by E-W to ENE-WSW  
100 faults developed (Roca, 1996; Roca and Guimerà, 1992). The most important fault, La Tet fault (roughly striking N60°E and dipping around 60°N) has associated a set of E-W extensional basins such as La Cerdanya, Conflent, La Seu d'Urgell and Cerc basins (Cabrera et al., 1988; Roca, 1996). The Cerc basin consists of a Stephano-Permian accumulation of volcanic rocks discordantly overlying Cambro-Ordovician materials from the Orri thrust sheet. This basin is thrust in its eastern limit by the Estamariu thrust, whereas the northern and southern boundaries correspond to two Neogene extensional faults, La Seu  
105 d'Urgell fault and the Ortedó fault, respectively (Hartevelt, 1970; Roca, 1996; Saura, 2004) (Fig. 1B, C). In the NW part of the basin, the limit between the Stephano-Permian unit and the Upper Ordovician sequence corresponds to a Stephano-Permian

**Eliminado:** of regional tectonic activity (

**Eliminado:** )

**Eliminado:** The integration of all these data within the studied geological setting in the Pyrenean basement will allow us

**Eliminado:** in relation to

**Con formato:** Español (España)

**Eliminado:** y

extensional fault formed coevally with the deposition of the volcanic sequence (Saura, 2004). This fault was reactivated during the latest stages of the Neogene extension (Saura, 2004) and is here referred as the Sant Antoni fault (Fig. 1C).

115 The Estamariu thrust is a basement-involved reverse fault originated during the Variscan orogeny with a minimum displacement of 27 km (Poblet, 1991). However, in its southwestern termination, it juxtaposes the Devonian Rueda Formation against the Stephano-Permian Erill Castell Formation. The Erill Castell Formation developed during the late to post-orogenic collapse of the Variscan belt (Lago et al., 2004; Martí, 1991, 1996; Ziegler, 1988), evidencing the reactivation of the Estamariu thrust during the Alpine Orogeny (Poblet, 1991; Saura, 2004).

120 Rocks cropping out around the Estamariu thrust and the Cerc basin range from Upper Ordovician to Miocene (Fig. 1C) and are deformed by successive Variscan, Alpine and Neogene phases (Saura and Teixell, 2006). Due to such a complex structural setting, the stratigraphic record is discontinuous and only Upper Ordovician, Devonian, Stephano-Permian and Neogene rocks are present in the study area. The basement lithologies consists of Upper Ordovician and Devonian metasedimentary rocks affected by multiscale folds and related pervasive axial plane regional foliation (Bons, 1988; Casas et al., 1989; Cochelin et al., 2018; Zwart, 1986). This deformation is linked to low-grade metamorphic conditions developed during the Variscan orogeny (Hartevelt, 1970; Poblet, 1991; Saura, 2004). The Upper Ordovician succession basically includes a centimetric to metric alternation of shales, sandstones, conglomerates, quartzites and phyllites and the Devonian sequence consists of a centimetric to decimetric alternation of limestones and black slates (Rueda Formation) (Mey, 1967). The Stephano-Permian sequence developed during the late to post-orogenic extensional collapse of the Variscan belt and in the study area is represented by a volcanic and volcanoclastic unit (the Erill Castell Formation) (Martí, 1991; Mey et al., 1968), involving tuffs and ignimbrites at the base and andesites in the upper part (Martí, 1996; Saura and Teixell, 2006). Finally, the Neogene sequence is constituted of detrital and poorly lithified sediments, mainly shales, sandstones and conglomerates deposited during the Neogene tectonic extension associated with the opening of the NW Mediterranean Sea (Roca, 1996).

### 3 Methods

135 This study integrates a field compilation of structural data and samples and petrological and geochemical analyses of calcite cements and related host rocks. The structural data includes bedding, foliation strike and fracture orientation, type, crosscutting relationships and kinematics. Such data were plotted in equal-area lower-hemisphere projections and different fracture sets were established according to their type, strike, mineral infillings, and relative age deduced from crosscutting relationships. All these data were integrated in a schematic map and a cross-section of the Estamariu thrust and the Cerc basin (Fig. 2A, B and  
140 3). Samples considered representative of the involved host rocks and all calcite vein generations observed in the different fracture sets and fault-related structures were selected for petrological and geochemical analyses. Thin sections of these samples were prepared and studied under a Zeiss Axiophot optical microscope and a Cold cathodoluminescence (CL) microscope model 8200 Mk5-1 operating between 16–19 kV and 350 µA gun current.

**Eliminado:** Rocks cropping out around the Estamariu thrust and the Cerc basin range from Upper Ordovician to Miocene (Fig. 1C) and are deformed by successive Variscan, Alpine and Neogene phases (Saura and Teixell, 2006). Due to such a complex structural setting, the stratigraphic record is discontinuous and only Upper Ordovician, Devonian, Stephano-Permian and Neogene successions are present in the study area. The Upper Ordovician consists mainly of a detrital sedimentary sequence affected by a low-graded metamorphism (Hartevelt, 1970; Poblet, 1991; Saura, 2004). This succession basically includes a centimetric to metric alternation of shales, sandstones, conglomerates, quartzites and phyllites. The Devonian succession consists of a centimetric to decimetric alternation of limestones and black slates (Rueda Formation) (Mey, 1967). The Stephano-Permian sequence is represented by a volcanic and volcanoclastic unit (the Erill Castell Formation) (Mey et al., 1968), involving tuffs and ignimbrites at the base and andesites in the upper part (Martí, 1996; Saura and Teixell, 2006). Finally, the Neogene sequence is constituted of detrital and poorly lithified sediments, mainly shales, sandstones and conglomerates (Roca, 1996).¶

**Eliminado:** and

**Eliminado:** Host rocks and calcite cements were sampled

**Eliminado:** were

**Con formato:** Color de fuente: Texto 1

Thirty-five representative samples of the different generations of calcite cements and the carbonate portion of the Devonian rocks were sampled for carbon and oxygen isotopy. Sampling was carried out with a 500  $\mu\text{m}$ -diameter microdrill. 50-100  $\mu\text{g}$  of powdered samples were reacted with 100% phosphoric acid during two minutes at 70  $^{\circ}\text{C}$ . The resultant  $\text{CO}_2$  was analyzed with an automated Kiel Carbonate Device attached to a Thermal Ionization Mass Spectrometer Thermo Electron MAT-252 (Thermo Fisher Scientific) according to the method of (McCrea, 1950). For calibration, the International Standard NBS-18 and the internal standard RC-1, traceable to the International Standard NBS-19, were used. The standard deviation is  $\pm 0.03\%$  for  $\delta^{13}\text{C}$  and  $\pm 0.05\%$  for  $\delta^{18}\text{O}$  expressed with respect to the VPDB standard (Vienna Pee Dee Belemnite).

The elemental composition of twelve samples of calcite cements and related host rocks were analyzed using a high resolution inductively coupled plasma-mass spectrometry (HR-ICP-MS, model Element XR, Thermo Fisher Scientific). 100 mg of powdered samples were dried at 40  $^{\circ}\text{C}$  during 24 h and then they were acid digested in closed polytetrafluoroethylene (PTFE) vessels with a combination of  $\text{HNO}_3 + \text{HF} + \text{HClO}_4$  (2.5 mL: 5 mL: 2.5 mL v/v). The samples were evaporated and 1 mL of  $\text{HNO}_3$  was added to make a double evaporation. Finally, the samples were re-dissolved and diluted with MilliQ water (18.2  $\text{M}\Omega\text{ cm}^{-1}$ ) and 1 mL of  $\text{HNO}_3$  in a 100 mL volume flask. A tuning solution containing 1  $\text{g L}^{-1}$  Li, B, Na, K, Sc, Fe, Co, Cu, Ga, Y, Rh, In, Ba, Tl, U was used in order to improve the sensitivity of the ICP-MS, and as internal standard, 20  $\text{mg L}^{-1}$  of a mono-elemental solution of  $^{115}\text{In}$ . Reference materials are the BCS-CRM n $^{\circ}$  393 (ECRM 752-1) limestone, JA-2 Andesite and JB-3 Basalt. The precision of the results was expressed in terms of two standard deviations of a set of eight reference materials measurements (reference material JA-2), whereas accuracy (%) was calculated using the absolute value of the difference between the measured values obtained during the analysis and the certified values of a set of eight reference material analysis (reference material BCS-CRM n $^{\circ}$  393 for major oxides and JA-2 for trace elements). The detection limit (DL) was calculated as three times the standard deviation of the average of ten blanks.

The  $^{87}\text{Sr}/^{86}\text{Sr}$  ratio was analyzed for eight representative samples of calcite cements and host rocks. Powdered samples were dissolved in 5 mL of 10% acetic acid. After centrifugation, the supernatant was dried and dissolved in 1 mL of 1M  $\text{HNO}_3$ . The solid residue generated after evaporation was diluted in 3 mL of 3M  $\text{HNO}_3$  and loaded into chromatographic columns to separate the Rb-free Sr fraction, using SrResinTM (crown-ether (4,4'(5')-di-t-butylcyclohexano-18-crown-6)) and 0.05M  $\text{HNO}_3$  as eluent. After evaporation, samples were loaded onto a Re filament along with 1  $\mu\text{L}$  of 1 M phosphoric acid and 2  $\mu\text{L}$  of  $\text{Ta}_2\text{O}_5$ . Isotopic analyses were carried out in a TIMS-Phoenix mass spectrometer performing a dynamic multicollection method, during 10 blocks of 16 cycles each one keeping a  $^{88}\text{Sr}$  beam intensity of 3-V. Possible  $^{87}\text{Rb}$  interferences and possible mass fractionation during sample loading and analysis were corrected and normalized with the reference value of  $^{88}\text{Sr}/^{86}\text{Sr} = 0.1194$ . The isotopic standard NBS-987 was analyzed six times during sample analysis, yielding an average value of 0.710243  $\pm 0.000009$  (standard deviation,  $2\sigma$ ). NBS 987 data have been used to correct the sample ratios for standard drift from the certified value. The analytical error in the  $^{87}\text{Sr}/^{86}\text{Sr}$  ratio, referred to two standard deviations, was 0.01%, whereas the internal precision is 0.000003. Sr procedural blanks were always below 0.5 ng.

The  $^{143}\text{Nd}/^{144}\text{Nd}$  ratios were analyzed in seven samples of calcite cements and host rocks. Samples were weighted in Teflon $^{\circledR}$  vessels, with enriched spike solution ( $^{149}\text{Sm}$ - $^{150}\text{Nd}$  - Oak Ridge) and dissolved in 5 mL of ultrapure HF and 3 mL of ultrapure

Eliminado: .

Eliminado: .

Eliminado: .

HNO<sub>3</sub> (Merck-Suprapur™). The PFA-vessels were placed 65 hours at 120 °C into an oven. After that, cold vials were evaporated at 120 °C on a heat plate. 4 mL of 6N distilled HCL were added to the dried samples and placed at 120 °C in an oven overnight. The solid residue generated after evaporation was dissolved in 3 mL of distilled and titrated 2.5 N HCL. Samples were centrifuged at 4000 rpm for 10 minutes to separate the possible dissolved fraction from the residue. Chromatographic separation of the whole group of REE was performed with a previously calibrated cation exchange resin DOWEX 50W-X8 200-400 mesh. After that, recovered REE fractions were dried and again dissolved in 200 µL HCl 0.18N. Such solutions were passed in a new chromatographic step (Ln-resin). The result is a complete separation between the Nd and the Sm fractions, using 0.3N HCl and 0.4N HCl as eluent, respectively. Dried Sm and Nd samples dissolved with 2 µL of 0.05M phosphoric acid were loaded onto a side Rhenium (Re) filament of a triple Re filament arrangement. Nd ratios were analysed in a mass spectrometer TIMS-Phoenix®, using a dynamic multicollection method, through 160 cycles at a stable intensity of 1V for the <sup>144</sup>Nd mass. In turn, Sm ratios were analysed in the same spectrometer, using a single static method through 112 cycles keeping 1V intensity for the <sup>149</sup>Sm mass. Nd analyses were corrected for <sup>142</sup>Ce and <sup>144</sup>Sm interferences, if any, and normalized to a ratio of <sup>146</sup>Nd/<sup>144</sup>Nd = 0.7219 to correct the possible mass fractionation during the processes of loading and analysing at the TIMS. Nd isotopic standard JNdi-1 was checked to correct the sample ratios for standard drift from the certified value. The analytical error (2STD) was 0.1% in the <sup>147</sup>Sm/<sup>144</sup>Nd ratio and 0.006% in the <sup>143</sup>Nd/<sup>144</sup>Nd ratio. Procedural blanks were always below 0.1 ng.

U-Pb geochronology of the calcite cements Cc1a to Cc5 was accomplished at FIERCE (Frankfurt Isotope and Element Research Center, Goethe University) using a laser ablation inductively coupled plasma mass spectrometry (LA-ICPMS).

Clumped isotope thermometry of the calcite cements was carried in order to determine the temperature and composition ( $\delta^{18}\text{O}_{\text{fluid}}$ ) of the vein-forming fluids. 2–3 mg aliquots from cements were measured with an automated line, the Imperial Batch Extraction system (IBEX), developed at Imperial College. Samples were dropped in 105% phosphoric acid at 90 °C and reacted during 30 min. The reactant CO<sub>2</sub> was separated with a poropak-Q column and transferred into the bellows of a Thermo Scientific MAT 253 mass spectrometer. The characterization of a replicate consisted of 8 acquisitions in dual inlet mode with 7 cycles per acquisition. The post-acquisition processing was completed with Easotope, a software for clumped isotope analyses (John and Bowen, 2016). During phosphoric acid digestion,  $\Delta_{47}$  values were corrected for isotope fractionation using a phosphoric acid correction of 0.069‰ at 90 °C for calcite (Guo et al., 2009). The data were also corrected for non-linearity applying the heated gas method (Huntington et al., 2009) and projected into the reference frame of (Dennis et al., 2011). Carbonate  $\delta^{18}\text{O}$  values were calculated with the acid fractionation factors of (Kim and O'Neil, 1997). Results were converted to temperatures applying the calibration method of (Kluge et al., 2015). Calculated  $\delta^{18}\text{O}_{\text{fluid}}$  values are expressed in ‰ with respect to the Vienna Standard Mean Ocean Water (VSMOW).



## 4 Results

### 4.1 Structure and associated calcite cements

235 The Estamariu thrust strikes N-S to NW-SE and dips between 40 and 70° towards the NE. It has a displacement of a few hundred meters and juxtaposes a Devonian alternation of limestones and shales in the hanging wall against Stephano-Permian andesites in the footwall (Poblet, 1991) (Fig. 2-4). The main slip plane is undulose and generates a 2 – 3 m thick thrust zone affecting both the hanging wall and footwall, but it is thicker in the hanging wall, up to 2.5 m thick. In the footwall, the thrust zone is less than 1 m thick and has associated minor restricted thrust zones developed as subsidiary accommodation structures related to the main thrust fault (Fig. 2A, B). All kinematic indicators, including S-C structures and slickenlines, indicate reverse displacement towards the west.

The mesostructures and microstructures observed in the study area are described below according to their structural position in relation to the Estamariu thrust, that is, hanging wall, thrust zone and footwall (Fig. 3, 4). U-Pb dating of the vein cements failed due to their high lead contents and low uranium contents and therefore, the relative timing of the different mesostructures and microstructures has been determined by means of crosscutting relationships and microstructural analysis.

#### 4.1.1 Hanging wall

In the studied outcrops, the Devonian Rueda Formation is characterized by a well-bedded alternation of dark to light grey limestones with subordinated dark grey shales ( $S_0$ ) (Fig. 5A). Limestones are made up of encrinites, which consist of a bioclastic packstone formed essentially of crinoid stems (Fig. 5B). Under cathodoluminescence, encrinites show dark to bright orange colors (Fig. 5C). Devonian rocks form a decametric anticline oriented NW-SE with a well-developed axial plane foliation ( $S_1$ ) concentrated in the pelitic intervals.  $S_1$ , which is oriented NNW-SSE, is a pervasive regional foliation dipping 30 to 55° towards the E and NE and is generally between 2 and 5 cm spaced. In the hinge of the anticline, bedding ( $S_0$ ) dips towards the SE and forms a high angle with  $S_1$  (Fig. 2B and 5A), whereas in its eastern limb, the regional foliation ( $S_1$ ) dips steeper than  $S_0$ . These geometric relationships between bedding and foliation have been used to determine the fold type at great scale (i.e., as it is shown in Fig. 2B).

#### 4.1.2 Thrust zone

The thrust zone consists of a deformation zone affecting both the hanging wall and the footwall. Within the hanging wall, the Devonian host rocks are still recognizable, but the intensity of deformation progressively increases towards the main thrust plane. This deformation consists of a penetrative thrust zone foliation ( $S_2$ ), two generations of stylolites (e1, e2) and three generations of calcite veins (V0, V1a and V1b) (Fig. 3, 6). These structures are described below in chronological order.

The foliation within the thrust zone affecting the Devonian hanging wall ( $S_2$ ) strikes NW-SE and dips 40 – 50° NE, similar to the regional foliation ( $S_1$ ), but it is more closely spaced, generally between 0.2 and 1 cm (Fig. 6A, B). This observation points

Eliminado: , producing changes in the strike direction and dip,

Eliminado: , which

Movido (inserción)[1]

Eliminado: calcite

Eliminado: Cc1a to Cc5

Eliminado: ur

Eliminado: ¶

Con formato: Título 3

Con formato: Color de fuente: Automático

Eliminado: from the hanging wall

Con formato: Fuente: 8 pto

Eliminado: (

Eliminado: are more abundant and

Con formato: Fuente: 10 pto

Eliminado: Deformation in the Devonian protolith (i.e., outside the thrust zone) corresponds to a decametric anticline (Fig. 2B), which has associated an axial plane pervasive regional foliation ( $S_r$ ) concentrated in the pelitic intervals (Fig. 5B). The  $S_r$  has a NW-SE mean orientation, dips 30 to 55° towards the E and NE and is generally between 2 and 5 cm spaced. The angular relationship between the Devonian bedding strike and the regional foliation is oblique and changes to nearly perpendicular when approaching the thrust zone (Fig. 2B).

Con formato: Título 3

Con formato: Inglés (Reino Unido)

Eliminado: the thrust zone affecting

Eliminado: intensity

Eliminado: ( $S_D$ )

Eliminado: in the protolith

285 out to a progressive transposition of the regional foliation within the thrust zone during thrusting. At mesoscale,  $S_2$  has related shear surfaces (Ci) defining centimetric S-C-type structures, indicating again reverse kinematics (Fig. 6A).

Stylolites e1 have a wave-like shape and trend subparallel to the thrust zone foliation ( $S_2$ ) (Fig. 6B, C). When present, these stylolites are very systematic exhibiting a spacing of 1 – 2 mm (Fig. 6C).

290 The first calcite vein generation (V0), only observed at microscopic scale (Fig. 6B, C), corresponds to up to 1 cm long and less than 1 mm thick veins cemented by blocky to elongated blocky calcite crystals featuring a dark-brown luminescence (cement Cc0). Veins V0 and stylolites e1 are perpendicular between them and show ambiguous crosscutting relationships. These microstructures are concentrated into discontinuous fragments of the Devonian host rocks within the thrust zone. Calcite veins V1a crosscut the previous vein generation (V0) as well as the stylolites e1 and are developed within  $S_2$  surfaces (Fig. 3, 6D).

These veins are the most abundant, exhibit a white to brownish color in hand sample and are up to 10 cm long and 1 cm thick. 295 The vein cement (Cc1a) is formed of up to 3-4 mm in size anhedral crystals displaying a blocky texture and a dark brown luminescence (Fig. 6E).

Stylolites e2, more abundant than stylolites e1, are up to 10 cm long and show spacing between 0.5 and 2 cm (Fig. 6D, F). These stylolites mainly correspond to sutured areas developed between the host rock and the calcite veins V1a and between foliation surfaces  $S_2$ .

300 Calcite veins V1b, up to 1 cm long and less than one mm thick, were also identified at microscopic scale (Fig. 6D, F). The vein cement (Cc1b) consists of up to 0.1 mm calcite crystals with a blocky texture and a bright yellow luminescence. These veins postdate the previous V0 and V1a generations and trend perpendicular to stylolites e2.

Towards the fault plane, the thrust zone foliation  $S_2$  is progressively more closely-spaced and stylolites e2 become more abundant (showing mm spacing) and exhibit ambiguous cross-cutting relationships with veins V1b (Fig. 6F). The main slip surface corresponds to a discrete plane that contains calcite slickensides (veins V2). The vein cement (Cc2) is milky white in hand sample and consists of up to 3 mm blocky to elongated blocky crystals (Fig. 6G) with a dull to bright orange luminescence (Fig. 6H).

310 Deformation in the footwall is concentrated within the main thrust zone and subsidiary thrust zones and corresponds to the thrust zone foliation ( $S_2$ ) and calcite veins V3 (Fig. 3). This foliation ( $S_2$ ) strikes NW-SE, dips towards the NE and is mm to cm spaced (Fig. 7A). Calcite veins V3 are generally 1 – 2 cm thick and strike NW-SE. They are parallel or locally branch off cutting the  $S_2$  planes in the subsidiary thrust zone (Fig. 7A, B). Outside the thrust zone, veins V3 are locally present but have a NE-SW strike. These veins are mostly less than 1 m long and are spaced between a few cm and 50 cm. The vein cement (Cc3) is made up of a milky white calcite characterized by up to 3 mm long fibrous crystals oriented perpendicular to the vein walls (Fig. 7C). Locally, anhedral blocky crystals ranging in size from 0.1 to 1 mm are also present. This cement displays a bright yellow to bright orange luminescence (Fig. 7D).

Eliminado: D

Eliminado: again

Eliminado: with densities between 5 and 8 stylolites/cm.

Eliminado: D

Eliminado: a

Eliminado: ( $S_{SP}$ )

Eliminado: ¶

Eliminado: e

Eliminado: foliation

### 4.1.3 Footwall

In the footwall, the Stephano-Permian Erill Castell Formation comprises massive, dark-greenish andesitic levels showing a rhythmic magmatic layering (Fig. 7E), which corresponds to a fluidal structure of the host rock. The local presence of pyroclastic and brecciated volcanoclastic levels is also ubiquitous mainly in the lower part of this sequence. Andesites are characterized by a porphyritic texture defined by a dark fine-grained spherulitic matrix partially devitrified and large zoned crystals of plagioclase (Fig. 7F), up to 2 – 3 cm long, and less abundant biotite and hornblende. These mafic phenocrystals are systematically pseudomorphosed by clay minerals and frequently show evidence of oxidation and chloritization. Andesites are affected by E-W striking open joints (J1) dipping indistinctively towards the north and south (Fig. 7E). These joints locally trend parallel to the magmatic layering (Fig. 3).

Finally, as described above, the northern and southern limits of both the Cerc basin and the Estamariu thrust correspond to two Neogene extensional faults, La Seu d'Urgell and the Ortedó fault systems (Fig 1C). These faults are subvertical or steeply dip towards the north. In the northern part, the slip plane of La Seu d'Urgell fault has not been observed and the limit between the Stephano-Permian rocks and the Neogene deposits is not well constrained due to the poor quality of the Neogene outcrops and the presence of Quaternary deposits. In the southern part, the Ortedó fault generates a several meter-thick dark greyish to brown fault zone, characterized by the presence of clay-rich incohesive fault rocks developed at the contact between Stephano-Permian and Upper Ordovician rocks. Related to these main fault systems, mesoscale normal faults commonly affect the andesites within the Cerc basin. These faults are mainly E-W and locally NE-SW, are subvertical and dip indistinctly towards the N and S. Fault planes are locally mineralized with calcite cement (veins V4) and exhibit two striae set generations indicating dip-slip and strike-slip movements (Fig. 8A). The calcite cement (Cc4) consists of up to 2 mm blocky to elongated blocky crystals (Fig. 8B) with a homogeneous dark orange luminescence (Fig. 8C). On the other hand, the main Estamariu thrust zone is locally displaced by shear fractures (Fig. 8D) and a later set of shear bands (Cn) (Fig. 8E), both having an overall NNW-SSE to NNE-SSW strike (Fig. 3) that indicate a minor normal displacement. Shear fractures are locally mineralized with calcite (veins V5). The vein cement consists of a greyish microsparite calcite cement (Cc5) (Fig. 8F-G).

### 4.2 Geochemistry of calcite cements and host rocks

The geochemistry ( $\delta^{18}\text{O}$ ,  $\delta^{13}\text{C}$ ,  $\delta^{18}\text{O}_{\text{fluid}}$ ,  $^{87}\text{Sr}/^{86}\text{Sr}$ ,  $^{143}\text{Nd}/^{144}\text{Nd}$  and elemental composition) and the calculated temperature of precipitation of the different calcite cements Cc1a to Cc5 are described below. Veins V0 and V1b were only observed at microscopic scale and their calcite cement Cc0 and Cc1b could not be sampled to perform these geochemical analyses.

The  $\delta^{18}\text{O}$  and  $\delta^{13}\text{C}$  isotopic composition of the carbonate fraction of the Devonian hanging wall and the different calcite cements (Cc1a to Cc5) are summarized in Table 1 and represented in Fig. 9. The micritic matrix of the Devonian packstone ranges in  $\delta^{18}\text{O}$  values between -10.5 and -8.4 ‰ VPDB and in  $\delta^{13}\text{C}$  values between +1.5 and +2.8 ‰ VPDB, whereas the calcite cements have a broader range of values depending on the cement generation (Fig. 9).

Con formato: Título 3

Con formato: Color de fuente: Automático, Inglés (Reino Unido)

Eliminado: (Sm)

Eliminado: greatly

Eliminado: (V4)

Eliminado: are also frequent affecting

Eliminado: (V5)

Eliminado: (V5)

Calcite cement Cc1a has  $\delta^{18}\text{O}$  values between -11.3 and -10.3 ‰VPDB and  $\delta^{13}\text{C}$  values between +0.8 and +2.1 ‰VPDB. Cc2 is characterized by  $\delta^{18}\text{O}$  values between -14.9 and -12.9 ‰VPDB and  $\delta^{13}\text{C}$  values between -1.2 and +1.5 ‰VPDB. Cc3 has  $\delta^{18}\text{O}$  values between -14.3 and -13.4 ‰VPDB and  $\delta^{13}\text{C}$  values between -9.3 and -6.9 ‰VPDB. Cc4 exhibits  $\delta^{18}\text{O}$  values between -13.8 and -13.4 ‰VPDB and  $\delta^{13}\text{C}$  values between -7.4 and -7.2 ‰VPDB and Cc5 ranges in  $\delta^{18}\text{O}$  between -8.1 and -5.7 ‰VPDB and in  $\delta^{13}\text{C}$  between -8.2 and -3.8 ‰VPDB. The calcite cement Cc1a, precipitated in the fault zone affecting the Devonian hanging wall, has enriched  $\delta^{13}\text{C}$  values, whilst the calcite cement within the fault plane (Cc2) exhibits either negative or positive  $\delta^{13}\text{C}$  values and the calcite cements hosted in the Stephano-Permian andesites (Cc3 to Cc5) have more depleted  $\delta^{13}\text{C}$  values (Fig. 9). In addition, calcite cements show a progressive depletion in  $\delta^{18}\text{O}$  from Cc1a to Cc4, whereas Cc5 displays more enriched  $\delta^{18}\text{O}$  values.

The obtained  $\Delta_{47}$  values from clumped isotope thermometry were converted into temperatures and  $\delta^{18}\text{O}_{\text{fluid}}$  (Table 1 and Fig. 10) using the equation of (Kluge et al., 2015) and (Friedman and O'Neil, 1977), respectively. Cc2 has a  $\Delta_{47}$  of 0.567, which translates into a temperature between 56 and 98 °C and a  $\delta^{18}\text{O}_{\text{fluid}}$  between -6.4 and -0.3 ‰VSMOW. For Cc3,  $\Delta_{47}$  is 0.045 and the calculated T and  $\delta^{18}\text{O}_{\text{fluid}}$  are 127 to 208 °C and +4.3 to +12.1 ‰VSMOW, respectively.  $\Delta_{47}$  for Cc4 is 0.48, which translates into a T and a  $\delta^{18}\text{O}_{\text{fluid}}$  between 102 to 167 °C and +0.9 to +8.1 ‰VSMOW, respectively. For Cc5 the  $\Delta_{47}$  is 0.77 and the calculated T and a  $\delta^{18}\text{O}_{\text{fluid}}$  are between -5 and +3 °C and between -12.4 and -10.1 ‰VSMOW, respectively.

The  $^{87}\text{Sr}/^{86}\text{Sr}$  ratio of calcite cements Cc1a to Cc5 and host rocks are reported in Table 1 and Fig. 11. Devonian limestones from the hanging wall have a  $^{87}\text{Sr}/^{86}\text{Sr}$  ratio of 0.710663, whilst the Stephano-Permian andesites in the footwall exhibit a more radiogenic  $^{87}\text{Sr}/^{86}\text{Sr}$  ratio of 0.743983. The calcite cements have more radiogenic  $^{87}\text{Sr}/^{86}\text{Sr}$  ratios than the Devonian limestones but less radiogenic values than the Stephano-Permian andesites. This ratio ranges from 0.713018 to 0.714092 in Cc1a, is 0.718294 for Cc2, 0.714619 for Cc3, 0.717706 for Cc4 and 0.716923 for Cc5. These results are compared with already published data from synkinematic veins and deformed rocks in other Pyrenean structures developed in the basement and in the sedimentary cover during the Pyrenean compression (Fig. 11). This comparison shows that values obtained in this study are: 1) significantly more radiogenic than the values of marine carbonates and synkinematic veins precipitated in the sedimentary cover (i.e., in the South Pyrenean fault and thrust belt); and, 2) within the same range of values of synkinematic veins and deformed rocks in the Pyrenean basement (Axial Zone).

The analyzed samples for  $^{143}\text{Nd}/^{144}\text{Nd}$  ratios in calcite cements and host rocks are reported in Table 1. However, due to the general low Nd concentrations in most of the analyzed calcite cements and the limited amount of powdered samples that were available, only calcite cement Cc5 and the andesite host rock (footwall) could be measured. Cc5 has a  $^{143}\text{Nd}/^{144}\text{Nd}$  ratio of 0.512178, which is similar to the one of its footwall host rocks, which is 0.512196.

The obtained elemental composition broadly varies among the different calcite cements and related host rocks (Table 2 and Fig. 12). In the thrust zone affecting the hanging wall, calcite cement Cc1a shows a similar trend to that of the Devonian limestones, both having high Sr, intermediate-high Mg and Fe and low Mn contents (Fig. 12). In the main thrust plane, calcite cement Cc2 has low Mg and Fe and intermediate Mn and Sr contents with respect to the other cements. In the footwall, Cc3 and Cc4 have similar elemental composition, characterized by high Mn, intermediate-high Sr, intermediate-low Fe and low

Mg contents. Finally, calcite cement Cc5 follows a similar trend to that of the Stephano-Permian andesites, both having the highest Fe and Mg and the lowest Sr and Mn contents with respect to the other cements and host rocks.

## 5 Discussion

### 5.1 Chronology of the observed structures

400 The Estamariu thrust, affecting basement rocks in the Axial Pyrenees, resulted from a long-lived tectonic history that lasted from Variscan to Neogene times.

The Paleozoic metasedimentary rocks from the Pyrenean basement are broadly affected by multiscale folds and axial plane regional foliation, developed during the main Variscan deformation phase (Bons, 1988; Cochelin et al., 2018; Zwart, 1986).

410 Similar structures, a decametric-scale anticline and pervasive axial plane foliation ( $S_1$ ), are found in the Devonian sequence located in the thrust hanging wall (Fig. 2B) and therefore, we consider them to be developed during the Variscan compression,

contemporaneous with the main activity of the Estamariu thrust. Veins V0 are perpendicular to stylonites e1 and show ambiguous crosscutting relationships between them. Thus, they are interpreted as originated coevally. Both microstructures are concentrated into discontinuous fragments of the Devonian host rocks and are therefore considered inherited microstructures likely developed in Variscan times. However, as pointed above, in the study area the Estamariu thrust affects

415 late- to post-Variscan Stephano-Permian andesites, confirming thus its reactivation during the Alpine orogeny. Accordingly, the structures that are strictly attributed to the Alpine reactivation of the thrust are those structures indicating reverse kinematics or associated with a compressional stress, which are found within the thrust zone deformation, at the contact between Devonian and Stephano-Permian units. Contrarily, the magmatic layering and joints J1 are broadly present in the andesitic footwall, outside the thrust zone, and in other Stephano-Permian basins, and are therefore considered inherited fluidal and cooling

structures, respectively. For this reason, the calcite veins V1a and V2 (and related cements Cc1a and Cc2), exclusively occurring within the thrust zone, have been associated with the reactivation of the Estamariu thrust. During this period, and associated with ongoing deformation and progressive shortening, stylonites e2 developed as sutured areas between host rock and veins V1a and between foliation surfaces, coevally with the development of veins V1b, as denoted by their crosscutting relationships and orientations.

420 Other structures present in the study area, such as veins V3 to V5 and related cements Cc3 to Cc5, are attributed to the Neogene extension. Veins V3 precipitated in the subsidiary thrust zone developed in the footwall of the Estamariu thrust. These veins strike parallel to the thrust zone foliation ( $S_2$ ) (Fig 7A, B) but are characterized by calcite fibers growing perpendicular to the vein walls and to the foliation surfaces (Fig. 7C), thus evidencing their extensional character. The presence of extensional calcite veins opened along previously formed foliation surfaces in a thrust zone has been reported in other structures in the

Pyrenees and has been considered to postdate the thrust activity (Lacroix et al., 2011, 2014). Veins V4 precipitated in subvertical and E-W mesoscale faults affecting the Stephano-Permian andesites (Fig. 8), outside the thrust zone (Fig. 3). The fault orientation and dip and the two striae set generations observed on the fault planes are compatible with the Neogene

425

**Movido hacia arriba[1]:** U-Pb dating of calcite cements Cc1a to Cc5 failed due to their high lead contents and low uranium contents and therefore, the timing of the different mesostructures and microstructures has been determined by means of crosscutting relationships and microstructural analysis.

**Eliminado:** n.

extensional faults that bound the Cerc basin and postdate the Estamariu thrust (Cabrera et al., 1988; Roca, 1996; Saura, 2004).

435 Calcite cements Cc3 and Cc4, occluding veins V3 and V4, have a similar geochemical composition (Fig. 9 – 12), supporting  
that their precipitation occurred during the same tectonic event and associated with a similar fluid regime (i.e., although these  
440 cements precipitated in different structures, they are likely contemporaneous). Finally, veins V5 (and related cement Cc5)  
precipitated locally in shear fractures crosscutting and postdating the thrust-related deformation (Fig. 3, 4 and 8D). These veins  
strike parallel to the shear bands (Cn) located in the main thrust zone (Fig. 8E), exhibiting normal slip kinematics, postdating  
the reverse structures and therefore indicating reactivation of the Estamariu thrust during the Neogene extension.

## 5.2 Fluid system during the Alpine reactivation of the Estamariu thrust

As veins V1a and V2 developed during the Alpine reactivation of the Estamariu thrust, the geochemistry of their related calcite  
cements Cc1a and Cc2 record the fluid system during this tectonic event.

445 Calcite cements Cc1a and Cc2 are characterized by high  $^{87}\text{Sr}/^{86}\text{Sr}$  ratios (from 0.713 to 0.714 for Cc1a and 0.718 for Cc2),  
significantly more radiogenic than ratios of Phanerozoic seawater (between 0.7070 and 0.7090) (McArthur et al., 2012). This  
may reflect the incorporation of radiogenic Sr from a fluid derived or interacted with Rb-rich and/or Sr-rich basement rocks  
such as those underlying the Estamariu thrust. Previous studies in the Pyrenees reported similar  $^{87}\text{Sr}/^{86}\text{Sr}$  ratios in Paleozoic  
450 rocks and in related synkinematic veins (Wayne and McCaig, 1998; McCaig et al., 1995; Banks et al., 1991; Bickle et al.,  
1988) (Fig. 11). Contrarily, rocks from the Mesozoic-Cenozoic cover in the Southern Pyrenean fold and thrust belt have similar  
or slightly higher  $^{87}\text{Sr}/^{86}\text{Sr}$  ratios with respect to Phanerozoic seawater (Fig. 11). On the other hand, Cc1a has a narrow range  
of  $\delta^{13}\text{C}$ , between +0.91 and +2 ‰VPDB, consistent with values of the Devonian marine limestones from the hanging wall  
(between +1.54 and +2.75 ‰VPDB) and within the range of Devonian marine carbonate values (Veizer et al., 1999). Likewise,  
the elemental composition of Cc1a follows a similar trend to that of its Devonian host, both having high Mg and Sr and low  
Mn contents with respect to the other calcite cements (Fig. 12). These geochemical similarities indicate high fluid-rock

455 interaction and buffering of the carbon and elemental composition of the precipitating fluid by the Devonian carbonates  
(Marshall, 1992). Calcite cement Cc2 has slightly lower  $\delta^{13}\text{C}$ , lower Mg and Sr and higher Mn contents with respect to both  
Cc1a and the Devonian host. On the other hand, the temperature and the  $\delta^{18}\text{O}$  composition of the vein-forming fluids, calculated  
from clumped isotope thermometry of Cc2, range between 56 °C and 96 °C and between -6.4 and -0.3 ‰SMOW, respectively.

These values are interpreted as the involvement of heated meteoric fluids. These fluids, which probably heated at depth and  
460 were enriched in radiogenic Sr during their flow and interaction with basement rocks, flowed preferentially along the thrust  
zone (Fig. 13A), as evidenced by the exclusive presence of calcite in this area, due to the enhanced permeability associated  
with the thrust discontinuity (McCaig et al., 1995; Trinca et al., 2017). As Cc1a and Cc2 precipitated during the same tectonic  
event but in different structural positions within the thrust zone, they likely precipitated from the same fluids, progressively  
increasing the fluid-rock interaction from the thrust plane (Cc2) towards the hanging wall (Cc1a). Previous studies already  
465 reported syntectonic migration of fluids that had interacted at depth with basement rocks before upflowing along thrust zones

Eliminado: c

Eliminado: crystalline

Eliminado: crystalline rocks

Eliminado: developed in the Pyrenean basement

Eliminado: trend

Eliminado: through

Eliminado: crystalline

Eliminado: channelized

Eliminado: channelized

Eliminado: fluid

Eliminado: the

in other structures from the Pyrenean basement, such as the Gavarnie thrust and the related Pic-de-Port-Vieux thrust (McCaig et al., 1995).

### 5.3 Fluid system during the Neogene extension

480 Calcite veins V3 to V5 are attributed to the Neogene extension and the geochemistry of their related calcite cements Cc3 to Cc5 characterize the fluid system during this period.

Cc3 and Cc4 have considerably high  $^{87}\text{Sr}/^{86}\text{Sr}$  ratios (0.714619 and 0.717706, respectively), similar to the ones reported for Cc1a and Cc2 (Fig. 11), indicating interaction with basement rocks. The  $\delta^{18}\text{O}_{\text{fluid}}$  calculated from clumped isotopes, between +4.3 and +12.1 ‰SMOW for Cc3 and between +0.9 and +8.1 ‰SMOW for Cc4, falls within the range of metamorphic and/or

485 formation brines (Taylor, 1987). The  $\delta^{18}\text{O}$ -depleted values of these cements (around -14 ‰VPDB) are due to the high temperatures of the fluids (between 127 °C and 208 °C for Cc3 and between 102 °C and 167 °C for Cc4). Assuming a normal geothermal gradient of 30 °C, these temperatures would have been reached at a minimum depth of 3 – 5 km. However, these veins have never reached such a burial depth, since during the Neogene extension the studied structure acquired its current configuration (Saura, 2004) and was only buried under the Devonian sequence (hanging wall), which has a maximum thickness

490 of several hundred meters (Mey, 1967). This assumption evidences the hydrothermal character of the circulating fluids, which probably migrated rapid enough through normal faults to maintain their high temperatures and to be in thermal disequilibrium with the surrounding rocks. Similarly, the high Mn content of Cc3 and Cc4 (around 7700-8300 and 4000 ppm, respectively), responsible of their bright luminescence (Fig. 7D, 8C), is consistent with hydrothermal waters (Pfeifer et al., 1988; Pomerol, 1983; Pratt et al., 1991). On the other hand, the  $\delta^{13}\text{C}$ -depleted values of these cements are indicative of the influence of organic

495 derived carbon (Cerling, 1984; Vilasi et al., 2006). The most probable source for these low  $\delta^{13}\text{C}$  values is the Silurian black shales that do not crop out in the study area but acted as the main detachment level during the Variscan compression, and locally during the Alpine compression, in the Pyrenean Axial Zone (Mey, 1967). These black shales have significant organic carbon contents (TOC around 2.3%), and around the Gavarnie thrust, they exhibit syntectonic carbonate veins yielding  $\delta^{13}\text{C}$  values between -2 and -8 ‰VPDB (McCaig et al., 1995). Thus, cements Cc3 and Cc4 precipitated from hydrothermal fluids

500 derived and/or equilibrated with basement rocks and expelled through newly formed and reactivated fault zones during deformation (Fig. 13B). The hydrothermal character of the fluids involved in this deformation event, and their relative high temperatures (up to 200°C) could have altered the clumped isotope composition of the previous calcite cement generations (Cc1a and Cc2). Clumped isotopes may be reset by recrystallization and by solid-state isotopic exchange reactions and diffusion within the mineral lattice (Shenton et al., 2015; Stolper and Eiler, 2015). However, in the studied vein samples, there is no evidence of calcite recrystallization (for instance, grain coarsening linked to grain boundary migration). Additionally, this hydrothermal event probably took place during a relatively short period of time (during precipitation of cements Cc3 and Cc4). Solid-state reordering needs temperatures in excess of 120°C during a period of at least 10 Ma, and probably longer (Henkes et al., 2014). Therefore, we conclude that although it is possible, there is little chance for crumpled isotopes of cements Cc1a and Cc2 to have been reset during precipitation of Cc3 and Cc4.

Eliminado: ,

Eliminado: these shales

Eliminado: have

Eliminado: crystalline

515 Finally, the isotopic signature of Cc5, ranging between -8.1 and -5.7 ‰VPDB for  $\delta^{18}\text{O}$  and between -8.2 and -3.8 ‰VPDB  
for  $\delta^{13}\text{C}$ , indicates a meteoric origin. The similar tendency in the elemental composition of this cement and the Stephano-  
Permian volcanic rocks, both having the highest Mg and Fe and the lowest Mn and Sr contents with respect to the other cements  
and host rocks, reveals high fluid-rock interaction with the footwall rocks. The significant water-rock interaction is also  
520 demonstrated by the Nd isotopic composition of Cc5 (0.512178), yielding to values of the volcanic host (0.512196). This fact,  
together with the scarcity and small size of Cc5 veins, indicate that this cement precipitated from percolation of meteoric fluids,  
which geochemistry was controlled by its volcanic host rock. The  $\delta^{18}\text{O}_{\text{fluid}}$  and the temperature of precipitation calculated from  
clumped isotopes, ranging between -12.4 and -10.1 ‰SMOW and between -5 and 3°C, respectively. These values corroborate  
525 the meteoric origin and may be indicative of high latitude and/or high altitude conditions (Dansgaard, 1964), because the  
 $\delta^{18}\text{O}_{\text{fluid}}$  and the temperature decrease with elevation (Huyghe et al., 2018). During the Neogene, the study area was  
approximately at the same latitude as today (Smith, 1996). Studies focused on infiltration of meteoric fluids and subsequent  
upflowing along La Tet fault during the Neogene extension, have shown that meteoric waters in the area infiltrate at high  
altitudes, around 2000 m, and low temperatures, around 5°C (Krimissa et al., 1994; Taillefer et al., 2018). On the other hand,  
the widespread presence of glacial and fluvio-glacial deposits has been reported unconformably overlying the Neogene basin  
infill and the Variscan rocks from the eastern Axial Pyrenees (Roca, 1996; Turu i Michels and Peña Monné, 2006). These  
530 deposits reflect several Quaternary glacial periods in the area, which in turn could have contributed to the low temperature and  
low  $\delta^{18}\text{O}_{\text{fluid}}$  (Gregory et al., 1989). In any case, precipitation of Cc5 probably took place during the latest stages of extension,  
after the fluid regime changed from upward fluid migration to percolation of cold meteoric waters, as also occurred in the  
Barcelona Plain (Catalan Coastal Ranges) (Cantarero et al., 2014).

In conclusion, the high  $^{87}\text{Sr}/^{86}\text{Sr}$  ratios of the different calcite cements (Cc1a to Cc5) evidence the interaction between the vein-  
535 forming fluids and Paleozoic basement rocks with higher radiogenic signature than those of the Mesozoic sedimentary cover  
(located in the Southern Pyrenees). The geochemical evolution of these cement generations also highlights the progressive  
change in the fluid regime and composition during successive compressional and extensional tectonic events (Fig. 13). The  
continuous increase in precipitation temperatures and enrichment in  $\delta^{18}\text{O}_{\text{fluid}}$  from calcite cements Cc1a and Cc2 (Alpine) to  
cements Cc3 and Cc4 (Neogene) is probably linked to higher extent of fluid-rock interaction with basement rocks. By contrast,  
540 during the latest stages of extension, the fluids responsible for precipitation of Cc5 are characterized by lower precipitation  
temperatures and lighter  $\delta^{18}\text{O}_{\text{fluid}}$ , evidencing a more significant change in the fluid regime and the infiltration of cold meteoric  
fluids (Fig. 13).

#### 5.4 Influence of Paleozoic basement rocks on fluid chemistry during deformation

545 In this section, we assess the influence of basement rocks on the chemistry of fluids during deformation. As pointed above,  
previous studies constrained the relationships between deformation and fluid migration in other structures from the Mesozoic  
and Cenozoic cover (Cruset et al., 2016, 2018; Travé et al., 1997, 2000), and to a lesser extent, from the Paleozoic basement

Con formato: Inglés (Reino Unido)

Eliminado: .

Eliminado: than

Con formato: No ajustar espacio entre texto latino y asiático,  
No ajustar espacio entre texto asiático y números

Con formato: Fuente: 10 pto

Con formato: Fuente: (Predeterminada) Times, Inglés (Reino Unido)

Eliminado: crystalline

Eliminado: The aim of this study was to provide insights into the behavior and evolution of fluids circulating through a long-lived thrust, and to determine

Eliminado: fluid



(Banks et al., 1991; McCaig et al., 1995, 2000b; Wayne and McCaig, 1998). The comparison between these studies and the new data provided in this contribution evidences that fluids migrating through basement or cover units have a different geochemical signature. This signature is recorded in the vein cements, particularly in their  $^{87}\text{Sr}/^{86}\text{Sr}$  ratios. Accordingly, the high  $^{87}\text{Sr}/^{86}\text{Sr}$  ratios (0.713 to 0.718) of the analyzed calcite cements, originated during successive compressional and extensional tectonic events, indicate that regardless of the origin of the fluids and the tectonic context, basement rocks have a significant influence on the fluid chemistry. This implies that cements precipitated from fluids that have circulated through basement rocks have significantly high  $^{87}\text{Sr}/^{86}\text{Sr}$  ratios ( $> 0.710$ ) (Fig. 11), reflecting the interaction between the vein-forming fluids and rocks with a high radiogenic signature. Similar high radiogenic  $^{87}\text{Sr}/^{86}\text{Sr}$  ratios have also been attributed to basement-derived fluids in the Glarus nappe (Swiss Alps) (Burkhard et al., 1992). By contrast, vein cements precipitated from fluids that have circulated through the Mesozoic–Cenozoic sedimentary cover in the Pyrenees (i.e., through younger rocks with a different radiogenic signature) have significantly lower  $^{87}\text{Sr}/^{86}\text{Sr}$  ratios ( $< 0.710$ ). Such lower values may be similar to Phanerozoic seawater values, evidencing interaction between the vein-forming fluids and marine carbonate units, or higher, evidencing interaction with siliciclastic rocks (Cruset et al., 2018; Travé et al., 2007). A previous study, focused on fluid flow along the Gavarnie thrust in the central-western Axial Pyrenees, used this limit value ( $^{87}\text{Sr}/^{86}\text{Sr} = 0.710$ ) to differentiate between the unaltered limestone protolith and the Cretaceous thrust-related carbonate mylonite affected by fluids carrying radiogenic Sr (McCaig et al., 1995).

Eliminado: means

Eliminado: crystalline

Eliminado: with Rb-rich source

#### 5.5 Fluid flow at regional scale: the NE part of the Iberian Peninsula during the Neogene extension

During the late Oligocene to middle Miocene, the opening of the NW Mediterranean Sea was responsible for the development of a complex ENE-WSW to NE-SW extensional fault system in the NE part of the Iberian Peninsula (Roca, 1996; Roca and Guimerà, 1992; Vergés et al., 2002). In the eastern Axial Pyrenees, La Tet fault is the main Neogene structure and has associated major E-W extensional faults, such as the Ortadó and La Seu d'Urgell faults, which crosscut the Alpine structures (e.g., the reactivation of the Estamariu thrust) and delimitate the Cerc basin (Fig. 1). Within this basin, E-W mesoscale normal faults (and related veins V4) also developed during this period and previously formed weakness surfaces were reopened (i.e., the thrust zone foliation associated with the Estamariu thrust, veins V3). During this episode, calcite cements Cc3 and Cc4 precipitated from hydrothermal fluids (temperatures between 102 and 208 °C) that interacted at depth with basement rocks before ascending through newly formed fault zones and reactivated structures. These interpretations are consistent with the presence of several hydrothermal springs (temperatures of 29 °C to 73 °C) currently upwelling aligned along La Tet fault and related Neogene deformation in the Pyrenean Axial Zone (Krimissa et al., 1994; Taillefer et al., 2017, 2018). Several studies indicate the origin of these hot water springs as meteoric fluids, infiltrated at high-elevated reliefs, above 2000 m, warmed at great depths by normal geothermal gradients, and migrated upwards along permeability anisotropies related to fault zones (Taillefer et al., 2017, 2018). The geochemical analysis of these springs, and in particular their high radiogenic  $^{87}\text{Sr}/^{86}\text{Sr}$  ratios, ranging between 0.715 and 0.730, according to French Geological Survey reports (Caballero et al., 2012), are within the range of values obtained in this study and also accounts for interaction between circulating fluids and basement lithologies. Studies

Eliminado: derived

Eliminado: crystalline

Eliminado: crystalline

Eliminado: rocks

595 based on numerical models suggest that La Tet fault and the involved **basement** rocks are still permeable down to 3 km depth (Taillefer et al., 2017, 2018), although the fault has been dormant since the Mio-Pliocene (Goula et al., 1999). These authors also suggest that the footwall topography is the major factor controlling the infiltration of meteoric fluids and the recharge of the hydrothermal system. The topography, which induces high hydraulic gradients and produces fluid advection, controls the circulation depth and therefore, the maximum temperature reached by the migrating fluids (Taillefer et al., 2017).

Eliminado: crystalline

600 A similar geological context and fluid regime evolution to that explained above is found in the Barcelona Plain and the Vallès Basin, located in the northeast part of the Catalan Coastal Ranges (CCR) (Fig. 1A). Consequently, the comparison between both geological contexts allows us to give insights into the fluid circulation in extensional basins at regional scale (in the NE part of Iberia). In these locations of the CCR, the main fault system associated with the Neogene extension acted as conduits for hydrothermal fluid circulation at temperatures between 130 and 150 °C during synkinematic periods (Cantarero et al., 2014; Cardellach et al., 2003), and is also responsible for the present-day circulation of hot water springs up to 70 °C (Carmona et al., 2000; Fernández and Banda, 1990). In both cases, fluids would have been topographically driven from elevated areas to

Eliminado: crystalline

610 great depths (Cantarero et al., 2014), where they circulated through **basement** rocks, acquiring high  $^{87}\text{Sr}/^{86}\text{Sr}$  ratios ( $> 0.712$ ) and high temperatures (Cardellach et al., 2003) before ascending through fault discontinuities. However, in the Penedès basin, which corresponds to the southwestern termination of the Neogene structure in the CCR, **basement lithologies** do not crop out and the extensional faults only involve Neogene deposits filling the basin and a Mesozoic sedimentary substrate. In this location, the main fault system acted as conduits for several episodes of meteoric fluids percolation during the Neogene extension and evidence of hydrothermal fluid circulation has not been reported in the area (Travé and Calvet, 2001; Travé et al., 1998; Baqués et al., 2012, 2010). This fact agrees with previous studies that highlight that hydrothermal activity, and in particular the occurrence of hot water springs in the Pyrenees and in the CCR, is preferably concentrated in basement rocks, which constitute the elevated footwall of the main extensional fault systems (Taillefer et al., 2017; Carmona et al., 2000).

Eliminado: crystalline

Eliminado: rocks

615 All these observations indicate that the fluids responsible for precipitation of synkinematic cements during Neogene times in the eastern Axial Pyrenees and in the northeast part of the CCR, and fluids currently flowing through Neogene extensional faults in both places are hydrothermal and **are sourced and/or interacted with similar basement rocks**. This evidences an open fluid system in the NE part of the Iberian Peninsula associated with the Neogene extensional deformation. Accordingly, this extensional fault system has acted as a conduit for **circulation of hot fluids in Neogene times and in the present**. This fault-controlled fluid flow could have been continuous through time or could be related to intermittent pulses. Fault control on upflowing of hot fluids along fault systems is a common process in different geological settings and has been reported in the Great Basin, USA (Faulds et al., 2010; Nelson et al., 2006), in the Western Turkey (Faulds et al., 2010), in the Southern Canadian Cordillera (Grasby and Hutcheon, 2001) **and in the southern Tuscany, Italy (Liotta et al., 2010)**.

Eliminado:

Eliminado: have crystalline basement rocks as a common reservoir

Eliminado: long-term

Eliminado: from

Eliminado: to

Eliminado: long-term

Eliminado: , in the Basin and Range Province (Nelson et al., 2006)

## 635 6 Conclusions

The Estamariu thrust, in the Pyrenean Axial Zone, resulted from a multistage Variscan to Neogene tectonic evolution. Our data, combining structural and petrological observations with geochemical analyses of synkinematic calcite veins and host rocks, provide a structural and diagenetic framework that constrains the fault-fluid system evolution and assesses the relationships between deformation and fluid migration in the **Paleozoic** Pyrenean basement. In the study area, the Variscan  
640 Estamariu thrust places a Devonian pre-Variscan unit against a Stephano-Permian late to post-Variscan sequence and therefore, the structures present within the thrust zone, affecting both sequences, are attributed to the Alpine and subsequent Neogene reactivation of the thrust. During the Alpine compression, the reactivation of the thrust resulted in the transposition of the Variscan regional foliation within the thrust zone and in the formation of a subsidiary thrust zone affecting the andesites in the footwall. During this period, meteoric fluids interacted with **basement rocks** and **migrated upwards along the thrust** and related  
645 structures at temperatures between 56 and 98 °C. These fluids progressively increased the fluid-rock interaction from the thrust plane towards the hanging wall. During the Neogene extension, the Estamariu thrust was reactivated and normal faults and shear fractures were formed. These structures allowed basement-derived fluids to flow upwards through reactivated and newly formed fault zones at temperatures up to 208 °C. Finally, during the latest to post stages of extension and uplift of the structure, the fluid regime changed to percolation of low temperature meteoric fluids that were buffered by the volcanic host rocks.

650 The comparison between our results and previously published data allows us to provide insights into the fluid characteristics and fluid regime at regional scale. On the one hand, the influence of basement rocks on the fluid chemistry during deformation in the Pyrenees has been assessed. In this sense, regardless the fluid origin and the tectonic context, the fluids that have interacted with **basement rocks** have a significantly higher  $^{87}\text{Sr}/^{86}\text{Sr}$  ratio ( $> 0.710$ ) with respect to those that have circulated through the sedimentary cover ( $< 0.710$ ). On the other hand, a similar fluid regime associated with the Neogene extension in  
655 the NE part of the Iberian Peninsula (including the eastern Pyrenees and the northeastern part of the Catalan Coastal Ranges) has been observed. In both settings, the extensional deformation structures have acted as conduits for **fluid migration in** Neogene times **and in the present**. **Fluids migrating during this period** are hydrothermal and have interacted with **basement** rocks before ascending through fault zones and related structures.

### Data availability

660 The data used in this study is included within the manuscript.

### Author contributions

Conceptualization, DM-L,GA, DC, IC; AT; data curation, DM-L; formal analysis, all authors; funding acquisition, AT; investigation and methodology, all authors; writing-original draft preparation, DM-L; writing-review and editing, all authors.

Eliminado: the crystalline

Eliminado: crystalline

Eliminado: long-term

Eliminado: from

Eliminado: to

Eliminado: M

Eliminado: fluids

Eliminado: crystalline

Con formato: Normal

### **Competing interest**

The authors declare that they have no conflict of interest.

Con formato: Normal

### 675 **Acknowledgments**

We acknowledge the constructive comments from Owen Callahan and Brice Lacroix, who helped to improve the quality of the manuscript, as well as the editorial guidance of Randolph Williams. We also thank Josep Maria Casas, from the Universitat de Barcelona, for showing us the location of the studied outcrops. Carbon and oxygen isotopic analyses were carried out at “Centre Científics i Tecnològics” of the Universitat de Barcelona. Strontium and Neodymium analyses were performed at the “CAI de Geocronología y Geoquímica Isotópica” of the Universidad Complutense de Madrid. The Elemental composition was analysed at the Geochemistry Facility of labGEOTOP of Geosciences Barcelona (GEO3BCN-CSIC). Clumped isotope thermometry was carried out at the Imperial College London. This research was carried out within the framework of DGICYT Spanish Project PGC2018-093903-B-C22 (Ministerio de Ciencia, Innovación y Universidades / Agencia Estatal de Investigación / Fondo Europeo de Desarrollo Regional, Unión Europea) and the Grup Consolidat de Recerca “Geologia Sedimentària” (2017-SGR- 824). The PhD research of DM-L is supported by the FPI2016 (BES-2016-077214) Spanish program from MINECO.

Eliminado: the Institute of Earth Sciences Jaume Almera

Eliminado: ICTJA

Con formato: Español (España)

### **References**

Arndt, M., Virgo, S., Cox, S. F. and Urai, J. L.: Changes in fluid pathways in a calcite vein mesh (Natih Formation, Oman Mountains): insights from stable isotopes, *Geofluids*, 14(4), 391–418, doi:10.1111/gfl.12083, 2014.

690 Banks, D., Da Vies, G., Yardley, B. W., McCaig, A. and Grant, N.: The chemistry of brines from an Alpine thrust system in the Central Pyrenees: An application of fluid inclusion analysis to the study of fluid behaviour in orogenesis, *Geochim. Cosmochim. Acta*, 55(4), 1021–1030, doi:10.1016/0016-7037(91)90160-7, 1991.

Baques, V., Trave, A., Roca, E., Marin, M. and Cantarero, I.: Geofluid behaviour in successive extensional and compressional events: a case study from the southwestern end of the Valles-Penedes Fault (Catalan Coastal Ranges, NE Spain), *Pet. Geosci.*, 18(1), 17–31, doi:10.1144/1354-079311-017, 2012.

Barker, S. L. L. and Cox, S. F.: Evolution of fluid chemistry and fluid-flow pathways during folding and faulting: an example from Taemas, NSW, Australia, *Geol. Soc. London, Spec. Publ.*, 359(1), 203–227, doi:10.1144/SP359.12, 2011.

Barker, S. L. L., Bennett, V. C., Cox, S. F., Norman, M. D. and Gagan, M. K.: Sm–Nd, Sr, C and O isotope systematics in hydrothermal calcite–fluorite veins: Implications for fluid–rock reaction and geochronology, *Chem. Geol.*, 268(1–2), 58–66, doi:10.1016/j.chemgeo.2009.07.009, 2009.

700 Beaudoin, N., Bellahsen, N., Lacombe, O., Emmanuel, L. and Pironon, J.: Crustal-scale fluid flow during the tectonic evolution

- of the Bighorn Basin (Wyoming, USA), *Basin Res.*, 26(3), 403–435, doi:10.1111/bre.12032, 2014.
- 705 Beaudoin, N., Huyghe, D., Bellahsen, N., Lacombe, O., Emmanuel, L., Mouthereau, F. and Ouahnon, L.: Fluid systems and fracture development during syn-depositional fold growth: An example from the Pico del Aguila anticline, Sierras Exteriores, southern Pyrenees, Spain, *J. Struct. Geol.*, 70, 23–38, doi:10.1016/j.jsg.2014.11.003, 2015.
- Bickle, M. J., Wickham, S. M., Chapman, H. J. and Taylor, H. P.: A strontium, neodymium and oxygen isotope study of hydrothermal metamorphism and crustal anatexis in the Trois Seigneurs Massif, Pyrenees, France, *Contrib. to Mineral. Petrol.*, 100(4), 399–417, doi:10.1007/BF00371371, 1988.
- 710 Bons, A.: Intracrystalline deformation and slaty cleavage development in very low-grade slates from the Central Pyrenees, *Geol. Ultraiectina*, 1988.
- Breesch, L., Swennen, R. and Vincent, B.: Fluid flow reconstruction in hanging and footwall carbonates: Compartmentalization by Cenozoic reverse faulting in the Northern Oman Mountains (UAE), *Mar. Pet. Geol.*, 26(1), 113–128, doi:10.1016/j.marpetgeo.2007.10.004, 2009.
- 715 Burkhard, M., Kerrich, R., Maas, R. and Fyfe, W. S.: Stable and Sr-isotope evidence for fluid advection during thrusting of the glarus nappe (swiss alps), *Contrib. to Mineral. Petrol.*, 112(2–3), 293–311, doi:10.1007/BF00310462, 1992.
- Caballero, Y., Gironde, C. and Le Goff, E.: Ressource en eau thermale de la station d' Amélie-les-Bains. Etat des lieux. Rapport BRGM/RP-60618-FR., 2012.
- 720 Cabrera, L., Roca, E. and Santanach, P.: Basin formation at the end of a strike-slip fault: the Cerdanya Basin (eastern Pyrenees), *J. Geol. Soc. London.*, 145(2), 261–268, doi:10.1144/gsjgs.145.2.0261, 1988.
- Cantarero, I., Travé, A., Alías, G. and Baqués, V.: Polyphasic hydrothermal and meteoric fluid regimes during the growth of a segmented fault involving crystalline and carbonate rocks (Barcelona Plain, NE Spain), *Geofluids*, 14(1), 20–44, doi:10.1111/gfl.12021, 2014.
- 725 Cantarero, I., Alías, G., Cruset, D., Carola, E., Lanari, P. and Travé, A.: Fluid composition changes in crystalline basement rocks from ductile to brittle regimes, *Glob. Planet. Change*, 171(March), 273–292, doi:10.1016/j.gloplacha.2018.03.002, 2018.
- Cardellach, E., Canals, À. and Grandia, F.: Recurrent hydrothermal activity induced by successive extensional episodes: the case of the Berta F–(Pb–Zn) vein system (NE Spain), *Ore Geol. Rev.*, 22(1–2), 133–141, doi:10.1016/S0169-1368(02)00112-9, 2003.
- 730 Carmona, J. M., Bitzer, K., López, E. and Bouazza, M.: Isotopic composition and origin of geothermal waters at Caldetes (Maresme-Barcelona), *J. Geochemical Explor.*, 69–70, 441–447, doi:10.1016/S0375-6742(00)00127-8, 2000.
- Casas, J. M., Domingo, F., Poblet, J. and Soler, A.: On the role of the Hercynian and Alpine thrusts in the Upper Paleozoic rocks of the Central and Eastern Pyrenees, *Geodin. Acta*, 3(2), 135–147, doi:10.1080/09853111.1989.11105181, 1989.
- Cerling, T. E.: The stable isotopic composition of modern soil carbonate and its relationship to climate, *Earth Planet. Sci. Lett.*, 735 doi:10.1016/0012-821X(84)90089-X, 1984.
- Choukroune, P.: The Eors Pyrenean deep seismic profile reflection data and the overall structure of an orogenic belt, *Tectonics*, doi:10.1029/TC008i001p00023, 1989.

- Cochelin, B., Lemirre, B., Denèle, Y., de Saint Blanquat, M., Lahfid, A. and Duchêne, S.: Structural inheritance in the Central Pyrenees: the Variscan to Alpine tectonometamorphic evolution of the Axial Zone, *J. Geol. Soc. London.*, 175(2), 336–351, doi:10.1144/jgs2017-066, 2018.
- 740 Cox, S. F.: Structural and isotopic constraints on fluid flow regimes and fluid pathways during upper crustal deformation: An example from the Taemas area of the Lachlan Orogen, SE Australia, *J. Geophys. Res.*, 112(B8), B08208, doi:10.1029/2006JB004734, 2007.
- Crespo-Blanc, A., Masson, H., Sharp, Z., Cosca, M. and Hunziker, J.: A stable and  $40\text{Ar}/39\text{Ar}$  isotope study of a major thrust in the Helvetic nappes (Swiss Alps): Evidence for fluid flow and constraints on nappe kinematics, *Geol. Soc. Am. Bull.*, 107(10), 1129–1144, doi:10.1130/0016-7606(1995)107<1129:ASAAA1>2.3.CO;2, 1995.
- 745 Crognier, N., Hoareau, G., Aubourg, C., Dubois, M., Lacroix, B., Branellec, M., Callot, J. P. and Vennemann, T.: Syn-orogenic fluid flow in the Jaca basin (south Pyrenean fold and thrust belt) from fracture and vein analyses, *Basin Res.*, 30(2), 187–216, doi:10.1111/bre.12249, 2018.
- 750 Cruset, D.: Sequential fluid migration along a fold and thrust belt SE pyrenees from late Cretaceous to Oligocene, PhD thesis, Universitat de Barcelona., 2019.
- Cruset, D., Cantarero, I., Travé, A., Vergés, J. and John, C. M.: Crestal graben fluid evolution during growth of the Puig-reig anticline (South Pyrenean fold and thrust belt), *J. Geodyn.*, 101, 30–50, doi:10.1016/j.jog.2016.05.004, 2016.
- Cruset, D., Cantarero, I., Vergés, J., John, C. M., Muñoz-López, D. and Travé, A.: Changes in fluid regime in syn-orogenic sediments during the growth of the south Pyrenean fold and thrust belt, *Glob. Planet. Change*, 171(October 2017), 207–224, doi:10.1016/j.gloplacha.2017.11.001, 2018.
- 755 Cruset, D., Cantarero, I., Benedicto, A., John, C. M., Vergés, J., Albert, R., Gerdes, A. and Travé, A.: From hydroplastic to brittle deformation: Controls on fluid flow in fold and thrust belts. Insights from the Lower Pedraforca thrust sheet (SE Pyrenees), *Mar. Pet. Geol.*, 120, 104517, doi:10.1016/j.marpetgeo.2020.104517, 2020a.
- 760 Cruset, D., Vergés, J., Albert, R., Gerdes, A., Benedicto, A., Cantarero, I. and Travé, A.: Quantifying deformation processes in the SE Pyrenees using U-Pb dating of fracture-filling calcites, *J. Geol. Soc. London.*, (August), jgs2020-014, doi:10.1144/jgs2020-014, 2020b.
- Dansgaard, W.: Stable isotopes in precipitation, *Tellus*, doi:10.3402/tellusa.v16i4.8993, 1964.
- Dennis, K. J., Affek, H. P., Passey, B. H., Schrag, D. P. and Eiler, J. M.: Defining an absolute reference frame for ‘clumped’ isotope studies of  $\text{CO}_2$ , *Geochim. Cosmochim. Acta*, 75(22), 7117–7131, doi:10.1016/j.gca.2011.09.025, 2011.
- 765 Dewever, B., Swennen, R. and Breesch, L.: Fluid flow compartmentalization in the Sicilian fold and thrust belt: Implications for the regional aqueous fluid flow and oil migration history, *Tectonophysics*, 591, 194–209, doi:10.1016/j.tecto.2011.08.009, 2013.
- Faulds, J., Coolbaugh, M., Bouchot, V., Moeck, I., Oğuz, K. and Cedex, O.: Characterizing Structural Controls of Geothermal Reservoirs in the Great Basin , USA , and Western Turkey : Developing Successful Exploration Strategies in Extended Terranes, *World, C(2010)*, 25–29, 2010.
- 770

- Fay-Gomord, O., Allanic, C., Verbiest, M., Honlet, R., Champenois, F., Bonifacie, M., Chaduteau, C., Wouters, S., Muechez, P., Lasseur, E. and Swennen, R.: Understanding Fluid Flow during Tectonic Reactivation: An Example from the Flamborough Head Chalk Outcrop (UK), *Geofluids*, 2018, 1–17, doi:10.1155/2018/9352143, 2018.
- 775 Fernández, M. and Banda, E.: Geothermal anomalies in the Valles-Penedes Graben Master Fault: Convection through the Horst as a possible mechanism, *J. Geophys. Res.*, 95(B4), 4887, doi:10.1029/JB095iB04p04887, 1990.
- Fitz-Diaz, E., Hudleston, P., Siebenaller, L., Kirschner, D., Camprubi, A., Tolson, G. and Puig, T. P.: Insights into fluid flow and water-rock interaction during deformation of carbonate sequences in the Mexican fold-thrust belt, *J. Struct. Geol.*, 33(8), 1237–1253, doi:10.1016/j.jsg.2011.05.009, 2011.
- 780 Foden, J.: Sr-isotopic evidence for Late Neoproterozoic rifting in the Adelaide Geosyncline at 586 Ma: implications for a Cu ore forming fluid flux, *Precambrian Res.*, 106(3–4), 291–308, doi:10.1016/S0301-9268(00)00132-7, 2001.
- Fontana, S., Nader, F. H., Morad, S., Ceriani, A., Al-Aasm, I. S., Daniel, J. M. and Mengus, J. M.: Fluid-rock interactions associated with regional tectonics and basin evolution, *Sedimentology*, 61(3), 660–690, doi:10.1111/sed.12073, 2014.
- Friedman, I. and O’Neil, J. R.: Compilation of stable isotope fractionation factors of geochemical interest, in *Professional Papers.*, 1977.
- 785 García-Sansegundo, J., Poblet, J., Alonso, J. L. and Clariana, P.: Hinterland-foreland zonation of the Variscan orogen in the Central Pyrenees: comparison with the northern part of the Iberian Variscan Massif, *Geol. Soc. London, Spec. Publ.*, 349(1), 169–184, doi:10.1144/SP349.9, 2011.
- Gasparrini, M., Ruggieri, G. and Brogi, A.: Diagenesis versus hydrothermalism and fluid-rock interaction within the Tuscan Nappe of the Monte Amiata CO<sub>2</sub>-rich geothermal area (Italy), *Geofluids*, 13(2), 159–179, doi:10.1111/gfl.12025, 2013.
- 790 Gomez-Rivas, E., Bons, P. D., Koehn, D., Urai, J. L., Arndt, M., Virgo, S., Laurich, B., Zeeb, C., Stark, L. and Blum, P.: The Jabal Akhdar dome in the Oman Mountains: Evolution of a dynamic fracture system, *Am. J. Sci.*, 314(7), 1104–1139, doi:10.2475/07.2014.02, 2014.
- Goula, X., Olivera, C., Fleta, J., Grellet, B., Lindo, R., Rivera, L. A., Cisternas, A. and Carbon, D.: Present and recent stress regime in the eastern part of the Pyrenees, *Tectonophysics*, doi:10.1016/S0040-1951(99)00120-1, 1999.
- 795 Grant, N. T., Banks, D. A., McCaig, A. M. and Yardley, B. W. D.: Chemistry, source, and behavior of fluids involved in alpine thrusting of the Central Pyrenees, *J. Geophys. Res.*, 95(B6), 9123, doi:10.1029/JB095iB06p09123, 1990.
- Grasby, S. E. and Hutcheon, I.: Controls on the distribution of thermal springs in the southern Canadian Cordillera, *Can. J. Earth Sci.*, 38(3), 427–440, doi:10.1139/cjes-38-3-427, 2001.
- 800 Gregory, R. T., Douthitt, C. B., Duddy, I. R., Rich, P. V. and Rich, T. H.: Oxygen isotopic composition of carbonate concretions from the lower Cretaceous of Victoria, Australia: implications for the evolution of meteoric waters on the Australian continent in a paleopolar environment, *Earth Planet. Sci. Lett.*, 92(1), 27–42, doi:10.1016/0012-821X(89)90018-6, 1989.
- Guo, W., Mosenfelder, J. L., Goddard, W. A. and Eiler, J. M.: Isotopic fractionations associated with phosphoric acid digestion of carbonate minerals: Insights from first-principles theoretical modeling and clumped isotope measurements, *Geochim. Cosmochim. Acta*, 73(24), 7203–7225, doi:10.1016/j.gca.2009.05.071, 2009.
- 805

- Hartevelt, J. J. A.: Geology of the Upper Segre and Valira Valleys, Central Pyrenees, Andorra, Spain, Geological Institute, Leiden University, Leiden, 1970.
- Henderson, I. H. C. and McCaig, A. M.: Fluid pressure and salinity variations in shear zone-related veins, central Pyrenees, France: Implications for the fault-valve model, *Tectonophysics*, 262(1–4), 321–348, doi:10.1016/0040-1951(96)00018-2, 810 1996.
- Henkes, G. A., Passey, B. H., Grossman, E. L., Shenton, B. J., Pérez-Huerta, A. and Yancey, T. E.: Temperature limits for preservation of primary calcite clumped isotope paleotemperatures, *Geochim. Cosmochim. Acta*, 139, 362–382, doi:10.1016/j.gca.2014.04.040, 2014.
- Huntington, K. W., Eiler, J. M., Affek, H. P., Guo, W., Bonifacie, M., Yeung, L. Y., Thiagarajan, N., Passey, B., Tripathi, A., 815 Daëron, M. and Came, R.: Methods and limitations of “clumped” CO<sub>2</sub> isotope ( $\Delta_{47}$ ) analysis by gas-source isotope ratiomass spectrometry, *J. Mass Spectrom.*, 44(9), 1318–1329, doi:10.1002/jms.1614, 2009.
- Huyghe, D., Mouthereau, F., Sébilo, M., Vacherat, A., Ségalen, L., Richard, P., Biron, P. and Bariac, T.: Impact of topography, climate and moisture sources on isotopic composition ( $\delta^{18}\text{O}$  &  $\delta\text{D}$ ) of rivers in the Pyrenees: Implications for topographic reconstructions in small orogens, *Earth Planet. Sci. Lett.*, 484(January), 370–384, doi:10.1016/j.epsl.2017.12.035, 2018.
- 820 John, C. M. and Bowen, D.: Community software for challenging isotope analysis: First applications of ‘Easotope’ to clumped isotopes, *Rapid Commun. Mass Spectrom.*, 30(21), 2285–2300, doi:10.1002/rcm.7720, 2016.
- Kim, S.-T. and O’Neil, J. R.: Equilibrium and nonequilibrium oxygen isotope effects in synthetic carbonates, *Geochim. Cosmochim. Acta*, 61(16), 3461–3475, doi:10.1016/S0016-7037(97)00169-5, 1997.
- Kluge, T., John, C. M., Jourdan, A.-L., Davis, S. and Crawshaw, J.: Laboratory calibration of the calcium carbonate clumped 825 isotope thermometer in the 25–250 °C temperature range, *Geochim. Cosmochim. Acta*, 157, 213–227, doi:10.1016/j.gca.2015.02.028, 2015.
- Krimissa, M., Chery, L., Fouillac, C. and Michelot, J. L.: Origin and Recharge Altitude of the Thermo-Mineral Waters of the Eastern Pyrenees, *Isot. Isot. Environ. Heal. Stud.*, 30(4), 317–331, doi:10.1080/00211919408046747, 1994.
- Lacroix, B., Buatier, M., Labaume, P., Travé, A., Dubois, M., Charpentier, D., Ventalon, S. and Convert-Gaubier, D.: 830 Microtectonic and geochemical characterization of thrusting in a foreland basin: Example of the South-Pyrenean orogenic wedge (Spain), *J. Struct. Geol.*, 33(9), 1359–1377, doi:10.1016/j.jsg.2011.06.006, 2011.
- Lacroix, B., Travé, A., Buatier, M., Labaume, P., Vennemann, T. and Dubois, M.: Syntectonic fluid-flow along thrust faults: Example of the South-Pyrenean fold-and-thrust belt, *Mar. Pet. Geol.*, 49, 84–98, doi:10.1016/j.marpetgeo.2013.09.005, 2014.
- Lacroix, B., Baumgartner, L. P., Bouvier, A.-S., Kempton, P. D. and Vennemann, T.: Multi fluid-flow record during episodic 835 mode I opening: A microstructural and SIMS study (Cotiella Thrust Fault, Pyrenees), *Earth Planet. Sci. Lett.*, 503, 37–46, doi:10.1016/j.epsl.2018.09.016, 2018.
- Lago, M., Arranz, E., Pocióvi, A., Galé, C. and Gil-Imaz, A.: Permian magmatism and basin dynamics in the southern Pyrenees: a record of the transition from late Variscan transtension to early Alpine extension, *Geol. Soc. London, Spec. Publ.*, 223(1), 439–464, doi:10.1144/GSL.SP.2004.223.01.19, 2004.



- 840 Liotta, D., Ruggieri, G., Brogi, A., Fulignati, P., Dini, A. and Nardini, I.: Migration of geothermal fluids in extensional terrains: the ore deposits of the Boccheggiano-Montieri area (southern Tuscany, Italy), *Int. J. Earth Sci.*, 99(3), 623–644, doi:10.1007/s00531-008-0411-3, 2010.
- Marshall, J. D.: Climatic and oceanographic isotopic signals from the carbonate rock record and their preservation, *Geol. Mag.*, doi:10.1017/S0016756800008244, 1992.
- 845 Martí, J.: Caldera-like structures related to Permo-Carboniferous volcanism of the Catalan Pyrenees (NE Spain), *J. Volcanol. Geotherm. Res.*, 45(3–4), 173–186, doi:10.1016/0377-0273(91)90057-7, 1991.
- Martí, J.: Genesis of crystal-rich volcanoclastic facies in the Permian red beds of the Central Pyrenees (NE Spain), *Sediment. Geol.*, 106(1–2), 1–19, doi:10.1016/0037-0738(95)00143-3, 1996.
- Martín-Martín, J. D., Travé, A., Gomez-Rivas, E., Salas, R., Sizun, J. P., Vergés, J., Corbella, M., Stafford, S. L. and Alfonso, P.: Fault-controlled and stratabound dolostones in the Late Aptian-earliest Albian Benassal Formation (Maestrat Basin, E Spain): Petrology and geochemistry constrains, *Mar. Pet. Geol.*, 65, doi:10.1016/j.marpetgeo.2015.03.019, 2015.
- 850 Martínez Casas, L. F., Travé, A., Cruset, D. and Muñoz-López, D.: The Montagut Fault System: Geometry and Fluid Flow Analysis (Southern Pyrennes, Spain), in *Petrogenesis and Exploration of the Earth's Interior. Proceedings of the 1st Springer Conference of the Arabian Journal of Geosciences (CAJG-1), Tunisia 2018*, pp. 211–214., 2019.
- 855 Matte, P.: Accretionary history and crustal evolution of the Variscan belt in Western Europe, *Tectonophysics*, doi:10.1016/0040-1951(91)90328-P, 1991.
- McArthur, J. M., Howarth, R. J. and Shields, G. A.: Strontium Isotope Stratigraphy, in *The Geologic Time Scale*, vol. 1–2, pp. 127–144, Elsevier., 2012.
- McCaig, A. ., Tritlla, J. and Banks, D. .: Fluid mixing and recycling during Pyrenean thrusting: evidence from fluid inclusion halogen ratios, *Geochim. Cosmochim. Acta*, 64(19), 3395–3412, doi:10.1016/S0016-7037(00)00437-3, 2000a.
- 860 McCaig, A. M., Wayne, D. M., Marshall, J. D., Banks, D. and Henderson, I.: Isotopic and fluid inclusion studies of fluid movement along the Gavarnie Thrust, central Pyrenees; reaction fronts in carbonate mylonites, *Am. J. Sci.*, 295(3), 309–343, doi:10.2475/ajs.295.3.309, 1995.
- McCaig, A. M., Wayne, D. M. and Rosenbaum, J. M.: Fluid expulsion and dilatancy pumping during thrusting in the Pyrenees: Pb and Sr isotope evidence, *Geol. Soc. Am. Bull.*, 112(8), 1199–1208, doi:10.1130/0016-7606(2000)112<1199:FEADPD>2.0.CO;2, 2000b.
- 865 McCrea, J. M.: On the isotopic chemistry of carbonates and a paleotemperature scale, *J. Chem. Phys.*, doi:10.1063/1.1747785, 1950.
- Mey, P. H. W.: The geology of the upper Ribagorzana and Baliera Valleys, Central Pyrenees, Spain, *Leidse Geol. Meded.*, 41, 153–220, 1967.
- 870 Mey, P. H. W., Nagtegaal, P. J. C., Roberti, K. J. and Hartevelt, J. J. A.: Lithostratigraphic subdivision of Post-Hercynian deposits in the South-Central Pyrenees, Spain, *Leidse Geol. Meded.*, 41(1), 221–228, 1968.
- Mouthereau, F., Filleaudeau, P. Y., Vacherat, A., Pik, R., Lacombe, O., Fellin, M. G., Castellort, S., Christophoul, F. and

- Masini, E.: Placing limits to shortening evolution in the Pyrenees: Role of margin architecture and implications for the Iberia/Europe convergence, *Tectonics*, 33(12), 2283–2314, doi:10.1002/2014TC003663, 2014.
- 875 Mozafari, M., Swennen, R., Balsamo, F., El Desouky, H., Storti, F. and Taberner, C.: Fault-controlled dolomitization in the Montagna dei Fiori Anticline (Central Apennines, Italy): record of a dominantly pre-orogenic fluid migration, *Solid Earth*, 10(4), 1355–1383, doi:10.5194/se-10-1355-2019, 2019.
- Muñoz, J. A.: Evolution of a continental collision belt: ECORS-Pyrenees crustal balanced cross-section, in *Thrust Tectonics*, pp. 235–246, Springer Netherlands, Dordrecht., 1992.
- 880 Muñoz, J. A.: Fault-related folds in the southern Pyrenees, *Am. Assoc. Pet. Geol. Bull.*, 101(04), 579–587, doi:10.1306/011817DIG17037, 2017.
- Muñoz, J. A., Martínez, A. and Verges, J.: Thrust sequences in the eastern Spanish Pyrenees, *J. Struct. Geol.*, 8, 399–405, 1986.
- 885 Nardini, N., Muñoz-López, D., Cruset, D., Cantarero, I., Martín-Martín, J., Benedicto, A., Gomez-Rivas, E., John, C. and Travé, A.: From Early Contraction to Post-Folding Fluid Evolution in the Frontal Part of the Bóixols Thrust Sheet (Southern Pyrenees) as Revealed by the Texture and Geochemistry of Calcite Cements, *Minerals*, 9(2), 117, doi:10.3390/min9020117, 2019.
- Nelson, S. T., Mayo, A. L., Gilfillan, S., Dutson, S. J., Harris, R. A., Shipton, Z. K. and Tingey, D. G.: Enhanced fracture permeability and accompanying fluid flow in the footwall of a normal fault: The Hurricane fault at Pah Tempe hot springs, Washington County, Utah, *Geol. Soc. Am. Bull.*, preprint(2008), 1, doi:10.1130/B26285.1, 2006.
- Pfeifer, H.-R., Oberhänsli, H. and Epprecht, W.: Geochemical evidence for a synsedimentary hydrothermal origin of Jurassic iron-manganese deposits at Gonzen (Sargans, Helvetic Alps, Switzerland), *Mar. Geol.*, 84(3–4), 257–272, doi:10.1016/0025-3227(88)90105-3, 1988.
- 895 Piessens, K., Muechez, P., Dewaele, S., Boyce, A., De Vos, W., Sintubin, M., Debacker, T. N., Burke, E. A. J. and Viaene, W.: Fluid flow, alteration and polysulphide mineralisation associated with a low-angle reverse shear zone in the Lower Palaeozoic of the Anglo-Brabant fold belt, Belgium, *Tectonophysics*, doi:10.1016/S0040-1951(01)00250-5, 2002.
- Poblet, J.: Estructura herciniana i alpina del vessant sud de la zona axial del Pirineu centra, PhD thesis, Universitat de barcelona., 1991.
- 900 Pomerol, B.: Geochemistry of the late Cenomanian-early Turonian chalks of the Paris Basin: Manganese and carbon isotopes in carbonates as paleoceanographic indicators, *Cretac. Res.*, 4(1), 85–93, doi:10.1016/0195-6671(83)90025-3, 1983.
- Pratt, L. M., Force, E. R. and Pomerol, B.: Coupled manganese and carbon-isotopic events in marine carbonates at the Cenomanian-Turonian boundary, *J. Sediment. Petrol.*, doi:10.1306/D4267717-2B26-11D7-8648000102C1865D, 1991.
- Roca, E.: The Neogene Cerdanya and Seu d'Urgell intramontane basins (Eastern Pyrenees), in *Tertiary basins of Spain*, edited by P. F. Friend and C. J. Dabrio, pp. 114–119, Cambridge University Press, Cambridge., 1996.
- 905 Roca, E. and Guimerà, J.: The Neogene structure of the eastern Iberian margin: Structural constraints on the crustal evolution of the Valencia trough (western Mediterranean), *Tectonophysics*, 203(1–4), 203–218, doi:10.1016/0040-1951(92)90224-T,

Con formato: Español (España)

1992.

Roure, F., Choukroune, P., Berastegui, X., Munoz, J. a., Villien, a., Matheron, P., Bareyt, M., Seguret, M., Camara, P. and

910 Deramond, J.: Ecors deep seismic data and balanced cross sections: Geometric constraints on the evolution of the Pyrenees, *Tectonics*, 8, 41-50, doi:10.1029/TC008i001p00041, 1989.

Rowland, J. V. and Sibson, R. H.: Structural controls on hydrothermal flow in a segmented rift system, Taupo Volcanic Zone, New Zealand, *Geofluids*, 4(4), 259–283, doi:10.1111/j.1468-8123.2004.00091.x, 2004.

Rye, D. M. and Bradbury, H. J.: Fluid flow in the crust; an example from a Pyrenean thrust ramp, *Am. J. Sci.*, 288(3), 197–

915 235, doi:10.2475/ajs.288.3.197, 1988.

Saura, E.: *Análisi estructural de la Zona de les Nogures (Pirineus Centrals)*, PhD thesis, Universitat de Barcelona., 2004.

Saura, E. and Teixell, A.: Inversion of small basins: effects on structural variations at the leading edge of the Axial Zone antiformal stack (Southern Pyrenees, Spain), *J. Struct. Geol.*, 28(11), 1909–1920, doi:10.1016/j.jsg.2006.06.005, 2006.

Shenton, B. J., Grossman, E. L., Passey, B. H., Henkes, G. A., Becker, T. P., Laya, J. C., Perez-Huerta, A., Becker, S. P. and

920 Lawson, M.: Clumped isotope thermometry in deeply buried sedimentary carbonates: The effects of bond reordering and recrystallization, *Geol. Soc. Am. Bull.*, 127(7–8), B31169.1, doi:10.1130/B31169.1, 2015.

Sibson, R. H.: Crustal stress, faulting and fluid flow, *Geol. Soc. London, Spec. Publ.*, 78(1), 69–84, doi:10.1144/GSL.SP.1994.078.01.07, 1994.

Sibson, R. H.: Selective fault reactivation during basin inversion: potential for fluid redistribution through fault-valve action,

925 *Geol. Soc. London, Spec. Publ.*, 88(1), 3–19, doi:10.1144/GSL.SP.1995.088.01.02, 1995.

Sibuet, J. C., Srivastava, S. P. and Spakman, W.: Pyrenean orogeny and plate kinematics, *J. Geophys. Res. B Solid Earth*, 109(8), 1–18, doi:10.1029/2003JB002514, 2004.

Srivastava, S. P., Schouten, H., Roest, W. R., Klitgord, K. D., Kovacs, L. C., Verhoef, J. and Macnab, R.: Iberian plate kinematics: A jumping plate boundary between Eurasia and Africa, *Nature*, doi:10.1038/344756a0, 1990.

930 Stolper, D. A. and Eiler, J. M.: The kinetics of solid-state isotope-exchange reactions for clumped isotopes: A study of inorganic calcites and apatites from natural and experimental samples, *Am. J. Sci.*, 315(5), 363–411, doi:10.2475/05.2015.01, 2015.

Suchy, V., Heijlen, W., Sykorova, I., Muechez, P., Dobes, P., Hladikova, J., Jackova, I., Safanda, J. and Zeman, A.:

935 *Geochemical study of calcite veins in the Silurian and Devonian of the Barrandian Basin (Czech Republic): evidence for widespread post-Variscan fluid flow in the central part of the Bohemian Massif*, *Sediment. Geol.*, 131(3–4), 201–219, doi:10.1016/S0037-0738(99)00136-0, 2000.

Taillefer, A., Soliva, R., Guillou-Frottier, L., Le Goff, E., Martin, G. and Seranne, M.: Fault-Related Controls on Upward Hydrothermal Flow: An Integrated Geological Study of the Têt Fault System, Eastern Pyrénées (France), *Geofluids*, 2017, 1–19, doi:10.1155/2017/8190109, 2017.

940 Taillefer, A., Guillou-Frottier, L., Soliva, R., Magri, F., Lopez, S., Courrioux, G., Millot, R., Ladouche, B. and Le Goff, E.: Topographic and Faults Control of Hydrothermal Circulation Along Dormant Faults in an Orogen, *Geochemistry, Geophys.*

Con formato: Español (España)

Geosystems, 19(12), 4972–4995, doi:10.1029/2018GC007965, 2018.

Taylor, B. D.: Stable isotope geochemistry of ore-forming fluids, in *Short Course Handbook.*, 1987.

945 Travé, A., Labaume, P., Calvet, F. and Soler, A.: Sediment dewatering and pore fluid migration along thrust faults in a foreland basin inferred from isotopic and elemental geochemical analyses (Eocene southern Pyrenees, Spain), *Tectonophysics*, 282(1–4), 375–398, doi:10.1016/S0040-1951(97)00225-4, 1997.

Travé, A., Labaume, P., Calvet, F., Soler, A., Tritlla, J., Buatier, M., Potdevin, J.-L., Séguret, M., Raynaud, S. and Briquieu, L.: Fluid migration during Eocene thrust emplacement in the south Pyrenean foreland basin (Spain): an integrated structural, mineralogical and geochemical approach, *Geol. Soc. London, Spec. Publ.*, 134(1), 163–188, doi:10.1144/GSL.SP.1998.134.01.08, 1998.

950 Travé, A., Calvet, F., Sans, M., Vergés, J. and Thirlwall, M.: Fluid history related to the Alpine compression at the margin of the south-Pyrenean Foreland basin: the El Guix anticline, *Tectonophysics*, 321(1), 73–102, doi:10.1016/S0040-1951(00)00090-1, 2000.

Travé, A., Labaume, P. and Vergés, J.: Fluid Systems in Foreland Fold-and-Thrust Belts: An Overview from the Southern Pyrenees, in *Thrust Belts and Foreland Basins*, edited by O. Lacombe, F. Roue, J. Lavé, and J. Vergés, pp. 93–115, Springer Berlin Heidelberg, Berlin, Heidelberg., 2007.

955 Travé, A., Roca, E., Playà, E., Parcerisa, D., Gómez-Gras, D. and Martín-Martín, J. D.: Migration of Mn-rich fluids through normal faults and fine-grained terrigenous sediments during early development of the Neogene Vallès-Penedès half-graben (NE Spain), *Geofluids*, 9(4), 303–320, doi:10.1111/j.1468-8123.2009.00258.x, 2009.

960 Trincal, V., Buatier, M., Charpentier, D., Lacroix, B., Lanari, P., Labaume, P., Lahfid, A. and Vennemann, T.: Fluid–rock interactions related to metamorphic reducing fluid flow in meta-sediments: example of the Pic-de-Port-Vieux thrust (Pyrenees, Spain), *Contrib. to Mineral. Petrol.*, 172(9), 78, doi:10.1007/s00410-017-1394-5, 2017.

Turu i Michels, V. and Peña Monné, J. L.: Las terrazas fluviales del sistema Segre-Valira (Andorra- La Seu d’Urgell-Organyà, Pirineos Orientales): relación con el glaciario y la tectónica activa., *Geomorfol. y Territ. IX Reun. Nac. Geomorfología*, (January 2006), 113–128, 2006.

Veizer, J., Ala, D., Azmy, K., Bruckschen, P., Buhl, D., Bruhn, F., Carden, G. A. F., Diener, A., Ebner, S., Godderis, Y., Jasper, T., Korte, C., Pawellek, F., Podlaha, O. G. and Strauss, H.:  $^{87}\text{Sr}/^{86}\text{Sr}$ ,  $\delta^{13}\text{C}$  and  $\delta^{18}\text{O}$  evolution of Phanerozoic seawater, *Chem. Geol.*, 161(1–3), 59–88, doi:10.1016/S0009-2541(99)00081-9, 1999.

970 Vergés, J.: Estudi geològic del vessant Sud del Pirineu Oriental i Central: Evolució cinemàtica en 3D. PhD thesis, University of Barcelona, Barcelona., 1993.

Vergés, J. and Fernández, M.: Tethys–Atlantic interaction along the Iberia–Africa plate boundary: The Betic–Rif orogenic system, *Tectonophysics*, 579, 144–172, doi:10.1016/j.tecto.2012.08.032, 2012.

Vergés, J. and Muñoz, J. A.: Thrust sequences in the southern central Pyrenees, *Bull. French Geol. Soc.*, 2, 265–271, 1990.

975 Vergés, J., Fernández, M. and Martínez, A.: The Pyrenean orogen: pre-, syn-, and post-collisional evolution, *J. Virtual Explor.*, 08(January 2002), doi:10.3809/jvirtex.2002.00058, 2002.

Con formato: Español (España)

Con formato: Español (España)

Vilasi, N., Swennen, R. and Roure, F.: Diagenesis and fracturing of Paleocene-Eocene carbonate turbidite systems in the Ionian Basin: The example of the Kelçyra area (Albania), *J. Geochemical Explor.*, 89(1-3 SPEC. ISS.), 409–413, doi:10.1016/j.gexplo.2005.11.018, 2006.

Voicu, G., Bardoux, M., Stevenson, R. and Jébrak, M.: Nd and Sr isotope study of hydrothermal scheelite and host rocks at

980 Omai, Guiana Shield: implications for ore fluid source and flow path during the formation of orogenic gold deposits, *Miner. Depos.*, 35(4), 302–314, doi:10.1007/s001260050243, 2000.

Warren, J., Morley, C. K., Charoentitirat, T., Cartwright, I., Ampaiwan, P., Khositchaisri, P., Mirzaloo, M. and Yingyuen, J.: Structural and fluid evolution of Saraburi Group sedimentary carbonates, central Thailand: A tectonically driven fluid system, *Mar. Pet. Geol.*, 55, 100–121, doi:10.1016/j.marpetgeo.2013.12.019, 2014.

985 Wayne, D. M. and McCaig, A. M.: Dating fluid flow in shear zones: Rb-Sr and U-Pb studies of syntectonic veins in the Néouvielle Massif, Pyrenees, *Geol. Soc. London, Spec. Publ.*, 144(1), 129–135, doi:10.1144/GSL.SP.1998.144.01.09, 1998.

Ziegler, P. A.: Evolution of the Arctic-North Atlantic and the Western Tethys, in *AAPG Memoir Volume 43: Evolution of the Arctic-North Atlantic and the Western Tethys.*, 1988.

Zwart, H. J.: The variscan geology of the Pyrenees, *Tectonophysics*, 129(1–4), 9–27, doi:10.1016/0040-1951(86)90243-X,

990 1986.

995

1000

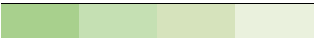
1005

**Table 1.**  $\delta^{18}\text{O}$ ,  $\delta^{13}\text{C}$ ,  $^{87}\text{Sr}/^{86}\text{Sr}$  and  $^{143}\text{Nd}/^{144}\text{Nd}$  ratios of the calcite cements and related host rocks. The calculated precipitation temperature and the  $\delta^{18}\text{O}_{\text{fluid}}$  of the parent fluids are also indicated. NR indicates analyzed samples in which no result was obtained.

Sample	Vein	Cement	$\delta^{18}\text{O}$ ‰VPDB	$\delta^{13}\text{C}$ ‰VPDB	$^{87}\text{Sr}/^{86}\text{Sr}$	$^{143}\text{Nd}/^{144}\text{Nd}$	$\Delta_{47}$	T (°C)	$\delta^{18}\text{O}_{\text{fluid}}$ ‰SMOW
C9	V1a	Cc1a	-11.2	+0.91					
C8B	V1a	Cc1a	-10.7	+2					
C8A.I	V1a	Cc1a	-10.4	+2					
C8A.II	V1a	Cc1a	-10.96	+1.3	0.713018	NR			
C8A.III	V1a	Cc1a	-10.9	+1.2					
C7.I	V1a	Cc1a	-10.9	+2.1					
C7.II	V1a	Cc1a	-10.8	+0.8					
C7.III	V1a	Cc1a	-10.4	+1.96					
C4B	V1a	Cc1a	-10.3	+1.9	0.714092	NR			
C3A.I	V1a	Cc1a	-11.2	+1.9					
C3A.II	V1a	Cc1a	-11.3	+1.7					
C3A.III	V1a	Cc1a	-10.5	+1.98					
C15.I	V2	Cc2	-14.9	-1.2	0.718294	NR	0.567	56 to 98	-0.3 to -6.4
C15.II	V2	Cc2	-13.3	+0.5					
C15.III	V2	Cc2	-12.91	+1.54					
C13	V3	Cc3	-13.8	-7.1	0.714619	NR	0.445	127 to 208	+4.3 to +12.1
C12.II	V3	Cc3	-14.3	-7.3					
C10	V3	Cc3	-14.2	-9.3					
C11A	V3	Cc3	-14.2	-8.7					
C13.II	V3	Cc3	-13.6	-7.2					
C14.I	V3	Cc3	-13.4	-6.9					
C14.II	V3	Cc3	-13.7	-7.4					
C16A	V3	Cc3	-13.8	-7.2					
C16B	V3	Cc3	-14	-7					
C16C	V3	Cc3	-14.1	-6.9					
C18.I	V4	Cc4	-13.4	-7.2	0.717706		0.48	102 to 167	+0.9 to +8.1
C18.II	V4	Cc4	-13.8	-7.4					
C12.I	V5	Cc5	-8.1	-7.8	0.716923	0.512178			
C6.I	V5	Cc5	-6.7	-8.2					
C6.II	V5	Cc5	-7.4	-7.4					
C11B	V5	Cc5	-5.7	-3.8					
C3A.HR	Devonian		-9.5	+2.4	0.710663	NR	0.77	-5 to +3	-12.4 to -10.1
C17.HR	carbonates		-10.5	+1.5					
C4.HR			-8.4	+2.7					
C11.HR	Andesites		-	-	0.743983	0.512196			

Table 2: Elemental composition (Ca, Mg, Fe, Mn, Sr) of the calcite cements Cc1a to Cc5 and host rocks from the hanging wall (HW) and footwall (FW). The qualitative scale in greens indicates different contents (for each element, the darkest green points to the highest concentration and vice versa).

Sample	Ca ppm	Mg ppm	Fe ppm	Mn ppm	Sr ppm
Cc1a	391618	1335.9	5603.5	1243.7	543.7
Cc1a	349063	1548.6	4121.3	781.6	460.2
Cc1a	351134	1231.8	5205.4	810.3	545.5
Cc1a	337588	1126.6	3914.9	680.7	704.0
Cc2	328169	501.2	1061.4	3629.3	248.5
Cc3	364995	331.9	1647.8	8277.9	122.3
Cc3	333123	909.5	5545.9	7695.5	424.9
Cc4	333563	624.4	3814.9	4034.6	72.2
Cc5	233784	2260.0	8656.6	161.4	72.1
Cc5	281741	1626.2	4078.0	138.8	25.3
HW	320038	2752.6	6289.0	621.1	449.4
FW	4234	12830.5	43107.1	466.6	18.6

Higher content  Lower content

Eliminado: higher concentrations when is darker.

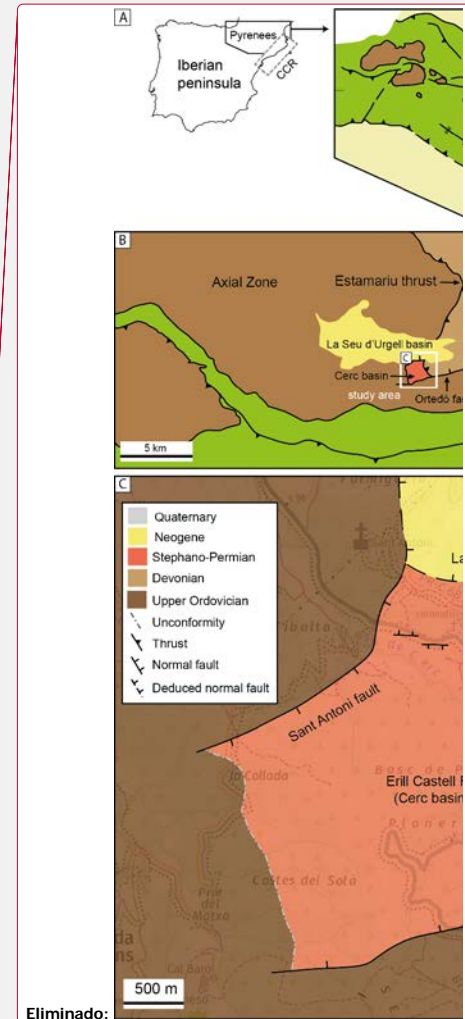
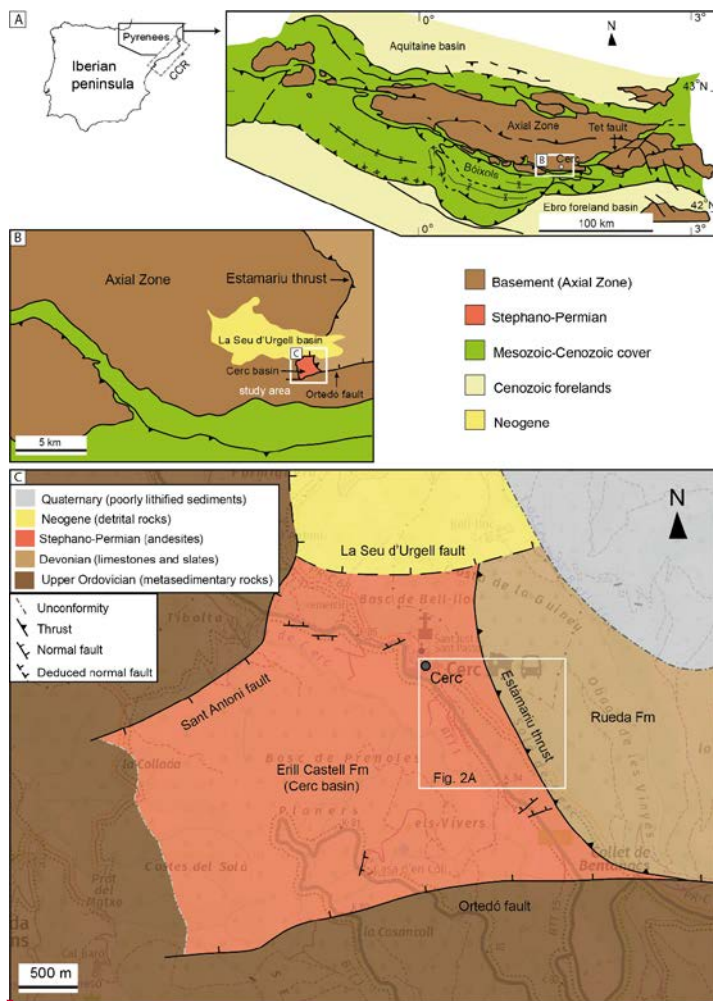


Figure 1: (A) Simplified geological map of the Pyrenees modified from (Muñoz, 2017) and its location in the Iberian Peninsula (location of the Catalan Coastal Range, CCR, is also shown). (B) Detail of the study area located within the Pyrenean Axial zone. (C) Geological map of the Cerc basin (using data from Saura (2004) and our own data) with the Estamariu thrust located in its eastern termination and the Neogene extensional faults in the northern and southern limits. The white square indicates the location of the main outcrop (Fig. 2A).



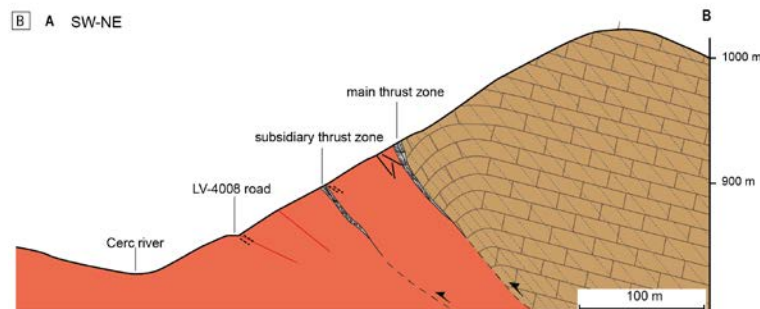
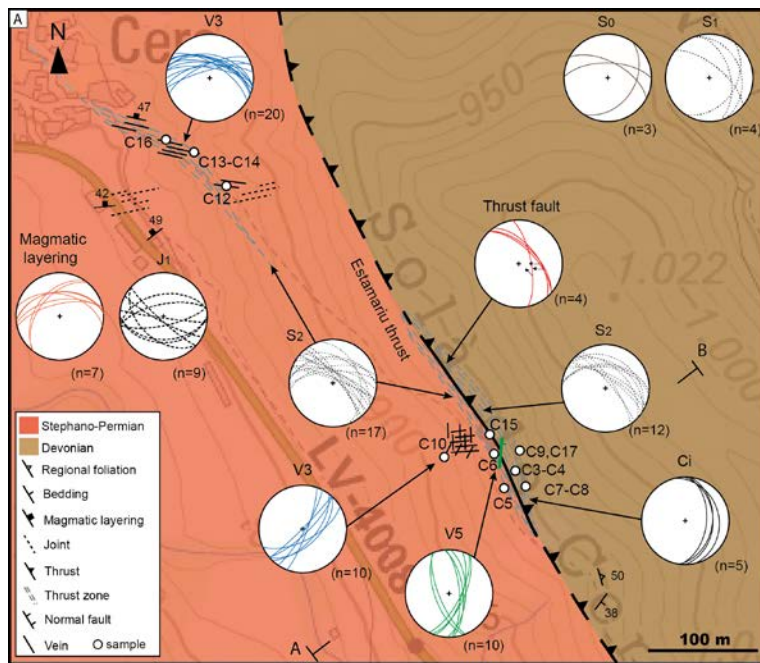
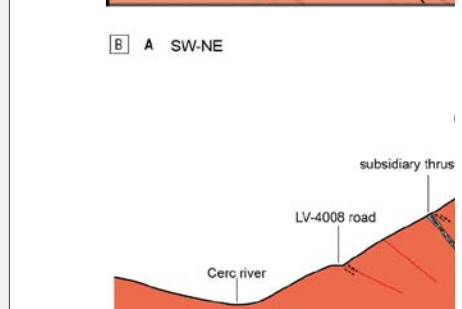
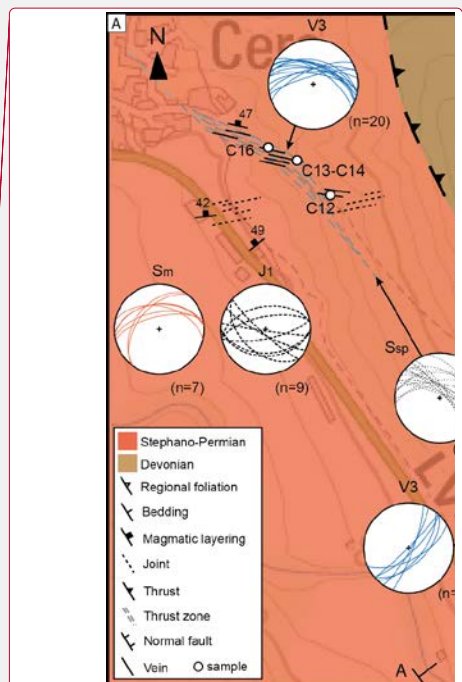


Figure 2: (A) Geological map and (B) cross-section of the Estamaru thrust, which juxtaposes a Devonian unit against a Stephano-Permian sequence (H=V, no vertical exaggeration). Lower-hemisphere equal-area stereoplots of the Devonian bedding (S<sub>0</sub>), regional foliation (S<sub>1</sub>), thrust zone foliation affecting the hanging wall and footwall (S<sub>2</sub>), magmatic layering and the different faults and veins observed in the study area are also included. Location in Fig. 1B.



Eliminado: Sr  
 Eliminado: (SD) ...nd footwall (S<sub>2</sub>SP..., magmatic layering (Sm)  
 Con formato: Subindice

035

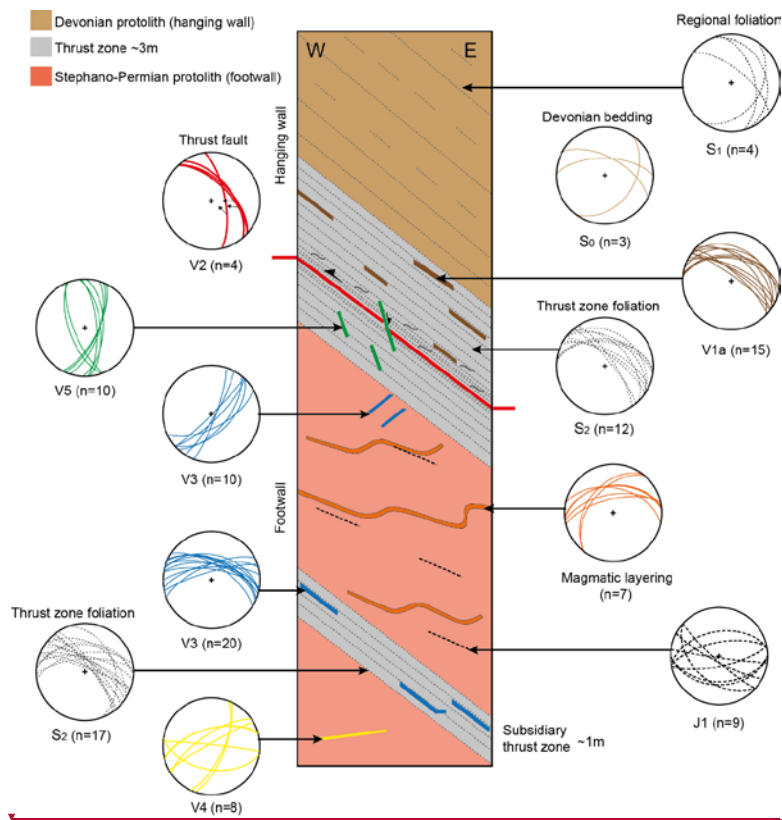
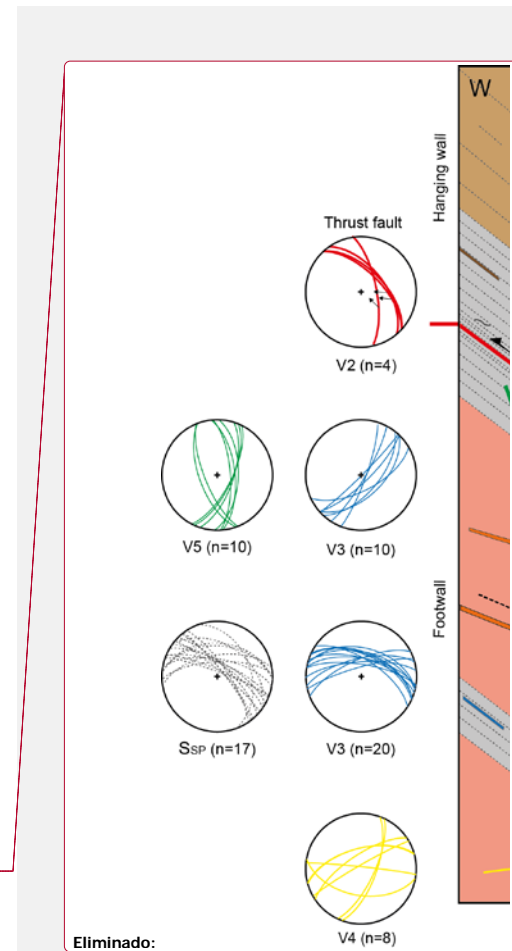


Figure 3: Sketch showing the spatial distribution of mesoscale structures within the main outcrop and lower-hemisphere equal-area stereoplots of the different mesostructures.



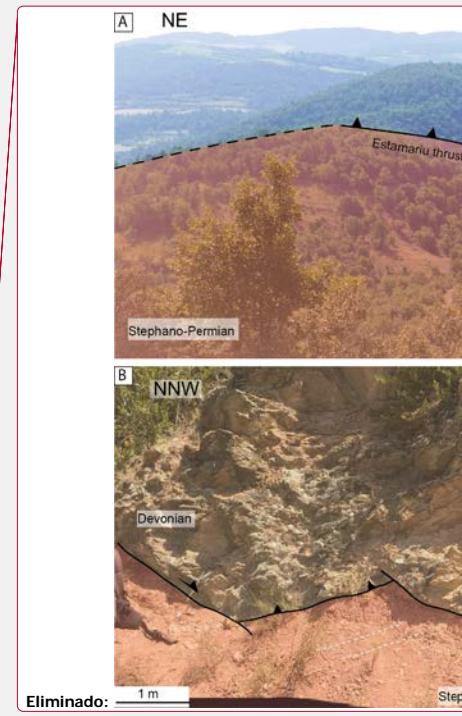
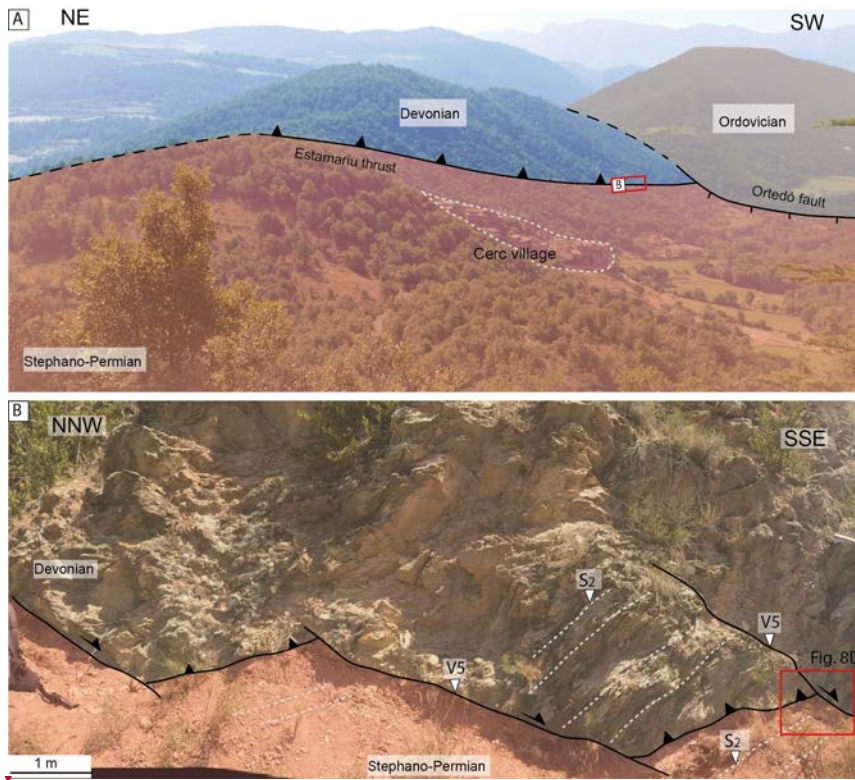


Figure 4: Main outcrop of the Estamariu thrust. A) Panoramic view from the Sant Antoni hill showing the extensional Ortedó fault postdating the Estamariu thrust. B) Main outcrop showing the Estamariu thrust and the related **thrust zone** foliation developed in the Devonian hanging wall and in the Stephano-Permian footwall, and in the Stephano-Permian footwall. The thrust is displaced by later shear fractures **locally mineralized with calcite (V5)**.

Eliminado: (SD)  
 Eliminado: SP

1055



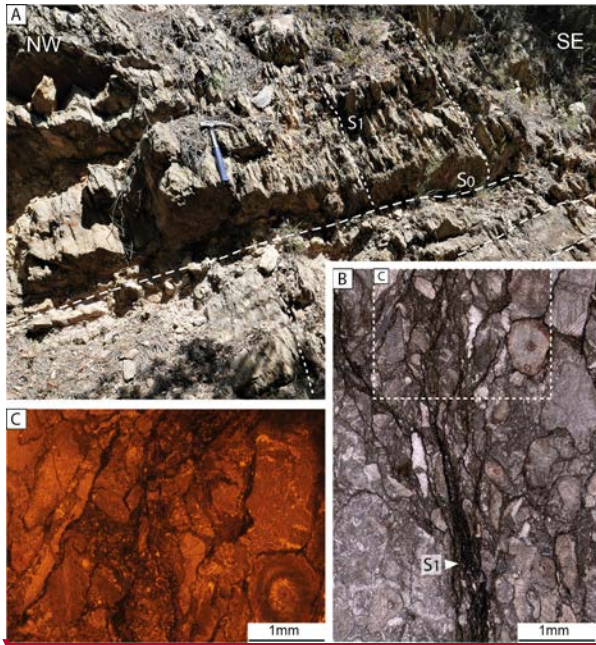
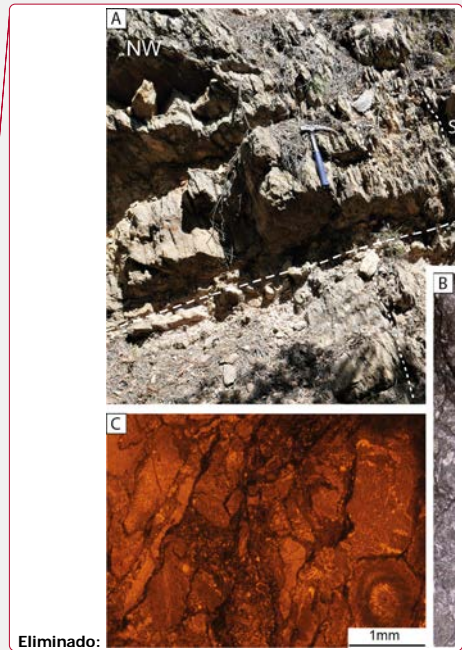


Figure 5: Devonian protolith. A) Field image showing the relationship between bedding ( $S_0$ ) and regional foliation ( $S_1$ ). B) Plane polarized light and C) Cathodoluminescence microphotographs of the encrinites alternating with pelitic rich bands, where the  $S_1$  is concentrated.



Eliminado:

Eliminado: r

Eliminado: r

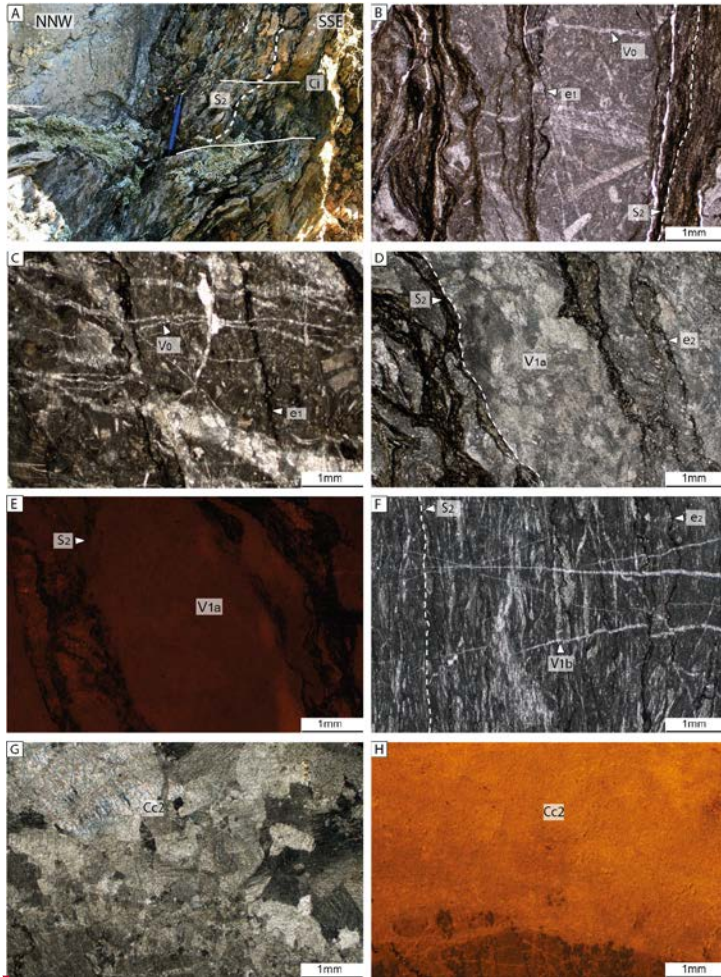
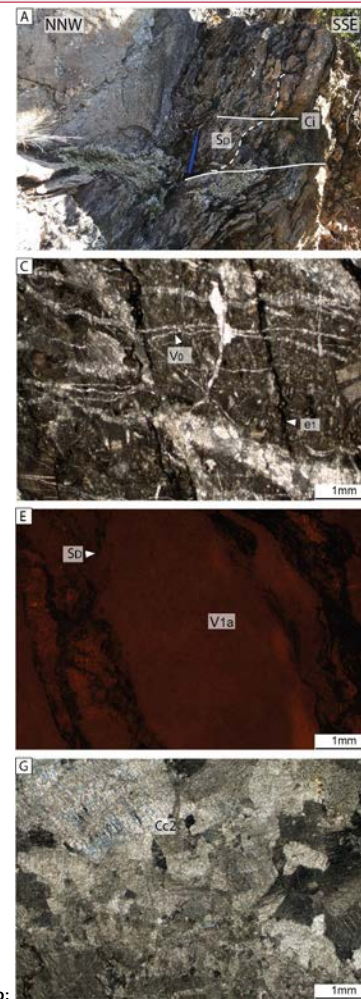


Figure 6: Mesostructures and microstructures found within the thrust zone affecting the hanging wall. A) Outcrop image of the thrust zone foliation ( $S_2$ ) and related C planes indicating reverse kinematics ( $C_1$ ). Microphotographs of B) thrust zone foliation ( $S_2$ ). C) stylolites  $e_1$  and veins  $V_0$  affecting the Devonian encrinites, D) Crossed polarized light and E) cathodoluminescence microphotographs of veins  $V_{1a}$  concentrated between foliation surfaces. F) Thrust zone foliation ( $S_2$ ) near the fault plane and ambiguous and perpendicular relationships between  $V_{1b}$  and  $e_2$ . G) Crossed polarized light and H) cathodoluminescence microphotographs of calcite cement  $Cc_2$  located on the main thrust plane ( $V_2$ ).



Eliminado:

Eliminado:  D

Eliminado:  D

1070

1075



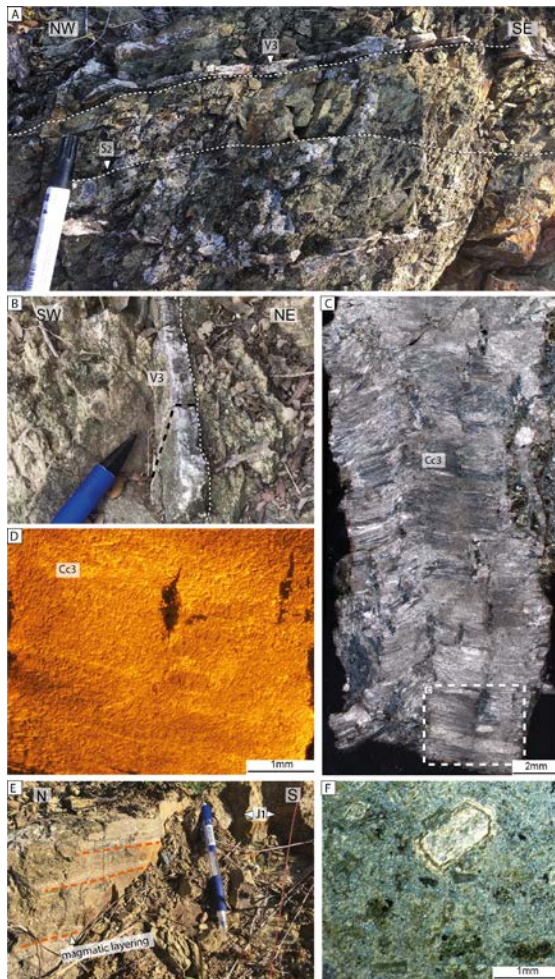
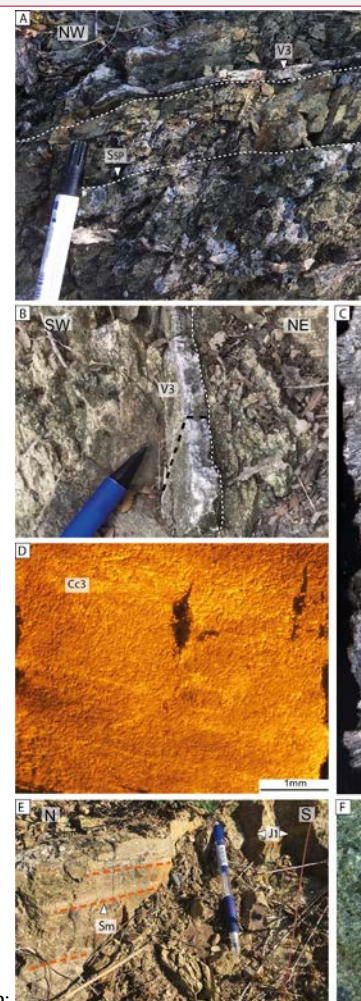


Figure 7: Mesostructures and microstructures present in the Stephano-Permian volcanic footwall. A) Field image of the subsidiary thrust zone in the footwall showing the thrust zone foliation ( $S_2$ ) and the veins V3. B) Detail of veins V3 also in the subsidiary thrust zone. The black dashed line indicates the original position of the thin section observed in C. C) Crossed polarized light and D) Cathodoluminescence microphotographs of veins V3, characterized by calcite fibers growing perpendicular to the vein walls (Cc3). E) Field image of the footwall andesites showing the magmatic layering and joints J1. F) Plane polarized light microphotograph of the volcanic andesites exhibiting a porphyritic texture with a large plagioclase crystal.

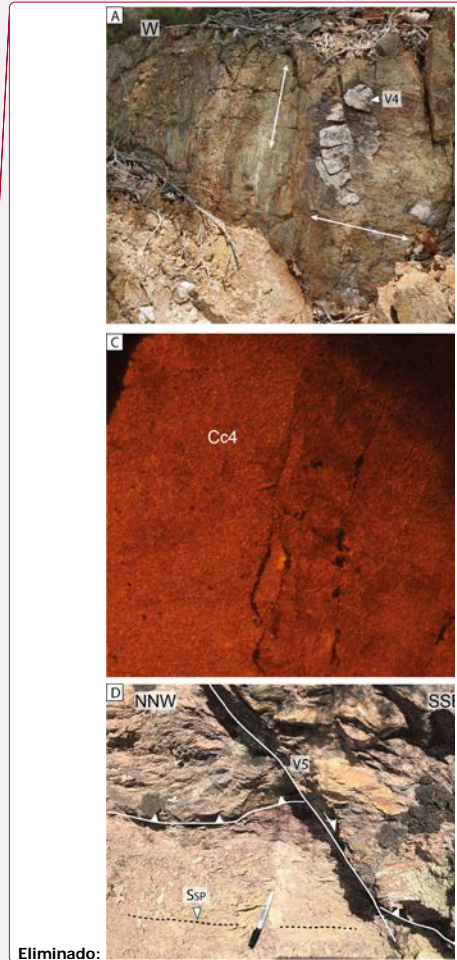
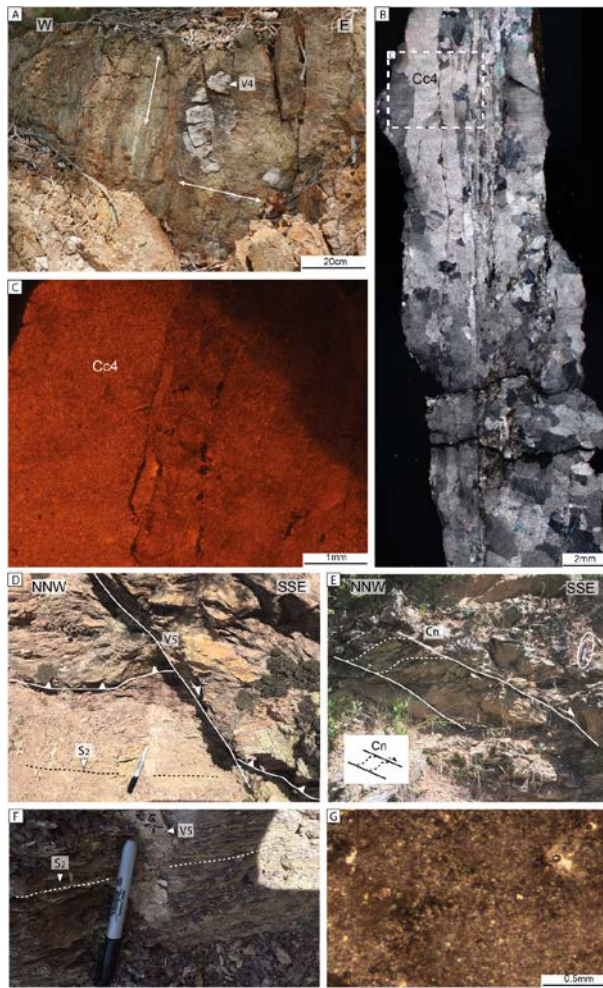


Eliminado:

Eliminado: SsP

Eliminado: c

Eliminado: (Sm)



Eliminado:

Figure 8: A) Field image of a subvertical and E-W fault plane mineralized with calcite (veins V4) and showing two striae set generations (white arrows) indicating dip-slip and strike-slip kinematics. B) Crossed polarized light and C) cathodoluminescence microphotographs of the vein-related calcite cement (Cc4). D) Shear fracture postdating the thrust zone foliation, locally mineralized with calcite veins V5. E) Shear bands (Cn) with normal kinematics located in the main thrust zone, indicating a later reactivation of the Estamariu thrust. (F) Field image of a calcite vein V5 and (G) Plane polarized light of the vein-related cement (Cc5).

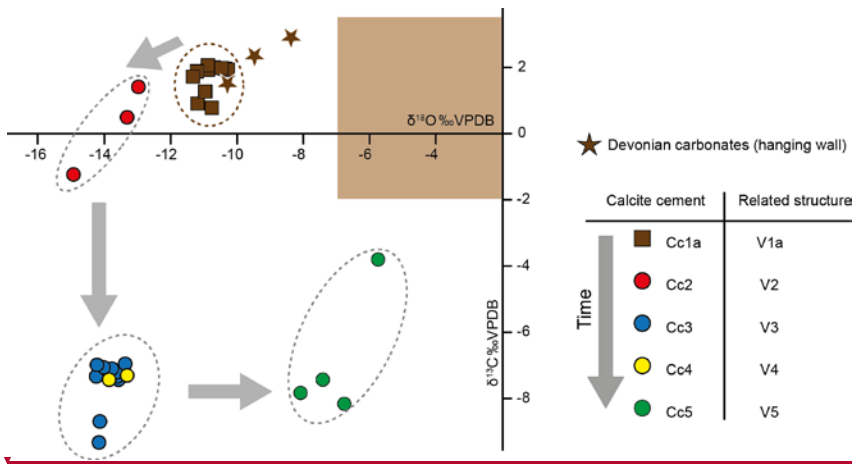
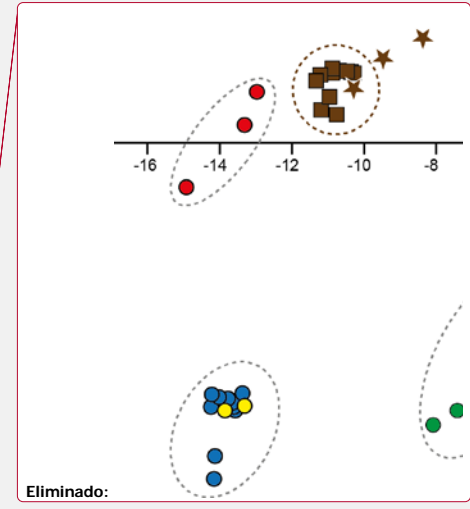


Figure 9:  $\delta^{18}\text{O}$  and  $\delta^{13}\text{C}$  values of calcite cements Cc1a to Cc5 and the Devonian carbonates from the hanging wall. Arrows indicate evolution over time according to the inferred relative timing of cements. The brown box refers to typical values of Devonian marine carbonates (Veizer et al., 1999).



1105

1110

1115



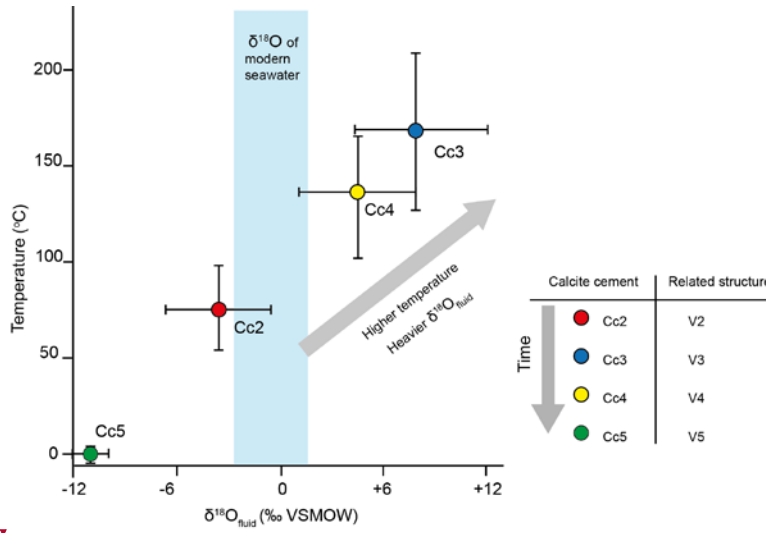
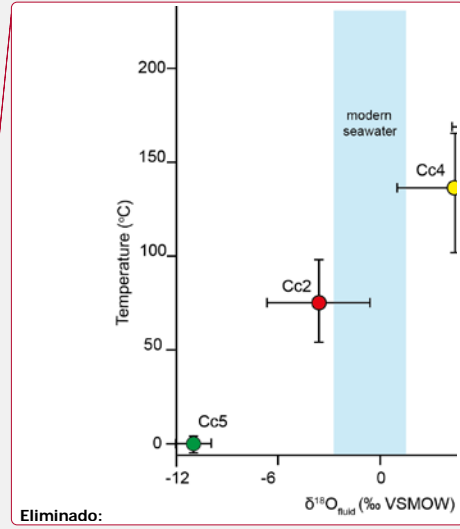


Figure 10: Temperatures (°C) vs  $\delta^{18}\text{O}_{\text{fluid}}$  calculated for cements Cc2 to Cc5. The typical  $\delta^{18}\text{O}$  values for modern seawater (blue band) are from (Veizer et al., 1999).



1120

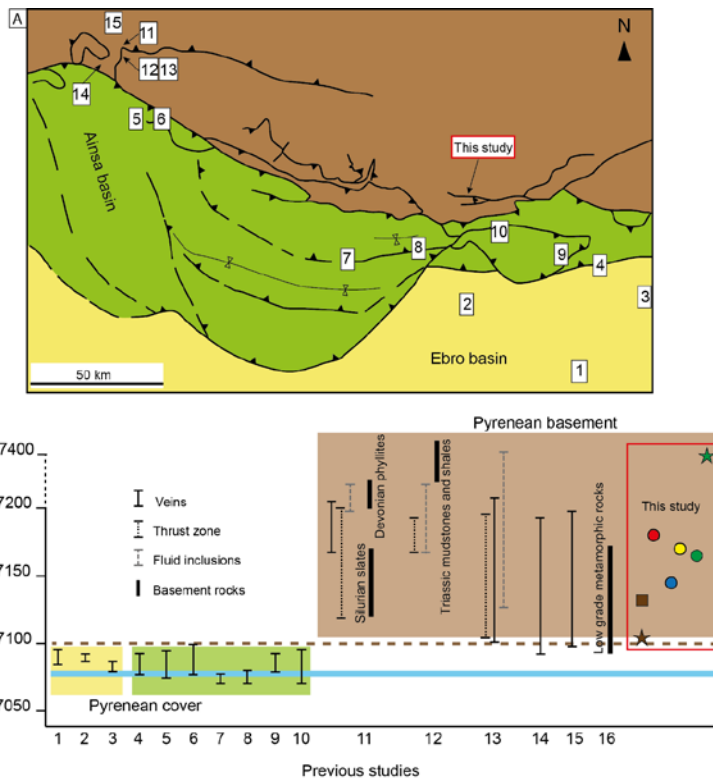


Figure 11: Simplified geological map of the south-central Pyrenees showing the location of structures where  $^{87}\text{Sr}/^{86}\text{Sr}$  analysis have been carried out. Below,  $^{87}\text{Sr}/^{86}\text{Sr}$  ratios from this study compared to results from other structures involving either cover units (1-10) or basement rocks (11-16). The blue thick line refers to the  $^{87}\text{Sr}/^{86}\text{Sr}$  range of Phanerozoic seawater and the dashed brown line represents the  $^{87}\text{Sr}/^{86}\text{Sr}$  limit value between basement and cover structures. 1. El Guix anticline (Travé et al., 2000), 2. Puig Reig anticline (Cruset et al., 2016), 3. L'Escala thrust (Cruset et al., 2018), 4. Valfogona thrust (Cruset et al., 2018), 5. Ainsa basin (Travé et al., 1997), 6. Ainsa-Bielsa area (McCaig et al., 1995), 7. Minor Bóixols thrust (Muñoz-López et al., under review), 8. Bóixols anticline (Nardini et al., 2019), 9. Lower Pedraforca thrust (Cruset et al., 2020a), 10. Upper Pedraforca thrust (Cruset, 2019), 11. Gavarnie thrust (McCaig et al., 1995), 12. Pic de Port Vieux thrust (Banks et al., 1991), 13. Pic de Port Vieux thrust (McCaig et al., 2000b), 14. Plan de Larri thrust (McCaig et al., 1995), 15. La Glere shear zone (Wayne and McCaig, 1998), 16. Trois Seigneurs Massif (not in the map) (Bickle et al., 1988).

Con formato: Español (España)

Código de campo cambiado

Con formato: Español (España)

Código de campo cambiado

Con formato: Español (España)

Código de campo cambiado

Con formato: Español (España)

Con formato: Español (España)

Código de campo cambiado

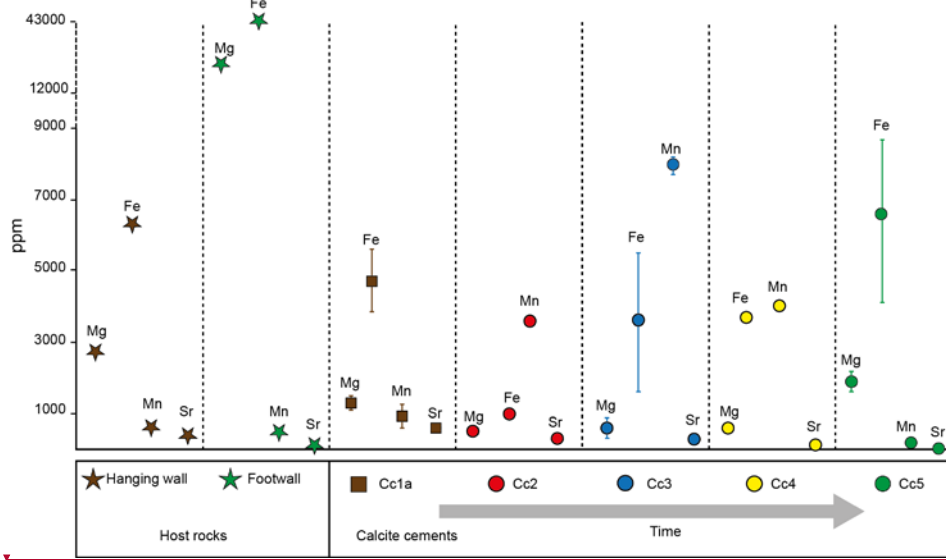
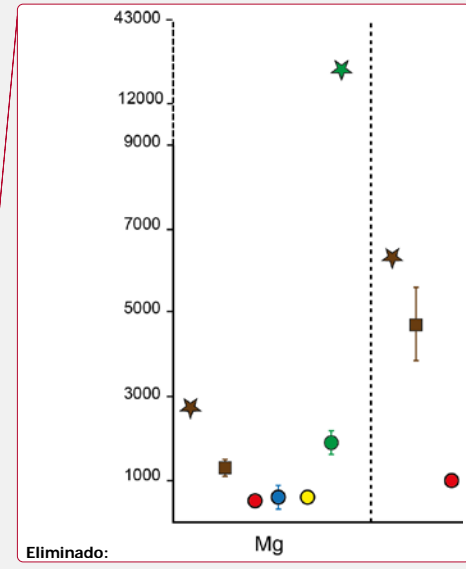


Figure 12: Elemental composition (including Mg, Fe, Mn and Sr) in ppm of the different calcite cements and host rocks. Bars indicate maximum, minimum and average composition.



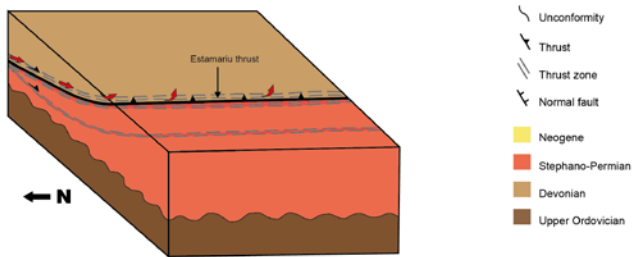
Eliminado:

Mg

Eliminado: <objeto>

**A Alpine compression**

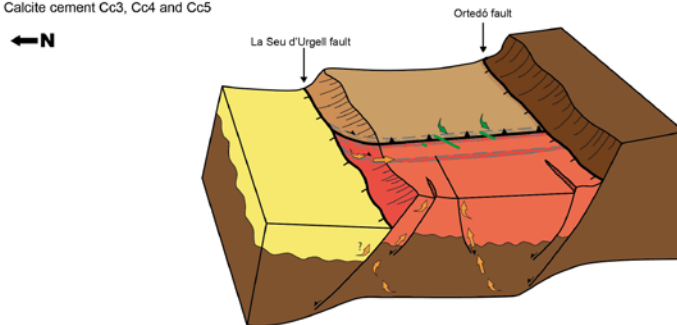
Reactivation of the Estamariu thrust. Calcite cements Cc1a and Cc2



Regional tectonism	A	Alpine compression		B			Neogene extension
Calcite cement		Cc1a	Cc2	Cc3	Cc4	Cc5	
Related structure		V1a	V2	V3	V4	V5	
Geochemistry	$\delta^{13}C_{calcite}$						
	$\delta^{18}O_{calcite}$						
	$^{87}Sr/^{86}Sr$						
	Mg						
	Fe						
	Mn						
	Sr						
$\delta^{18}O_{fluid}$							
Temperature							
Fluid source		Upward meteoric fluid		Upward hydrothermal fluid		Downward meteoric fluid	
Implications		Change in the fluid regime. Increasing extent of fluid-rock interaction			Main change in the fluid regime		

**B Neogene extension**

Reactivation of the Estamariu thrust and development of normal faults  
Calcite cement Cc3, Cc4 and Cc5



150 | Figure 13: Tectonic and geochemical evolution of the study area (not to scale) and relationships with the evolution of the fluid system. A) During the Alpine reactivation of the Estamariu thrust, a meteoric fluid (red arrows) interacted at depth with basement rocks and then migrated along the fault plane towards the hanging wall, precipitating cements Cc1a and Cc2. B) During the Neogene extension, basement-derived hydrothermal fluids (orange arrows) flowed upwards through newly formed and reactivated fault zones. This fluid precipitated calcite cements Cc3 and Cc4. Finally, during ongoing deformation, meteoric fluids (green arrows) percolated in the system and precipitated Cc5, revealing a main change in the fluid regime.

Eliminado: yellow

Eliminado: channelized

Eliminado: blu

Eliminado: e